1985

Comparison of the Optical Techniques of Caustic and Photoelasticity as Applied to Fracture

Himanshu Nigam
University of Rhode Island

COMPARISON OF THE OPTICAL TECHNIQUES OF

CAUSTIC AND PHOTOELASTICITY

AS APPLIED TO

FRACTURE

BY

HIMANSHU NIGAM

A THESIS SUBMITTED IN PARTIAL FULFILLMENT OF THE

REQUIREMENT FOR THE DEGREE OF

MASTER OF SCIENCE

IN

MECHANICAL ENGINEERING

UNIVERSITY OF RHODE ISLAND

1985

MASTER OF SCIENCE THESIS

OF

HIMANSHU NIGAM

APPROVED:

    Thesis Committee

        Major Professor _Arun Shukla_

                                Thomas J. Kim

                                Cheng-Jmng Chang

                                L. A. Michel

                    DEAN OF THE GRADUATE SCHOOL

UNIVERSITY OF RHODE ISLAND

1985

ABSTRACT

Photoelastic and caustic experiments are conducted to obtain stress intensity factor, K, for both stationary and moving cracks. For the stationary crack the values of K are compared with the available theoretical and numerical solutions. Results show that the accuracy varies with the location of the crack tip for both the methods. Six parameter analysis of the photoelastic data gives better values as compared to the caustic results which in turn are better than the values obtained by three parameter photoelastic analysis.

Dynamic photoelastic experiments are conducted with SEN, DCB and DCB/SEN specimens. The data obtained from these experiments namely the stress intensity factor and crack velocity, is compared with existing results and also with the values obtained from dynamic caustic experiment with SEN specimen. Values from caustic analysis are significantly lower. Stress intensity factor as a function of crack velocity is plotted and the results show a dependence on specimen geometry for cracks moving at high velocities.

ACKNOWLEDGEMENTS

TABLE OF CONTENTS

LIST OF FIGURES

LIST OF TABLES

LIST OF SYMBOLS

v	Crack tip velocity
c1	dilatational wave velocity
c2	shear wave velocity
C_R	Raleigh wave velocity
f'	material fringe value
$\bar{N}$	fringe order
σox	remote parallel stress
τmax	maximum in-plane shear stress
σ,τ	stress components
h	thickness of model
l	crack length
ro,Ro	radius of initial curve
rostat	ro for static crack
rodyn	ro for dynamic crack
K,KI	mode I stress intensity factor
Ko	initiating stress intensity factor
KIm	minimum stress intensity factor
KI3	KI by three parameter analysis
KI6	KI by six parameter analysis
KIdyn	dynamic stress intensity factor
KID	dynamic fracture toughness
KII	mode II stress intensity factor
P	applied load
t	time
Δs	path length change

n	refractive index
ν	Poisson's ratio
E	modulus of elasticity
m	magnification factor
Zo,zo	distance to reference plane
f,k,c	constants for caustic analysis
F	correction factor for dyn.caustic
D	diameter of caustic

CHAPTER 1

INTRODUCTION

Stress intensity factor is one of the most important parameters that describes the stress field around a crack tip[3]. It is of both theoretical and practical interest. Practical because most of the fracture criteria are based on it. Even the fatigue failure depends on the instantaneous values of K [4]. Theoretical interest arises from the fact that dynamic fracture characterization may be possible in terms of the stress intensity factor and crack velocity for a given material [5,6].

The value of K is currently obtained by investigators using two different optical techniques, the method of caustics[1] and the method of photoelasticity[2].

Till now photoelasticity has been the most widely used experimental technique for fracture related studies. In recent years the technique of caustics has been used by some investigators but the stress intensity factor-crack velocity data obtained through it is not seen to tally with the existing photoelastic data[6]. Kalthoff[6], who has used the method of caustics, and Kobayashi,et al.[7],who have used photoelasticity, have measured such data and conclude that the K-v-curves are not unique but depend on specimen geometry. Dally et al.[8] also performed such experiments and argue that the K-v -curves are unique for a material and

the variation in the data is due to the variation in experimental conditions and analysis procedure. The controversies yet remain unresolved. The scatter in the data obtained from these is large. It is partially because of the nature of the problem and partially because of the techniques being used. So there is a need to establish a confidence in experimental methods employed for such studies.

This study critically evaluates the optical techniques of caustic[1] and photoelasticity[2] as applied to fracture. Dynamic experiments have been conducted with the same sheet of material under identical loading conditions using both techniques to eliminate the errors arising because of the variation in properties. An attempt is also made to investigate the uniqueness of dynamic stress intensity factor as a function of crack velocity for Homalite100. The effects of the distance of measurement from the crack tip on the accuracy of result has been studied for the method of caustics on plexiglass[9]. The result shows the effect of three dimensonal nature of stress field on the evaluated stress intensity factor.

This thesis consists of six chapters. First chapter is on introduction. The next chapter briefly reviews the past work done in the refinement of the two techniques and in the study of the K-v characteristics. The camera used and the modifications made on it as a part of this work are discussed in chapter 3. Fourth chapter describes the two

techniques. The details of the experiments performed and the data obtained are given in the fifth chapter. Results are discussed in the chapter on conclusions.

CHAPTER 2

REVIEW OF PAST WORK

1 PHOTOELASTICITY AS APPLIED TO FRACTURE

Photoelasticity is a technique which has been widely used for the determination of both static and dynamic stress intensity factors for a field around a crack tip.

Post [10] and Wells and Post[11] in the early 50's were the first investigators to show the application of photoelasticity to fracture mechanics. Irwin[12], in a discussion to reference [11], showed that the stress intensity factor could be determined from a single isochromatic fringe loop at the crack tip. Irwins method is only applicable if the shearing mode stress intensity factor KII=0. The accuracy which can be achieved with Irwin's approach depends upon the location of the apogee point and the precision of locating it[13]. Error of ±3 degrees in locating are common and can result in large errors. Bradly and Kobayashi [14]and Schroedl and Smith [15] modified Irwin's approach and employed a differencing technique to obtain KI and σox. Etheridge and Dally [16] introduced a third parameter into the analysis by modifying the Westergaard stress function to more closely account for stress field variations near the crack tip.

4

All these methods were based on measurements taken from particular points and there was no way to average the errors which might be occuring. Sanford and Dally [17] suggested a multi-point method which uses more number of points than the number of unknowns. It uses the method of least squares coupled with Newton Raphson method to minimise error in arriving at the solution. It is global in nature and the use of full field data permits a significant improvement in the accuracy of determining the stress intensity factors.

Kobayashi and Ramulu[18] derived a relationship between the dynamic stress intensity factors KI,KII and remote stress component σox and the dynamic isochromatic fringes. This relation, together with the overdeterministic method of Sanford and Dally can be used for the evaluation of the three parameters. Using the series representation of stress fields given by Irwin[19] and Atluri et.al[20] a relation between the isochromatic fringes and the stress field parameters, which constitute the higher order terms, is derived to extract KI from the fringe patterns. Studies [9] show that the higher order terms are necessary to reduce the errors in determining KI.

2 CAUSTICS AS APPLIED TO FRACTURE

Caustics as opposed to photoelasticity is a fairly new technique. It was introduced in 1964 by Manogg [21,22], who

performed a shadow optical analysis for a stationary crack under mode-I loading. His study was done on transparent materials. Theocaris and co-workers [23,24] generalized the method of caustics to non-transparent materials by using reflection and applied it to fracture problems of general interest in various branches of engineering science. Theocaris and Gdoutos [25,26] applied the method of caustics in reflection to experimentally examine the deformation fields near the tips of stationary crack in metal plates. In this case, which apparently was the first application of the method to metal specimens, plastic deformation occured locally and the optical data were analysed by assuming a plane stress Dugdale-Barenblatt model for the crack tip plastic zone. Also, Rosakis, Duffy and Freund[27] demonstrated the use of this method to study dynamic fracture phenomenon in metals.

Beinert and Kalthoff[1], Maier[28], Rosakis[29] and Rossmanith[30] have employed the method for dynamic measurements of stress intensity factors. In the initial cases the influence of inertial effects of the spatial dependence on the crack tip was not taken into account. Kalthoff et al.[31], introduced an approximate correction factor to account for the potentially large error introduced by assuming static local field in data analysis. The exact equations of the caustic envelope formed by the reflection of parallel incident light from the surface of the specimen containing a rapidly growing crack were obtained by

Rosakis[29] for mixed mode plane stress crack growth. It was found that, for some typical laboratory materials used in crack propagation studies, the neglect of the influence of inertia on the crack tip stress field could lead to errors of up to 30-40 percent in the value of the elastic stress intensity factor inferred from the measured caustic diameter.

Rossmanith[32] included the higher order terms of the Westergaard type stress functions and discussed their effect on the shape and extension of the highly constrained zone surrounding a crack tip. For a singular solution it was found that the dynamic K-values associated with larger shadow spots are lower than their static counterparts. Higher order terms induce a generalized evaluation formula for the stress intensity factor where powers of the order $n+5/2$ ($n=0,1,...$) of the caustic diameter appear. The dynamic correction is negligible for small and moderate crack velocities justifying the use of static equations for practical purposes.

In a detailed report on crack tip stress state, Rosakis and Ravi Chander [33] discussed the effect of three dimensional stress state on the evaluated results which are based on two dimensional analysis. They tried to identify the regions in which local experimental measurements based on two dimensional theory can be performed with confidence. They concluded that the three dimensional nature of the crack tip field scales with thickness. No signifant plane

7

strain region exists around the crack tip(extremely small).

Rosakis with Freund [34] also studied the effect of the crack tip plasticity on the determination of dynamic stress intensity factors and found that the error introduced through the neglect of plasticity effects in the analysis of data will be small as long as the distance from the crack tip to the initial curve ahead of the tip is more than about twice the plastic zone size. They also found that the error introduced through the neglect of inertial effects will be small as long as the crack speed is less than about 20 percent of the longitudinal wave speed.

Effect of higher order stress terms on mode-I caustics in birefringent materials has been recently studied by Phillips and Sanford [35]. They developed a theory to determine the sizes, shapes and location of the double caustics produced in statically loaded birefringent plates containing mode-I cracks. It was found that the transverse diameters of the inner and outer parts of the double caustic have an average value essentially equal to the transverse diameter of the single caustic produced by optically isotropic material having the same optical constant. They also observed that with the superposition of a constant (tensile or compressive) stress parallel to the crack, each part of the double caustic deforms independently but in such a way as to maintain this average transverse diameter.

3 <u>STUDIES PERTAINING TO STRESS INTENSITY FACTOR AND CRACK VELOCITY RELATIONSHIP</u>

Both the mentioned techniques have been used to study dynamic fracture and obtain the K-v-plots and it is believed, though with some skepticism, that these plots characterize the dynamic fracture behaviour of a material[36]. The Fracture Mechanics group at the University of Maryland[5,37,38], University of Washington[39] and other institutions have made important contributions to the charecterization of dynamic crack propagation by means of relationship between the crack velocity and the stress intensity factor.

Irwin, Dally and others [5] performed a series of fracture experiments with various types of specimens fabricated from Homalite 100 and observed that the K vs v curve had three distinct regions, the stem, the slope range and the plateau, as shown in figure 1. In the stem region, the crack velocity is independent of K. Small changes of K cause considerable changes in the crack velocity, up to velocities of about 200 m/s. The slope range is the transition region covering crack velocities from 200 to 381 m/s. For higher velocities, a large increase in K is needed even for small increase in v. This is the plateau region. The highest velocity of crack propagation recorded in these experiments was 432 m/s. Rossmanith and Irwin [38] suggested that the K vs v relationship, as obtained from

experiments with test specimens, depends in the high velocity region on the type of test specimen used. Though Dally argued [8] that the different results are due to insufficiencies of the current data evaluation procedures and speculated that the K-v-curve is unique.

Irwin et al[5] concluded that KIm, which is the stress intensity factor below which the crack cannot propagate, can be treated as a material property. Though it has been shown theoretically[40] that the maximum crack velocity which can be achieved is $v = C_R$, the Raleigh wave speed. This value is not attained for most of the materials in practice because branching occurs at lower velocities and the energy driving the crack is divided.

Kalthoff and his colleagues performed dynamic caustic experiments with DCB, SEN and DCB/SEN specimens and got two different K-v-curves. From that he concluded that these curves are not unique, but depend on specimen geometry [6]. Kobayashi[7] also concluded that these curves are not unique. To explain the difference in the values for the two types of specimens Kalthoff has differentiated the dynamic stress intensity factor KIdyn, a pure stress field quantity and dynamic fracture toughness KID [6], a material property and contends that KID(v) is a lower bound for all possible KIdyn(v) curves (from energy considerations). This raises a question whether KIdyn is unique and completely describes the fracture phenomenon. Experiments have been performed [41] to show that KIdyn has a tendency to be larger than

10

KID.

Ravi-Chander and Knauss[42] also employed the method
of caustics with Homalite100. The loading of the crack in
an unbounded medium was dynamic and achieved with an
electromagnetic loading device for the duration of the
experiment (0.150 m.sec). The results of this experiment
indicate that there is not one-to-one relationship between
KI and v.

The difference in the viewpoint on the uniqueness of
the K-v relation is clear from the above review. To better
judge which is the correct viewpoint, it is required that
one carefully consider the details of the experiment and the
methods used to determine the values of both KI and v from
either isochromatic fringe loops or shadow spots[36].

In this project the two techniques have been studied
and the results compared. The dynamic experiment data
generated has been used to verify the K-v relationship
described above.

CHAPTER 3

THE MULTIPLE-SPARK CAMERA

Dynamic photoelasticity and the method of caustics are the two most popular techniques used today to study dynamic fracture. The photoelastic method is commonly employed in the United States whereas the technique of caustic is used both in Europe and the US.

Although both techniques require a high speed recording device, usually the multiple spark camera which was originally designed by Cranz and Schardin [43], the light sources required by the two approaches are quite different. This chapter will briefly discuss the two techniques in the perspective of camera design and the component systems comprising the camera.

Many transparent non-crystalline materials that are optically isotropic when free of stress become optically anisotropic and display characteristics similar to crystals when they are stressed. These characteristics persists while loads on the material are maintained but disappear when the loads are removed. This behaviour is called temporary double refraction and the method of photoelasticity is based on this physical behaviour of transparent non-crystalline materials[2].

For experimentation, the model is fabricated from a polymeric, transparent, birefringent material. When

circularly polarized light passes through the stressed model and then through another circular polarizer, an optical interference produces a series of light and dark bands which are termed isochromatic fringe patterns(they are lines of constant maximum shear stress). The stress-optic law, which relates the stress state of the model to the order of the associated interference pattern is given by

$$2\tau m = \sigma 1 - \sigma 2 = \bar{N} f'/h$$

where $\sigma 1$ and $\sigma 2$ are the inplane principal stresses, τm the maximum inplane shear stress, $\bar{N}$ the fringe order, f' the material fringe value and h the thickness of the model.

Method of caustics is based on a totally different phenomenon. When a material is stressed there is a change in the thickness and shape of the material. This leads to the deflection of light reflected from its surface or refraction of light passing through it in some particular way which depends on the stress field present. The image obtained on the reference plane of the light thus deflected gives the information of the stress field present in the material.

1 THE CAMERA

In the photomechanics laboratory here, there existed a Cranz-Schardin multiple spark camera which could be used for photoelasticity work only. Also the range of time intervals

13

available was restrictive. As a part of this research the camera has been modified to suit the caustic set up and the inductive coils, which determine the time delay, were redesigned to extend the range to allow recording slow phenomena such as a slow moving crack etc. Following is a brief description of the three main subdivisions of the camera, viz., the optical arrangement, the spark gap and the control circuit.

1.1 Optical Arrangement

Altough both the techniques require similar arrangements, the light sources required by the two approaches are quiet different. Photoelastic applications require about 100 times more light energy than is needed for caustics, as the light has to pass through at least three different filters before exposing the film. Also the film used for photoelasticity is relatively slow. On the other hand the method of caustics requires much less light - which must emanate from a "point light source" to ensure a sharp caustic. Thus a light source designed for caustics cannot be used for photoelastic applications and vice versa. The optical bench for the two is shown in figure 2 and figure 3.

For photoelastic experiments two circular polarizers are kept on either side of the specimen. As an example, light from the spark SG1 passes through a field lens, the first polarizer, the specimen, the second polarizer and the

second field lens onto the camera lens L1. In a similar manner, light from the spark gaps SG2,SG3 etc. is focused on the corresponding lenses L2,L3 etc. The spark gaps, the field lenses and the camera lenses are so placed that the light from one particular spark falls on one particular camera lens so that the image from one camera lens is due to one spark only. So twenty pictures of the propagating crack are obtained at twenty different spots on the same film. Kodak Wrattan No.8 filters and Kodak Grauvre Positive 4135 film are used, the combination of film and filter yielding blue light of wavelength of 4920 A°. The light from the spark gaps is picked up by a fiber optic light guide which then acts as a light source for the camera. The light guide is a 1/4 inch thick bundle of fibers which provides sufficient light to generate sharp, well-defined isochromatic-fringe pattern.

For caustic experiments the polarizer sheets and the filters are removed. The fiber-optic light guides which are used for photoelastic work are replaced by a new set of fiber-optics which contains a step index of refraction fibers 200 microns in diameter. The fiber optic end adjacent to the spark is positioned at the focal point of a micro lens as shown in figure 4. These micro lenses pick up light at a diverging angle of about 5 degrees from the spark gaps and concentrate it on the fiber. This unique optical arrangement permits sufficient light to record clearly defined caustics. Since the distance of the reference plane

from the specimen (Zo) is critical in determining the caustic, the camera and the lenses are moved back to achieve sufficient Zo (see figure 3). The film used is a high speed (1000 ASA) Kodak Royal Pan film 4141.

1.2 Spark Circuit

The Multiple Spark circuit is shown in figure 5. In the camera which is used in this research, there are twenty spark gaps (SG), each of them connected to L-C circuit in series. TSG is the trigger spark gap. In operation the condensors are charged to about 15kv and the circuit L1C1 is closed by applying a trigger to the spark gap TSG. The firing sequence is initiated at a predetermined time after the crack initiation by applying a 30kv pulse to the trigger gap. When the trigger is fired, the capacitor C1 discharges to below the ground potential. When the voltage on C1 becomes sufficiently negative, a spark occurs at the gap SG1 and the capacitor C1* discharges, providing a short, intense flash of light.

The timing between the first and second sparks depends on the inductance L2 in the C1*-L2-C2 loop. When the gap SG1 fires, the voltage on C2 decays with time and the gap SG2 fires when the voltage on C2 is sufficiently negative. Like wise, all twenty gaps fire. The light from the spark gap is let out of the camera by fiber optics.

1.3 Control Circuit

The control circuit is used to initiate the firing sequence at a required delay after the dynamic event has started. A schematic of the circuit is shown in figure 6[44]. When the conductive paint on the specimen is broken by the moving crack, a 20volt pulse is emitted which initiates a Digital Delay Generator(Model 103CR of California Avionics Labs Inc.) and a Nicolet Oscilloscope(Model 206).

The light from the sparks is picked up by a high frequency response photocell and its output is recorded on the oscilloscope as an intensity-time trace. The timings of the peaks on this trace represent the time at which the picture of the crack was taken. The delay generator holds the pulse from the broken conductive paint line for a predetermined interval of time. Once the pulse is passed to the Trigger Spark Gap after the required delay, the voltage at the trigger gap is stepped up to 30kv, after which the firing occurs in the sequence described before.

CHAPTER 4

ANALYSIS OF DATA

In this research experiments have been done both with isochromatic and caustic set ups. Following is a brief description of the two techniques and the method of analysis.

1 PHOTOELASTICITY:

When a birefringent material is placed in a polariscope, the stresses in it lead to the formation of interference fringes as discussed in chapter 3. These fringes are related to the stresses present in the material by the following stress optic law:

$$\left(\frac{\bar{N}f'}{2h}\right)^2 = \tau_{max}^2 = \frac{1}{4}(\sigma_{xx} - \sigma_{yy})^2 + \tau_{xy}^2 \tag{4.1}$$

where f' is the fringe sensitivity of the model material, $\bar{N}$ is the order of the fringe and h is the model thickness. Now, the stresses are represented in terms of the stress intensity factors and other terms comprising a series(equations given later). Depending on the type of series and the number of terms included for analysis we get two different models-the three parameter model and the six parameter model. These models are discussed here for the dynamic case. Static analysis is a special case with the

18

crack velocity set to zero.

1.1 Three Parameter Model:

In this model[18] first two terms of the mode I series involving KI and σox and the first term of the mode II series involving KII are included. So the three stresses σx,σy and τxy at any point r and θ are reprsented in terms of KI,KII and σox. These expressions when substituted in equation(4.1) give the value of τmax as

$$\tau_{max}^2 = \frac{1}{4}\left(\frac{H^2}{r} + \frac{2H\sigma_{ox}}{\sqrt{r}} + \sigma_{ox}^2\right) + \frac{J^2}{r} \tag{4.2}$$

where

$$H = \frac{K_I}{\sqrt{\pi}} B_I \cdot \left\{(1+s_1^2)\left[f(c_1)+g(c_1)\right]^{1/2} - \frac{4s_1s_2}{(1+s_2^2)}\left[f(c_2)+g(c_2)\right]^{1/2}\right\}$$

$$- \frac{K_{II}}{\sqrt{\pi}} B_{II} \cdot \left\{(1+s_1^2)\left[f(c_1)-g(c_1)\right]^{1/2} - (1+s_2^2)\left[f(c_2)-g(c_2)\right]^{1/2}\right\} \tag{4.3}$$

$$J = \frac{K_I}{\sqrt{\pi}} B_I \cdot s_1 \left\{\left[f(c_1)-g(c_1)\right]^{1/2} - \left[f(c_2)-g(c_2)\right]^{1/2}\right\}$$

$$+ \frac{K_{II}}{4\sqrt{\pi}\, s_2} B_{II} \left\{4s_1s_2\left[f(c_1)+g(c_1)\right]^{1/2} - (1+s_2^2)^2\left[f(c_2)+g(c_2)\right]^{1/2}\right\} \tag{4.4}$$

$$B_I = \frac{1+s_2^2}{4s_1s_2-(1+s_2^2)^2} \tag{4.5}$$

$$B_{II} = \frac{2s_2}{4s_1s_2-(1+s_2^2)^2} \tag{4.6}$$

$$f(c_1) = \left(1-\frac{v^2}{c_1^2}\sin^2\theta\right)^{-1/2} \qquad f(c_2) = \left(1-\frac{v^2}{c_2^2}\sin^2\theta\right)^{-1/2} \tag{4.7}$$

$$g(c_1) = f(c_1)^2 \cos\theta \qquad g(c_2) = f(c_2)^2 \cos\theta \tag{4.8}$$

19

$$S_1^2 = 1 - \frac{v^2}{c_1^2} \qquad\qquad S_2^2 = 1 - \frac{c^2}{c_2^2} \qquad (4.9)$$

For any point k in the field (defined by r and θ) having fringe order $\bar{N}k$, equation(4.2) can be rewritten in the following form

$$G_k(K_1, K_{11}, \sigma_{ox}) = \left(\frac{\bar{N}_k f'}{2h}\right)^2 - \frac{1}{4}\left[\frac{H_k^2}{T_k} + \frac{2H_x \bar{\sigma}_{ox}}{\sqrt{T_k}} + \sigma_{ox}^2\right] + \frac{J_k^2}{T_k} = 0 \qquad (4.10)$$

Just three points would be sufficient to give three equations of the above form which can be solved simultaneously to obtain the solution. Instead of using this approach a multipoint overdeterministic method is used which is a combination of least squares and Newton-Raphson techniques. The overdeterministic method suggested by Sanford and Dally [17] is discussed below.

For the sake of generality equation(4.10) can be considered to be of the form

$$G_k (x_1, x_2, x_3, \ldots, x_n) = 0 \qquad\qquad (4.11)$$

where n is the number of unknown constants. The unknowns (x1,x2,...) have to be determined to make Gk=0. Though equation (4.10) can be solved in closed form, the algebra becomes quite involved and the simpler numerical method based on the Newton-Raphson technique is employed.

In the overdeterministic method, the function Gk is evaluated at a large number of data points in the stress field. If initial estimates are given for the constants in

20

equation(4.10), Gk ≠ 0, since the initial estimates will usually be in error. To correct the estimates, a series of iterative equations based on a Taylor series expansion of Gk are written as

$$(G_k)_{i+1} = (G_k)_i + \left[\frac{\partial G_k}{\partial x_1}\right] \Delta x_1 + \left[\frac{\partial G_k}{\partial x_2}\right] \Delta x_2 + \dots \qquad (4.12)$$

where the subscript i refers to the ith iteration step and $\Delta x_1, \Delta x_2$ etc. are corrections for the previous estimates of x_1, x_2 etc.

The corrections are determined so that $(Gk)_{i+1} = 0$ and thus equation(4.12) gives

$$\left[\frac{\partial G_k}{\partial x_1}\right] \Delta x_1 + \left[\frac{\partial G_k}{\partial x_2}\right] \Delta x_2 + \dots = -(G_k)_i \qquad (4.13)$$

The method of least squares involves the determination of the series coefficients so that equation(4.10) is fitted to a large number of data points in the isochromatic field.

Equation(4.13) in the matrix form gives

$$-\begin{bmatrix} G_1 \\ G_2 \\ \vdots \\ \vdots \\ G_N \end{bmatrix} = \begin{bmatrix} \Delta x_1 \\ \Delta x_2 \\ \vdots \\ \vdots \\ \Delta x_n \end{bmatrix} * \begin{bmatrix} \dfrac{\partial G_1}{\partial x_1} & \dfrac{\partial G_1}{\partial x_2} & \dots & \dfrac{\partial G_1}{\partial x_n} \\ \dfrac{\partial G_2}{\partial x_1} & \dfrac{\partial G_2}{\partial x_2} & & \dfrac{\partial G_2}{\partial x_n} \\ \vdots & \vdots & & \vdots \\ \dfrac{\partial G_N}{\partial x_1} & \dfrac{\partial G_N}{\partial x_2} & \dots & \dfrac{\partial G_N}{\partial x_n} \end{bmatrix} \qquad (4.14)$$

where N is the total number of the data points considered. The above equation can be put in the form

$$[G] = [a][\Delta x] \qquad (4.15)$$

where

21

$$[G] = \begin{bmatrix} G_1 \\ G_2 \\ \vdots \\ G_N \end{bmatrix} \qquad [\Delta X] = \begin{bmatrix} \Delta X_1 \\ \Delta X_2 \\ \vdots \\ \Delta X_n \end{bmatrix}$$

and

$$[a] = \begin{bmatrix} \dfrac{\partial G_1}{\partial x_1} & \dfrac{\partial G_1}{\partial x_2} & \cdots & \dfrac{\partial G_1}{\partial x_n} \\ \dfrac{\partial G_2}{\partial x_1} & \dfrac{\partial G_2}{\partial x_2} & \cdots & \dfrac{\partial G_2}{\partial x_n} \\ \vdots & \vdots & & \vdots \\ \dfrac{\partial G_N}{\partial x_1} & \dfrac{\partial G_N}{\partial x_2} & \cdots & \dfrac{\partial G_N}{\partial x_n} \end{bmatrix}$$

Premultiplying by aT (Transpose of a),

$$[a]^T [G] = [a]^T [a] [\Delta x] \quad \circ$$

$$\text{or} \quad [d] = [c][\Delta x]$$

$$\text{where} \quad [d] = [a]^T [G] \quad \text{and} \quad [c] = [a]^T [a]$$

The correction factors are given by

$$[\Delta X] = [c]^{-1} [d] \tag{4.16}$$

The iterative procedure is employed till the series constants are determined to obtain a close fit of the function G to the N data points.

The x's in case of three parameter model are KI,KII and σox and the differentials of G with respect to them are given below[18]

22

$$\frac{\partial G_\kappa}{\partial k_1} = \frac{1}{4}\left(\frac{2H_\kappa}{r_\kappa}\frac{\partial H_\kappa}{\partial k_1} + \frac{2\sigma_{0x}}{\sqrt{r_\kappa}}\frac{\partial H_\kappa}{\partial k_1}\right) + \frac{2J_\kappa}{r_\kappa}\frac{\partial J_\kappa}{\partial k_1} \qquad (4\cdot17)$$

$$\frac{\partial G_\kappa}{\partial k_{11}} = \frac{1}{4}\left(\frac{2H_\kappa}{r_\kappa}\frac{\partial H_\kappa}{\partial k_{11}} + \frac{2\sigma_{0x}}{\sqrt{r_\kappa}}\frac{\partial H_\kappa}{\partial k_{11}}\right) + \frac{2J_\kappa}{r_\kappa}\frac{\partial J_\kappa}{\partial k_{11}} \qquad (4\cdot18)$$

$$\frac{\partial G_\kappa}{\partial \sigma_{0x}} = \frac{1}{2}\left(\frac{H_\kappa}{\sqrt{r_\kappa}} + \sigma_{0x}\right) \qquad (4\cdot19)$$

where

$$\frac{\partial H_\kappa}{\partial k_1} = \frac{\beta_1}{\sqrt{\pi}}\left\{(1+s_1^2)\left[f(c_1)+g(c_1)\right]^{1/2} - \frac{4s_1 s_2}{(1+s_2^2)}\left[f(c_2)+g(c_2)\right]^{1/2}\right\} \qquad (4\cdot20)$$

$$\frac{\partial H_\kappa}{\partial k_{11}} = -\frac{\beta_{11}}{\sqrt{\pi}}\left\{(1+s_1^2)\left[f(c_1)-g(c_1)\right]^{1/2} - (1+s_2^2)\left[f(c_2)-g(c_2)\right]^{1/2}\right\} \qquad (4\cdot21)$$

$$\frac{\partial J_\kappa}{\partial k_1} = \frac{\beta_1 s_1}{\sqrt{\pi}}\left\{\left[f(c_1)-g(c_1)\right]^{1/2} - \left[f(c_2)-g(c_2)\right]^{1/2}\right\} \qquad (4\cdot22)$$

$$\frac{\partial J_\kappa}{\partial k_{11}} = \frac{\beta_{11}}{4\sqrt{\pi}}\left\{4s_1 s_2\left[f(c_1)+g(c_1)\right]^{1/2} - (1+s_2^2)^2\left[f(c_2)+g(c_2)\right]^{1/2}\right\} \qquad (4\cdot23)$$

1.2 Six Parameter Model

In six parameter model the stresses are represented as the sum of two series with three terms each. The coefficients of the six terms are the six parameters to be evaluated. These coefficients happen to include KI and σox which are of primary interest. A short description of the model is given here. Irwin [19] has shown, that for a crack tip stress pattern translating in the positive x-direction at a fixed speed, stresses at a point (x,y) can be expressed as

$$\sigma_{xx} = \frac{1}{[\Omega - (1 + s_2^2)]} \left[(1 + 2s_1^2 - s_2^2) \, \text{Re} Z_1 - \Omega \, \text{Re} Z_2 \right]$$

$$+ \frac{1}{(s_1^2 - s_2^2)} \left[(1 + 2s_1^2 - s_2^2) \, \text{Re} Y_1 - (1 + s_2^2) \, \text{Re} Y_2 \right] \qquad (4.24)$$

$$\sigma_{yy} = \frac{1}{[\Omega - (1 + s_2^2)]} \left[-(1 + s_2^2) \, \text{Re} Z_1 + \Omega \, \text{Re} Z_2 \right]$$

$$+ \frac{(1 + s_2^2)}{(s_1^2 - s_2^2)} \left(\text{Re} Y_2 - \text{Re} Y_1 \right) \qquad (4.25)$$

$$\tau_{xy} = \frac{1}{[\Omega - (1 + s_2^2)]} \, 2 s_1 \left(\text{Im} Z_2 - \text{Im} Z_1 \right)$$

$$+ \frac{1}{(s_1^2 - s_2^2)} \left[\frac{(1 + s_2^2)^2}{2 s_2} \, \text{Im} Y_2 - 2 s_1 \, \text{Im} Y_1 \right] \qquad (4.26)$$

where

$$\Omega = 4 s_1 s_2 / (1 + s_1^2)$$

$$Y = \sum_{m=0} B_m z^m \qquad (4.27)$$

$$Y_1 = Y(z_1) \qquad \qquad Y_2 = Y(z_2)$$

$$Z = \sum_{n=0} A_n z^{n - \frac{1}{2}} \qquad (4.28)$$

$$Z_1 = Z(z_1) \qquad \qquad Z_2 = Z(z_2)$$

$$z_1 = x + i y_1 \qquad \qquad z_2 = x + i y_2$$

$$y_1 = s_1 y \qquad \qquad y_2 = s_2 y$$

24

Now from equations(4.24) and (4.25) we get

$$\frac{\sigma_{yy} - \sigma_{xx}}{2} = \frac{1}{[\Omega - (1+S_1^2)]} \left[\Omega \, \mathrm{Re} Z_2 - (1+S_1^2) \, \mathrm{Re} Z_1 \right]$$

$$+ \frac{1}{(S^2 - S_2^2)} \left[(1+S_2^2) \, \mathrm{Re} Y_2 - (1+S_1^2) \, \mathrm{Re} Y_1 \right] \qquad (4.29)$$

The first three terms in each of the series Z and Y are included in the analysis. So Z1 and Z2 can be expressed as follows:

$$Z_1 = A_0 \, z_1^{-\frac{1}{2}} + A_1 \, z_1^{\frac{1}{2}} + A_2 \, z_1^{\frac{3}{2}} \quad \text{and} \qquad (4.30)$$

$$Z_2 = A_0 \, z_2^{-\frac{1}{2}} + A_1 \, z_2^{\frac{1}{2}} + A_2 \, z_2^{\frac{3}{2}} \qquad (4.31)$$

and Y1 and Y2 can be expressed as

$$Y_1 = B_0 + B_1 z_1 + B_2 \, z_1^2 \qquad (4.32)$$

$$Y_2 = B_0 + B_1 z_2 + B_2 \, z_2^2 \qquad (4.33)$$

where $A_0\sqrt{2\pi}$ = KI, the stress intensity factor and remote stress σ_{ox} = 2Bo.

Substituting the series in (4.26) and (4.29) we can obtain expressions for $(\sigma_y - \sigma_x)/2$ and τ_{xy} in terms of the series constants and the coordinates of the point x and y. Now substituting these values in the stress optic law (equation 4.1) we get the following for the kth point in the fringe field

$$G_k(A_0, A_1, \dots B_1, B_2) = \left(\frac{\bar{N}_k f'}{2h}\right)^2 - \left(\frac{\sigma_{yy} - \sigma_{xx}}{2}\right)^2 - \tau_{xy}^2 = 0 \qquad (4.34)$$

This equation is of the same form as equation(4.10) obtained for the three parameter model and is again solved using the

25

overdeterministic approach where the x's are the unknown coefficients of the series: A0,A1,A2,B0,B1 and B2.

Both the equations -(4.10), which constitute the three parameter model, and (4.34), which constitutes the six parameter model, have been used with the overdeterministic approach to evaluate the stress intensity factors from the experimental fringe patterns.

2 METHOD OF CAUSTICS

2.1 Case Of A Stationary Crack

The physical method underlying the method of caustics also known as the method of shadow patterns is illustrated in figure 7. A loaded specimen is illuminated with light generated by a point light source. The stress intensification in the region surrounding the crack tip causes a reduction of both the thickness of the specimen and the refractive index of the material. As a consequence, the area surrounding a crack tip acts similar to a divergent lens: the light transmitted through the specimen is deflected outwards. Therefore, in the shadow image of the crack on a plane at a distance Zo behind the specimen, the crack tip appears surrounded by a dark spot called the caustic. The shadow pattern is shown schematically on the right side of the figure.

The shadow optical analysis consists of calculating the light deflections and resulting shape and size of the

shadow pattern for a given stress distribution with a given stress intensity factor. The principle of Manogg's procedure [21] which apply likewise for stationary and propagating cracks, is described below.

A light beam is considered which traverses the specimen at the point $P(r,\theta)$ in the object plane E as shown in figure 8. The non-deflected beam would pass the shadow image plane E' which is also called the reference plane, at the point Pm defining the vector $\vec{r}m$. Due to the light deflection in P, however, the beam is displaced to the point $P'(x',y')$ by a vector $\vec{w}$. $\vec{w}$ is a function of the co-ordinates r, θ of the point P. As can be seen from the figure, the vector $\vec{r'}$ of the image point P'is given as

$$\vec{r}' = \vec{r}_m + \vec{w}(r, \theta) \tag{4.35}$$

The shadow optical image is completely described by equation(4.35):For each point $P(r,\theta)$ of the object, the corresponding image point $P'(x',y')$ of the shadow image is obtained.

After passing the object, the deflected light beams envelope a shadow space (see figure 7). On the image plane which is the cross section of this space, they form a caustic. As an envelope, the caustic is a singular curve of the image equation(4.35). A necessary condition for the existence of such a singularity is that the Jacobian functional determinant J of equation(4.35) vanishes,i.e.

$$J = \frac{\partial x'}{\partial r} \frac{\partial y'}{\partial \theta} - \frac{\partial x'}{\partial \theta} \frac{\partial y}{\partial r} = 0 \tag{4.36}$$

Those points P whose co-ordinates (r, θ) fulfill the condition (4.36) are imaged on to the caustic. The caustic itself then results by inserting these points (r, θ) into the image equation(4.35).

Thus the main problem in analysing a shadow pattern is finding for the given physical problem the vectors $\vec{r}m$ and $\vec{w}$ in the image equation(4.35). The vector $\vec{r}m$ is the projection of $\vec{r}$ onto the image plane and can easily be determined. The vector $\vec{w}$, according to the theory of eikonal, is given as

$$\vec{w}(r, \theta) = z_0 \, \text{grad} \, \Delta s (r, \theta) \qquad (4.37)$$

where Δs is the change of the optical path length caused by the object and Zo is the reference distance which is defined as the distance from the object plane E to the shadow plane E' (figure 8). The path length change $\Delta s(r, \theta)$ in equation(4.37) is correlated to the stresses $\sigma(r, \theta)$ in the object by elasto-optical relations. The stresses σ at each point P near the crack tip are given by fracture mechanics equations.

Due to a tensile load, its initial thickness h and its refractive index n are reduced to h-Δh and n-Δn, respectively. Then for normally incident light, Δs is given as

$$\Delta s = (n-1) \Delta h + d \Delta n \qquad (4.38)$$

The correlation between the change Δn of the refractive index and the principal stresses $\sigma 1, \sigma 2$ and $\sigma 3$ in the plate

28

is described by Maxwell-Neumann's law:

$$\Delta n_1 = A \sigma_1 + B (\sigma_2 + \sigma_3)$$
$$\Delta n_2 = A \sigma_2 + B (\sigma_1 + \sigma_3)$$

(4.39)

$\Delta n1$ and $\Delta n2$ are the refractive index changes for the light polarized parallel to the principal stresses $\sigma 1$ and $\sigma 2$, respectively, and propagating in the direction of $\sigma 3$ and A and B are elasto-optical material constants.

For plane stress conditions $\sigma 3 = 0$ and due to Hooke's law

$$\Delta h = - \frac{\nu}{E} (\sigma_1 + \sigma_2) h$$

(4.40)

Where ν is Poisson's ratio and E is Young's modulus. Then, by using the equations(4.39), equation(4.38) becomes

$$\Delta s_1 = (a \sigma_1 + b \sigma_2) h$$
$$\Delta s_2 = (a \sigma_2 + b \sigma_1) h$$

(4.41)

with

$$a = A - (n-1) \frac{\nu}{E}$$

(4.42a)

$$b = B - (n-1) \frac{\nu}{E}$$

(4.42b)

where $\Delta s1$ and $\Delta s2$ are the path length changes for light polarized parallel to the principal srtesses $\sigma 1$ and $\sigma 2$, respectively. It can be written in a convenient form as

$$\Delta s_{1,2} = ch [\sigma_1 + \sigma_2 \pm \lambda (\sigma_1 - \sigma_2)]$$

(4.43)

where the positive (negative) sign of λ relates to $\Delta s1$ ($\Delta s2$), and

$$c = (a + b)/2 \qquad (4.44)$$

$$\lambda = (a - b)/(a + b)$$

For a crack under mode I loading conditions in linear elastic materials the stress distribution in the vicinity of the crack tip is given by Sneddon and Williams [45]:

$$\sigma_{xx} = \frac{K_1}{\sqrt{2\pi r}} \cos\frac{\theta}{2}\left(1 - \sin\frac{\theta}{2}\sin\frac{3\theta}{2}\right) + \sigma_{0x} \qquad (4.45a)$$

$$\sigma_{yy} = \frac{K_1}{\sqrt{2\pi r}} \cos\frac{\theta}{2}\left(1 + \sin\frac{\theta}{2}\sin\frac{3\theta}{2}\right) \qquad (4.45b)$$

$$\tau_{xy} = \frac{K_1}{\sqrt{2\pi r}} \cos\frac{\theta}{2}\sin\frac{\theta}{2}\cos\frac{3\theta}{2} \qquad (4.45c)$$

Now, the vector rm in figure 8 is given as

$$\vec{r}_m = m\vec{r} \qquad (4.46)$$

Where m is a scale factor. In present work parallel incident light is used, therefore m=1. Using equations (4.43) and (4.37), equation(4.35) can be written as

$$\vec{r}' = m\vec{r} + ch z_0 \, grad[\sigma_1 + \sigma_2 \pm \lambda(\sigma_1 - \sigma_2)] \qquad (4.47)$$

The principal stresses $\sigma 1, \sigma 2$ can be determined from the equations(4.45) using the relations

$$\sigma_1 + \sigma_2 = \sigma_x + \sigma_y \qquad (4.48)$$

$$\sigma_1 - \sigma_2 = \left[(\sigma_x - \sigma_y)^2 + 4\tau_{xy}^2\right]^{1/2}$$

For optically isotropic materials ($\lambda = 0$), the components x' and y' of $\vec{r}$ in the image equation(4.47) are then

$$x' = mr\cos\theta - \frac{K_1}{\sqrt{2\pi}} chz_0 r^{-3/2} \cos\frac{3\theta}{2} \qquad (4.49a)$$

$$y' = mr\sin\theta - \frac{K_1}{\sqrt{2\pi}} chz_0 r^{-3/2} \sin\frac{3\theta}{2} \qquad (4.49b)$$

with $-\pi \leq \theta \leq \pi$

The determinant condition (4.36) leads to

$$r = \left(\frac{3}{2} \frac{K_1}{\sqrt{2\pi}} \frac{1}{m} chz_0 \right)^{2/5} \equiv r_0 \qquad (4.50)$$

where ro is a constant independent of θ and it represents a circle around the crack tip called the initial circle. This circle is imaged onto the caustic. The equation for the caustic, therefore, is obtained by replacing r in the image equation(4.49) by ro:

$$x' = mr_0 \left(\cos\theta + \frac{2}{3} \cos\frac{3\theta}{2} \right) \qquad (4.51a)$$

$$y' = mr_0 \left(\sin\theta + \frac{2}{3} \sin\frac{3\theta}{2} \right) \qquad (4.51b)$$

with $-\pi \leq \theta \leq \pi$

The equations(4.51) show that only the size, but not the shape of the caustic depends on the value of ro and hence on the value of KI (equation(4.50). From the equations(4.51) the maximum caustic diameter 2y'max=D (see figure 7) can be determined. D can be written as

D=m*ro*f

where f is a constant. Inserting ro from equation(4.50) one obtains the wanted correlation between the experimentally measurable caustic diameter D and the stress intensity

31

factor KI:

$$K_I = \frac{2\sqrt{2\pi}}{3 m^{3/2} f^{5/2} |c| h z_0} D^{5/2} \qquad (4.53)$$

2.2 Case Of A Propagating Crack

For a crack propagating with a crack velocity v, the near field stress distribution is given in [46] as

$$\sigma_{xx} = \frac{K_1 \beta_1}{\sqrt{2\pi}} \left[\frac{(1 + 2s_1^2 - s_2^2)}{\sqrt{r_1}} \cos\frac{\theta_1}{2} - \frac{4 s_1 s_2}{(1 + s_2^2)\sqrt{r_2}} \cos\frac{\theta_2}{2} \right] \qquad (4.54a)$$

$$\sigma_{yy} = \frac{K_1 \beta_1}{\sqrt{2\pi}} \left[-\frac{(1 + s_2^2)}{\sqrt{r_1}} \cos\frac{\theta_1}{2} + \frac{4 s_1 s_2}{(1 + s_2^2)\sqrt{r_2}} \cos\frac{\theta_2}{2} \right] \qquad (4.54b)$$

$$\tau_{xy} = \frac{K_1 \beta_1}{\sqrt{2\pi}} \left[2s_1 \left(\frac{1}{\sqrt{r_1}} \sin\frac{\theta_1}{2} - \frac{1}{\sqrt{r_2}} \sin\frac{\theta_2}{2} \right) \right] \qquad (4.54c)$$

x,y now represents a moving co-ordinate system with its origin in the crack tip. The co-ordinates r1,θ1 and r2,θ2 are connected with this system by the relations

$$x = r_1 \cos\theta_1 = r_2 \cos\theta_2 \qquad (4.55)$$
$$y = (r_1/\alpha_1) \sin\theta_1 = (r_2/\alpha_2) \sin\theta_2$$

A computation analog to that which leads in the static case to the image equations(4.49), yields the corresponding equations for the dynamic case. These equations, which give for each point P(r,θ) in the specimen the image point P'(x',y') in the shadow image, are

$$x' = mr\cos\theta - \frac{K_1}{\sqrt{2\pi}} ch z_0 r^{-3/2} F^{-1} G_1(s_1, \theta) \tag{4.56a}$$

$$y' = mr\sin\theta - \frac{K_1}{\sqrt{2\pi}} ch z_0 r^{-3/2} F^{-1} G_2(s_1, \theta) \tag{4.56b}$$

where the abbreviations used are:

$$F = \frac{4s_1 s_2 - (1 + s_1^2)^2}{(s_1^2 - s_2^2)(1 + s_2^2)} \tag{4.57}$$

$$G_1(s_1, \theta) = \frac{-1}{\sqrt{2}} (q^{1/2} + \cos\theta)^{1/2} (q^{-1/2} - q^{-1}\cos\theta - 2q^{-3/2}\cos^2\theta) \tag{4.58a}$$

$$G_2(s_1, \theta) = \frac{1}{\sqrt{2}} (q^{1/2} + \cos\theta)^{-1/2} (s_2^2 q^{-1}\sin\theta + s_1^2 q^{-3/2}\sin 2\theta) \tag{4.58b}$$

with

$$q = (s_1^2 - 1)\sin^2\theta + 1 \tag{4.59}$$

The determinant condition(4.36) leads to a quadratic equation in $r^{-3/2}$, the solution of which has the form

$$r = \left[\frac{3}{2} \frac{K_1}{\sqrt{2\pi}} \frac{1}{m} ch z_0 F^{-1} H(s_1, \theta) \right]^{2/5} \equiv r_0^{dyn} \tag{4.60}$$

where r ,in analogy to equation(4.50), is denoted as rodyn and H is a complicated function dependent only on s1 and θ. A comparison with the analog relation(4.50) for the stationary crack shows that

$$r_0^{dyn} = F^{-2/5} H^{2/5}(s_1, \theta) r_0^{stat} \tag{4.61}$$

where ro from equation (4.50) is denoted as rostat.

F is a constant for a given crack velocity v. The function H(s1,θ) can be computed numerically [28]. When crack velocities are considered within a range typical for fracture experiments the value of $H^{2/5}$ for all angles θ

33

nearly equals one. Thus

$$\gamma_0^{dyn} = F^{-2/5} \gamma_0^{stat} \tag{4.62}$$

This means that the line which is imaged onto the caustic is practically a circle for the dynamic case also. The radius of this circle is enlarged in comparison to the static case by the factor $F^{-2/5}$.

Inserting rodyn from equation (4.61) into the image equations (4.56) yields the expression for the dynamic caustic which can be written in the form

$$x' = m \, r_0^{dyn} \left(\cos\theta + C_1(s_1, \theta) \right) \tag{4.63}$$
$$y' = m \, r_0^{stat} \left(\sin\theta + C_2(s_1, \theta) \right)$$

where C1 and C2 are functions of s1 and θ, and influence the shape of the caustic. In analogy to equation(4.52)as in the static case, and using equation (4.62) the caustic diameter 2y'max=D can be written as

$$D = m \, r_0^{dyn} f = F^{-2/5} m \, r_0^{stat} f \tag{4.64}$$

Inserting rostat from equation (4.50), one obtains the evaluation equation for the dynamic caustic

$$K_1 = \frac{2\sqrt{2\pi}}{3 \, m^{3/2} f^{5/2} |c| h z_0} F \, D^{5/2} \tag{4.65}$$

A comparison with the corresponding static evaluation formula (4.53) shows that the static formula can also be used for the evaluation of the caustic for propagating cracks, when modified with the crack velocity dependent correction factor F defined by equation (4.57). For the evaluation of caustic in static experiments relation (4.53)

34

has been used and for the dynamic case relation (4.65) has been used.

35

CHAPTER 5

EXPERIMENTAL PROCEDURE AND RESULTS

The experiments performed for this study can be categorized as follows

1.   Static Experiments

    a   Static isochromatic

    b   Static caustic

2.   Dynamic Experiments

    a   Dynamic isochromatic

    b   Dynamic caustic

These experiments are discussed below in the above order.

1.1 Static Isochromatic Experiments

A series of experiments were conducted to get a relationship between stress intensity factor and crack length for a constant load. The model geometry used in these experiments was a single edge notch specimen as shown in figure 9. The specimen dimensions were large so that the stress field from loading pins did not influence the crack tip stress field region. The width was such as to provide both the regions away from the boundary as well as close to it while the crack length was varied.   The model material was chosen to be 1/4" thick polycarbonate. This material has high photoelastic sensitivity and a high fracture

36

toughness as such many fringes could be seen even below the critical load for fracture. The cracks were made with a band saw and the crack tip was blunted with a fine jewellers round file. Blunting was important because the presence of any nicks at the crack tip can lead to local stress concentration and hence the failure of the specimen by propagation of the crack.

The model was loaded on the INSTRON testing machine. The fringes were recorded on the Polaroid Type 55 black and white land film which yielded both the negative and the print. Fringe patterns thus obtained were analysed using the multi-point method of alalysis. From these fringe plots (figure 10) 40 data points were taken and their locations with respect to the crack tip and the crack line is fed into the main analysis program through a Hitachi Hicomscan data tablet digitizer (model HDG-1216) and the value of the stress intensity factor was obtained using both the three parameter model(KI3) and the six parameter model(KI6). The three parameter model is effectively two parameter model because in these experiments mode II loading did not exist. Data was taken from a region neither too close nor too far from the crack tip with $0.1" < r < 0.5"$.

Experiments were conducted with crack length to width ratio(l/w) of 0.1,0.2,...,0.9 and for each crack length fringe patterns at four different loads were recorded. The data has been tabulated in table 1. and has been plotted in figures 11 to 28. These plots indicate the theoretical

stress intensity factor expected for loads (bold lines of the form y=Cth*x), the actual data points and the least square fits of the form y=mx, y=a+bx and y=bx are also shown. But for comparison's sake, only the fit of the form y=mx is used. Consolidated results are shown as a KI vs 1/w plot for a load of 1.0N in figure 29 and the values are listed in tables 2 and 3.

1.2 Static Caustic

Purpose of this set of experiments was to obtain similar results as for the case of static photoelasticity. The goemetry of the specimen is shown in figure 30. It is a single edge notch specimen made of 1/4" thick PMMA. The dimensions are again chosen such that proper stress conditions exist at the crack tip. PMMA is chosen because it is optically isotropic, not brittle, easy to machine and readily available. The loading frame used to load it in uniaxial tension is shown in figure 31. Load was applied using ENERPAC hydraulic cylinders and the loads were recorded by an in-line PCB model 200A quartz transducer (of Piezotronics, Inc.), used in conjunction with a 484B line power unit. The transducer had built-in ICP(Integrated circuit Piezoelectric) amplifiers.

Again, like for the isochromatic experiment, the objective was to obtain plots of stress intensity factor

against load for various values of crack length to width(l/w) ratio. But before this could be done it was necessary to ascertain that proper Zo(distance between the refrence plane and the specimen) was chosen for the experiment to obtain large enough ro. As discussed in the previous chapter, a caustic is a mapping of points forming the initial circle on the specimen. If the radius of this circle is too small and falls in the plasticity zone the results will be erroneous. The initial curve should be sufficiently large so that, at points which form the caustic, proper two-dimensional stress field conditions exist. For points closer than that 3-D field exist and the equations derived for stress intensity factor (eqn.4.53) do not hold good. To ensure this an experiment was performed to obtain the plot of K/Kth vs ro/h. The thickness, h, was choosen to normalize ro because it is the only relevent length scale. The thicker the material the longer the distance has to be from the crack tip for plane stress conditions to prevail. A crack length to width ratio of 0.5 was choosen so that the boundary effects are minimum and the crack is subjected to pure opening tensile load.

The specimen was loaded to various loads which gave different values of ro/h and for each of these Kexp/Kth was evaluated. This data, with other data obtained from experiments described next, is tabulated in table 4. The plot is given in figure 32 for a crack extending to the center of the specimen and in figure 33 data for other l/w

39

has been included. It is seen that for lower values of ro/h, (say ro/h=0.17) the experimental value is only 0.4 times the theoretical value but as the value of ro/h is increased K/Kth approaches a stable value which is close to 1.0. Above ro/h=0.38 the curve stabilizes and further increase in ro does not change the value of the ratio of experimentally evaluated stress intensity factor to the theoretical one. In all the experiments performed the value of ro/h has been kept above this value to ensure that the data points are sufficiently away from the crack tip.

For static caustic experiments the specimen was loaded to various loads(2795N to 4570N) for an initial crack length to width ratio of 0.1. For each of these pictures (figure 34) were taken and analysed to obtain the experimental stress intensity factor. The crack was then extended such that l/w became 0.2 and the procedure was repeated. This was done for all l/w ranging from 0.1,0.2,...,0.9. For analysis printing was not necessary and the measurements were taken off the negative itself by the use of an optical comparator(Micro Vu model 400). The data is given in table 5 and a plot of the theoretical curve together with the experimental plots is given in figures 35 through 43. Again as for the case of static isochromatic data various least square fits are provided and KI is plotted against l/w in figure 44. The values are listed in table 6.

2.1 Dynamic Isochromatic Experiments

Experiments with three specimen geometries were performed in an attempt to obtain a wide range of crack velocities and stress intensity factors ranging from the crack arrest value to crack branching value. Analysis was done with both three and six parameter models. Loading was such that mode II conditions did not exist and three parameter analysis was effectively two parameter analysis.

2.1.1 Single Edge Notch Experiment -

In the first experiment a single edge notch specimen was used the geometry of which is shown in figure 30. The material used is 1/2" thick Homalite 100. The specimen was cut from a section of material which did not have any casting residual stresses which could interfere with the stress field of the crack. Also, to minimize machining stresses the specimen was routed and good edges were achieved. This is an important requirement for dynamic experiments because the waves that get reflected from the boundaries can interfere with the moving crack tip. The loading for this experiment was identical to the case of static caustic experiments. The speecimen was loaded to 4.8kN which gave an initial KI, (Ko), of 1.242MPa$\sqrt{m}$. The grips were held in position (constant displacement) and then with the help of a solenoid operated knife the crack was initiated to propagate. The timings of sparks were recorded

on the oscilloscope with a high frequency response diode as described in chapter 3. The electronic circuitry was triggered by breaking the continuity of a conducting silver paint placed just below the crack. The crack length vs time plot is shown in figure 45. The velocity is constant throughout being equal to a high value of 360 m/s. The isochromatic fringes (figure 46) are analysed with both three and six parameter models by taking 60 points and the results are tabulated in table 7. The plots of KI3 and KI6 against the crack length are given in figure 47. The single edge notch specimen geometry is an increasing K geometry i.e. K increases with the crack length. As can be seen from the plot of KI vs l, such a trend does exist. KI3 starts from a value of .954MPa√m̅ and rises to a value of 1.555MPa√m̅ with slight oscillations. Whereas KI6 starts with a high value of 1.274MPa√m̅ falls to 1.038MPa√m̅ and then rises to a value of 2.064MPa√m̅. The photograph of the crack surface is shown in figure 48 which shows that surface roughness increases with the stress intensity factor.

2.1.2 <u>Double</u> <u>Cantilevered</u> <u>Beam</u> <u>Experiment</u> -

In the second experiment the specimen used was the double cantilevered beam (DCB) type. The geometry is shown in figure 49. The load is applied at the two pins so that they tend to open the crack apart. The loading arrangement is shown in figure 50. In this experiment instead of load, displacement was monitered. The specimen was loaded to a

displacement (opening increase) of 0.0442in" between the two pins and the crack was initiated using the knife. The displacement was recorded by an accurate eddy current transducer (Model KD 2300-2S of Kaman Measuring Systems) and recorded on the digital oscilloscope.

The crack-length vs time plot is shown in figure 51. The velocity is seen to decrease continuously with the crack length. This is expected because in a DCB specimen the loading is such that it tends to close the moving crack and tries to stop it (arrest it). Again the fringes obtained (figure 52) were analysed both with the three parameter and the six parameter models taking 40 data points off each pattern. The values are tabulated in table 8. The results KI3 and KI6 are plotted against crack length in figure 53. The three parameter model indicates that KI falls from $1.137MPa\sqrt{m}$ to a value of $0.510MPa\sqrt{m}$ where as the six parameter shows values from $1.299MPa\sqrt{m}$ to $0.570MPa\sqrt{m}$. In general, the values from six parameter analysis are higher than those obtained from the three parameter analysis of the same data. The fracture surface is shown in figure 54 being rough in the begining and as K decreases it becomes smooth.

2.1.3 DCB/SEN Experiment –

The third experiment was performed with a DCB/SEN geometry as shown in fig.55. Kalthoff[6] has performed experiments with T-shaped (DCB/SEN) specimens using caustics and obtained plots showing two distinct regions in the

43

K-v-curve for the two sections of the specimen. One of the reasons for choosing this geometry was to obtain similar data and compare it with Kalthoff's results. The loading is applied the same way as for the DCB specimen. The specimen was loaded to an opening displacement of 0.0704in" and the crack was then initiated. Due to this peculiar T-shaped geometry the crack velocity decreases and then increases again as can be seen from the time-crack length plot in figure 56. Typical fringes, as shown in fig.57, are analysed using both three and six parameter models with 30 point data input. The results are plotted in figure 58 and tabulated in table 9. Both of them show similar trends. $KI3$ starts from 1.111MPa$\sqrt{m}$ and falls to 0.397MPa$\sqrt{m}$ and then again rises to 0.523MPa$\sqrt{m}$ where as the corresponding values for six parameter model are 1.432, 0.414 and 0.547MPa$\sqrt{m}$. The fracture surface is shown in figure 59. In the begining it is rough and then smoothes out and does not show signs of roughening again. This is a long specimen with a complex geometry so the waves do reflect and effect the propagating crack. The crack starts moving in a straight line but later on the path becomes somewhat wavy as shown in figure 60.

2.2 Dynamic Caustic Experiment

The specimen geometry, material and the loading were the same as for the case of SEN dynamic isochromatic experiment.The purpose was to compare the results with the

ones obtained using photoelasticity, so the conditions were kept identical. The crack was again initiated at a load of 4.8kN. The experimental setup is shown in figure 3. In caustic experiment the camera is not focused on the specimen but on a reference plane away from it. For this reason the crack tip is not visible but has to be calculated by measuring the distance to the end of shadow pattern and subtracting the value k*D from it as described in [1]. D is the caustic diameter and k is a constant given in table 11. The crack length vs time plot is shown in figure 61. The velocity turns out to be 384 m/s. The values of the stress intensity factors have been calculated by the measured diameters of the shadow spots (see fig.62), using relation 4.65 and are listed in table 10. The plot of KI vs crack length is shown in fig.63. It is seen that a crack starts with a KI of 0.825MPa$\sqrt{m}$ fall slightly to 0.770Mpa$\sqrt{m}$ and then continues to rise to 1.080MPa$\sqrt{m}$. Fracture surface shown in fig.64 shows that surface roughens as the crack grows. Features are identical to the corresponding photoelasticity experiment so similar values of K were expected but the actual values obtained are much lower.

3 ERROR ANALYSIS

For the case of static experiments theoretical results are available[47] and the error is evaluated as the percentage deviation from the theoretical value

45

(%err.=(Kth-K)/Kth*100). The errors are listed in tables 2,3 and 6. But in case of dynamic experiments no such results are available to compare with and for that reason the two techniques are compared with each other. For six parameter analysis the number of coefficients necessary for an adequate representation of stress field over the data acquisition region can be estimated by examining the value of the average fringe order error which depends on the specified fringe order, the calculated fringe order and the number of data points. Typically errors less than tenth of a fringe order were obtained showing accurate results[9].

CHAPTER 6

DISCUSSION AND CONCLUSIONS

In this work the techniques of caustics and photoelasticity have been compared. The plot of the stress intensity factor as a function of crack tip velocity has been generated and compared with the existing results.

Results of the static photoelastic experiments are plotted in figures 11 to 28 and the overall extracted information is given in tables 2 and 3. Some interesting observations can be made from the values obtained. Six parameter analysis(KI6) of the data consistently gives higher estimates of the stress intensity factor as compared to the values obtained from the three parameter analysis(KI3). The values of KI6 are more closer to the theoretical solution. A plot of Kth, KI6 and KI3 vs l/w ratio for a given load shown in figure 29 indicates that for six parameter analysis errors are small(table 2) being -8.55% for l/w=0.1, it decreases to lessthan 2% for l/w between 0.3 and 0.5 and than again increases as the crack goes close to the boundary being 11.13% for l/w=0.9. For 3 parameter analysis errors are always larger(table 3). The estimated values are much less than the theoretical one. The error is about 11% for l/w=0.1, it decreases to about 10% for l/w=0.3 and then keeps increasing to 24% when l/w reaches 0.9. From these it can be concluded in the cases

where mode II loading does not exist six parameter analysis gives results closer to the theoretical results.

In case of caustics it is necessary that initial curve lie in a region where plane stress conditions exist. To find the region a plot of K/Kth against ro/h is generated (figure 32) for a crack length to width ratio of 0.5. From this plot it is seen that when ro is less than 0.38h the experimental value is considerably lower than the theoretical value. As ro is increased the value of K/Kth increases and finally stabilizes at a value of 0.96. So for caustic experiments with plexiglas the value of ro/h should be greater than this value to ensure consistent and accurate results. Recently, Rosakis and Ravi Chander[33] also conducted a similar experiment with varying thickness of the specimen and obtained similar results. Interesting results can be seen when data for other l/w ratio (different from 0.5) is also included (fig. 33). The value of K/Kth is seen to stabilize at a different value being about 0.865 for l/w=0.7 and 1.040 for l/w=0.2.

The results of the static caustic experiment set are presented in table 6 and plotted in figures 35 to 43. Percentage error (see table) is very low for l/w=0.1, increases to a value of about 15%(-ve) then it changes sign and goes to about 13% for l/w=0.7 and again decreases to 2% for l/w=0.9. Caustic is the black spot surrounded by a bright light region and the diameter which should be used is the outer diameter of the dark spot,as also required by

theoretical considerations, and not the center of the bright region as suggested by some investigators[1], which gives higher values. A plot of the theoretical value of K and the experimental value obtained through the method of caustics against the l/w ratio given in figure 44 better shows the results discussed above. The values obtained from caustics are closer to the theoretical value when compared with the three parameter analysis for isochromatic fringes. Six parameter photoelastic analysis gives better results than caustics. None of the techniques give exact results in the whole range of crack locations.

For the dynamic Photoelastic experiment with the single edge notch specimen it is seen that the stress intensity factor increases with the crack length. Six parameter values are considerably higher than the three parameter values. There is scatter in the data partially because of the errors in locating the crack tip and the fringes and partially because of the waves that get reflected from the boundaries.

In case of DCB specimens the geometry and loading is such that K decreases as the crack progresses. It is noticed that the volocity also decreases from a starting value of 370 m/s to 180 m/s. On the K-v plot this gives points in between the stem and the plateau region (figs.67,68). Decreasing KI is also reflected by the shrinking fringe size in fig.52. Seeing the fracture surface(figure 54) it is concluded that roughness increases

with the K value. If the stress intensity factor is very low for a moving crack the surface formed is extremely smooth and shining.

DCB/SEN experiment data shows a decrease and then an increase in the K value as does the crack velocity which falls from 364m/s to 136m/s and then rises to 200m/s. KI6 falls from 1.432 to 0.414 and then rises to 0.547MPa$\sqrt{m}$. Again because of the reflected waves there is not a continuous drop in the K value but it shows a tendency to increase in between. From the sequence of photographs (fig.57) it can be seen that the fringes change in shape, size and tilt. Size of the fringes decrease and in the last picture increases again signifying an increase in KI. In the DCB section and in the beginning of the SEN section of the specimen the fringes are leaning backward, but in the last picture the lean is forward. The lean is related to remote parallel stress, σox[18]. Thus the fringes indicate that σox changes sign as crack propagates across the specimen. In general, six parameter K values are higher than the three parameter values. Rough fracture surface in the beginning is seen to smoothen out as the crack moved through the specimen. The waviness in the crack path is seen to be due to the unsymmetry in the existing stress fields around the crack tip as can be seen in the fourth and fifth photographs of fig.57.

Dynamic caustic experiment showed considerable scatter in crack tip location-time data. The crack tip cannot be

seen directly in the photograph and has to be evaluated from theoretical relations[1]. This has been found to be a disadvantage of caustics over isochromatic method when velocity is not known apriori and the effect of slight changes in velocity are to be studied. The SEN experiment with photoelasticity and caustics were conducted under identical conditions and the results are compared. The K vs crack length plots are given together in fig.65. It is observed that the caustic values follow the same trend as the KI6 values but the numerical values are significantly lower, for instance, at a crack length of 100mm KI6 is $1.264MPa\sqrt{m}$, KI3 is $1.154MPa\sqrt{m}$ where as the value obtained from caustics is only $0.878MPa\sqrt{m}$. The rate of rise in K value is not as steep as for the case of KI6 when the crack approaches the boundary. A possible explanation is that caustic analysis takes only the first term of stress field series as compared to six terms in case of six parameter analysis.

The purpose of generating the K-v plot for Homalite-100 was to compare it with the existing results shown in fig.1 and in fig.66. A plot of K vs v for the values KI3 and KI6 given in fig.67 and fig.68 shows that at lower velocities the points of both DCB and DCB/SEN experiments merge and form the stem region of the curve but as the velocity rises the two separate (fig.67) with DCB values being higher than that for DCB/SEN. In the stable part of the curve(the plateau region) SEN data falls at an

51

intermediate velocity. This is similar to the results shown in fig.1 where R-DCB values are above the SEN values. The value of stress intensity factor corresponding to the stem(KIm) is 0.414MPa$\sqrt{m}$ from three parameter analysis whereas from six parameter analysis it has a higher value of 0.476MPa$\sqrt{m}$. These values match well with the values obtained by other investigators for a ring specimen of Homalite-100[48]. From the split in the plateau region it can be concluded that K does depend upon the specimen geometry at higher velocities while the stem is independent. But the split observed by Kalthoff[6] is not seen. The DCB and SEN section data of the DCB/SEN specimen did not fall on separate curves. Also the difference in the values of K was not as large for the three geometries as observed by Kalthoff.

It can be seen that there is little data in the low velocity-low K region. More experiment should be done preferably around crack arrest and crack branching values of K. Caustics experiments with DCB and DCB/SEN specimen cannot be performed with the existing set up of transmitted light caustic because of space limitations which restrict the ro/h value attainable at lower K values and so reflected light caustic is recommended.

REFERENCES

1. Beinert,J. and Kalthoff,J.F., "Experimental determination of dynamic stress intensity factors by shadow patterns", Mechanics of Fracture, vol VII, G.C.Sih,ed., Noordhoff Int. Publishing, London, The Netherlands, 1981.

2. Dally,J.W. and Riley,W.F., "Experimental Stress Analysis", McGraw-Hill, (1978).

3. Broek,D., "Elementary Engineering Fracture Mechanics", Marinus Nijhoff Publishers, 1982.

4. Collins,J.A., "Failure of Materials in Mechanical Designs", Wiley Intersciences Publications.

5. Irwin,G.R., Dally,J.W, Kobayashi,T., Fourney,W.L., Etheridge,M.J. and Rossmanith,H.P., "On he Determination of the a-K Relaionship for Birefringent Polymers", Experimental Mechanics, vol. 19, No. 4, 121-128, April 1979.

6. Kalthoff,J.F., "On some Current problems in Experimental Fracture Dynamics"

7. Kobayashi,A.S. and Mall,S., "Dynamic Fracture Toughness of Homalite-100", Experimental Mechanics, 18(1978) 11-18.

8. Dally,J.W., Kobayashi,T. and Fourney,W.L., "Influences of Specimen Geometry on Crack Propagation and Arrest Behaviour", VIth Intl. Conf. Exptl. Stress Analysis, Society for Exptl. Stress Analysis, Munich, West Germany, Sept. 18-22, 1978.

9. Sanford,R.J., Chona,R., Fourney,W.L. and Irwin,G.R., "A Photoelastic Study of the Influence of Non-singular Stresses in Fracture Test Specimens", Univ. of Maryland Report, p.1, Aug.1981.

10. Post,D., "Photoelasitc Stress Analysis for an Edge Crack in a Tensile Field", Proc. of SESA, 12(1), 99-116(1954).

11. Wells,A. and Post,D, "The Dynamic Stress Distribution Surrounding a Running Crack- A Photoelasic Analysis", Proc. of SESA, 16(1), 69-92(1958).

12. Irwin,G.R., "Discussion of Wells and Post Paper (in Proc. of SESA, 16(1)), Proc. of SESA, 16(1), 93-96(1958).

13. Etheridge,J.M. and Dally,J.W., "A Critical Review of Methods for Determining Stress Intensity Factors from Isochromatic Fringes", Exptl. Mech., 17(7), 248-254 (1977).

14. Bradley,W.B. and Kobayashi,A.S., "An Investigaion of Propagating Crack by Dynamic Photoelasicity", Exptl. Mech., 10(3), 106-113 (1970).

15. Schroedl,M.A. and Smith,C.W., "Local Stresses near Deep Surface Flaws Under Cylindrical Bending Fields", Progress in Flaw Growth and Fracture Toughness Testing, ASTM STP 536, pp.45-63 (1973).

16. Etheridge,J.M. and Dally,J.W., "A Three Parameter Method for Determining Stress Intensity Factor from Isochromatic Fringe Loops", J. Strain Analysis, 13(2), 91-94 (1978).

17. Sanford,R.J. and Dally,J.W., "A General Method for Determining Mixed-mode Stress Intensity Factor from Isochromatic Fringe Patterns, J. of Engr. Fract. Mech., 11,621-633 (1979).

18. Kobayashi,A.S. and Ramulu,M., "Dynamic Stress Intensity Factors for Unsymmetric Dynamic Isochromatics", Exptl. Mech., vol.21, No.1, Jan 1981, 1141-1148.

19. Irwin,G.R., "Series Representation of the Stress Field Around Constant Speed Cracks", Univ. of Maryland Lecture Notes, 1980.

20. Atluri,S.N. and Nishioka,T., Engr. Fract. Vol. 18, No.1, pp1-22, (1983).

21. Manogg,P., "Anwendung der Schattenoptik zur Untersuchung des Zerreissvorgangs von Platten", Dissertation, Freiburg, Germany (1964).

22. Manogg,P., "Investigation of the rupture of a Plexiglas Plate by means of an Optical Method Involving High-speed Filming of the Shadows Originating Around Holes Drilling in the Plate", Intl. J. Frac. Mech., 2,pp 604-613 (1966).

23. Theocaris,P.S., "Local Yielding Around a Crack Tip in Plexiglas", J. Appl. Mech., 37 ,509-514, (1970).

24. Theocaris,P.S., "Caustics for the Determination of Singularities in Cracked Plates", Proc. IUT Symposium on Optical Methods in Mechanics of Solids, Univ. of Poitires, (1979).

25. Theocaris,P.S. and Gdoutos,E.E., "Verification of the Validity of the Dugdale-Barenblatt Model by the Method of Caustics", Engr. Frac. Mech., vol.6, pp 523-535,(1974).

26. Theocaris,P.S. and Gdoutos,E.E., "The Modified Dugdale-Barenblatt Model Adapted to Various Fracture Configurations in Metals", Intl. J. Frac., vol 10, pp 549-564, (1974).

27. Rosakis,A.J., Duffy,J. and Freund,L.B., "Experimental Study of the Dynamic Crack Propagation Resistance of a Structured Steel by the Optical Method of Caustics"

28. Beinert,J., Kalthoff,J.F. and Maier,M., "Neuere Ergebnesse zur Anwendung des Schatten-fleckverfahrens auf stehende und Schnellaufende Bruche", VIth Intl. Conf. Expt. Stress Analysis, VDI Nr.313, 791-798 (1978).

29. Rosakis,A.J., "Analysis of the Optical Method of Caustics for Dynamic Crack Propagation", Report ONR-79-1 Division of Engineering Brown Univ., Mar.1979, Engineerring Fracture Mech., vol.13, pp.331-347, (1980).

30. Rossmanith,H.P., "Determination of Stress Intensity Factors by the Dynamic Method of Caustics for Optically Isotropic Materials", Ingenieur Archiv, 362-381, 48(1979)

31. Kalthoff,J.F., Beinert,J. and Winkler,S., "Influence of Dynamic Effects on Crack Arrest", EPRI 1022-1, First Semi-annual Progress Report, Report V9/78, Institut fur Festkopermechanik, Freiburg, Germany, Aug (1978).

32. Rossmanith,H.P., "General Mode-1 Caustic Evaluation for Optically Anisotropic Materials", Ingenieur-Archiv, 73-83, 50(1981).

33. Rosakis,A.J. and Ravi Chander,K., "On Crack Tip Stress State: An Experimental Evaluation of Three Dimensional Effects", Caltech Report, SM84-2, March 1984.

34. Rosakis,A.J. and Freund,L.B., "The Effect of Crack Tip Plasticity on the Determination of Dynamic Stress Intensity Factors by the Optical Method of Caustics", Trans. of the ASME, J. Appl. Mech., vol.48, pp.302-308, June 1981.

35. Phillips,J.W. and Sanford,R.J., "Effect of Higher-order Stress Terms on Mode-1 Caustics in Birefringent Materials", Special Technical Publication 743, ASTM.

36. Irwin,G.R., Dally,J.W. and Fourney,W.L., "On the Uniqueness of the Stress Intensity Factor-Crack Velocity Relationship", To be published.

37. Dally,J.W., "Dynamic Photoelastic Studies of Fracture", Expt. Mech., vol.19, No.10, pp.349-361, Oct(1979).

38. Rossmanith,H.P. and Irwin,G.R., "Analysis of Dynamic Isochromatic Crack Tip Stress Patterns", Univ. of Maryland Report.

39. Kobayashi,A.S. et al., "Crack Branching in Homalite-100 Sheets", Engr. Frac. Mech., vol.6, pp.81-92, (1974).

40. Yoffe,E.H., "The Moving Griffith Crack", Philosophical Magazine, Series 7, 42,739(1951).

41. Shockey,D.A., Kalthoff,J.F., Klemm,W. and Winkler,S., "Simultaneous Measurements of Stress Intensity and Toughness for Fast Running Cracks in Steel", Expt. Mech. Vol.23, No.2, June 1983.

42. Ravi-Chander,K. and Knauss,W.G., "Process Controlling the Dynamic Fracture of Brittle Solids", Workshop on Dynamic Fracture, Calif. Inst. of Tech., pp.119-128, Feb.(1983).

43. Cranz,C. and Schardin,H., Zeits.f.Phys., 56, 147-83, (1929).

44. Shukla,A., "Crack Propagation in Ring Type Fracture Specimens", M.S.Thesis, Univ. of Maryland, p.50, (1978).

45. Williams,M.L., "On the Stress Distribution at the Base of a Stationary Crack", J.Appl. Mech., 24, pp.109-114(1957).

46. Rice,J.R., "Mathematical Analysis in the Mechanics of Fracture", Fracture, ed. Liebowitz,H., Academic press, NY-London, pp235-238(1968).

47. Tada,Irwin,G.R. and Paris, "The Stress Analysis of Cracks Handbook", Del Research Corporation, 1973.

48. Chona,R., Fourney,W.L., Sanford,R.J. and Shukla,A., "Determining Stress Intensity Factor for Running Cracks", Proc. of CFC10, "Modeling Problems in Crack Tip Mechanics", at Univ. of Waterloo, Aug.24-26,1983.
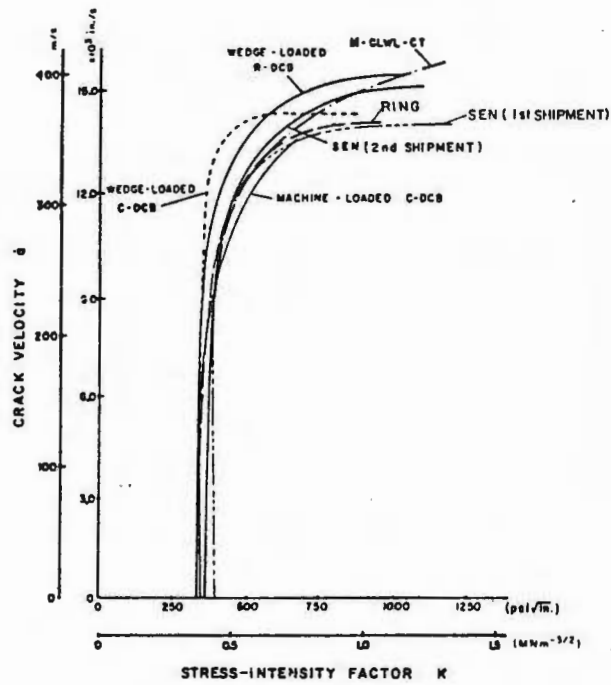
Fig.1. K-v curves for several different types of
fracture specimens.(from[5]).
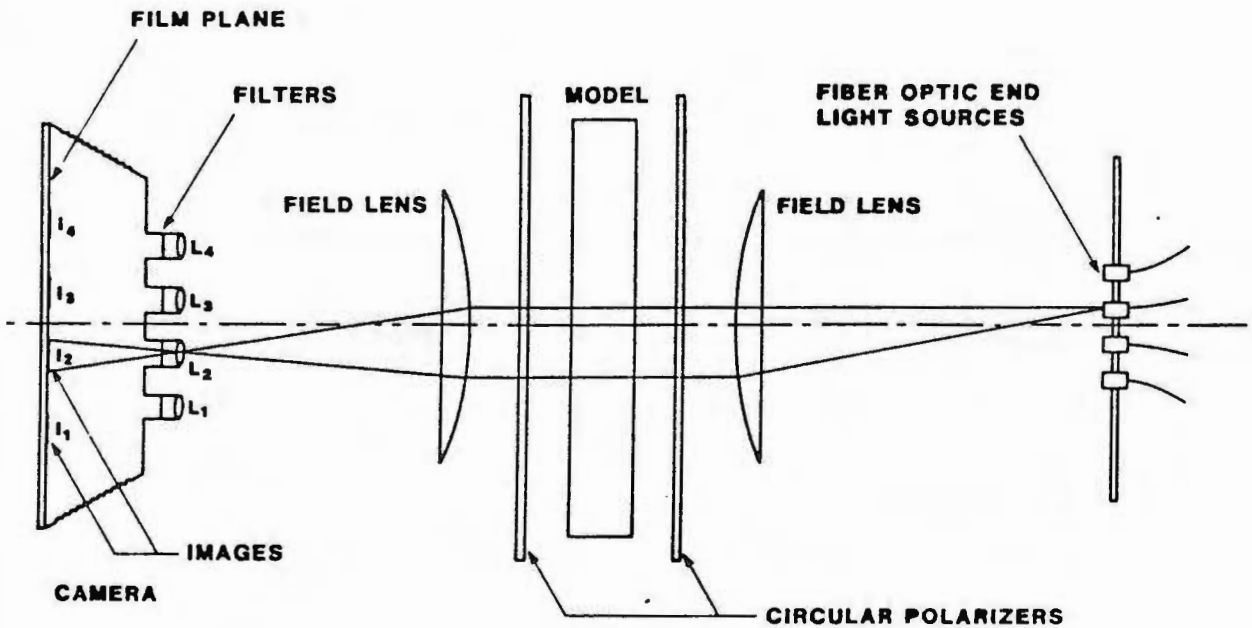
Fig.2. Optical arrangement of the camera for obtaining
isochromatics.

57
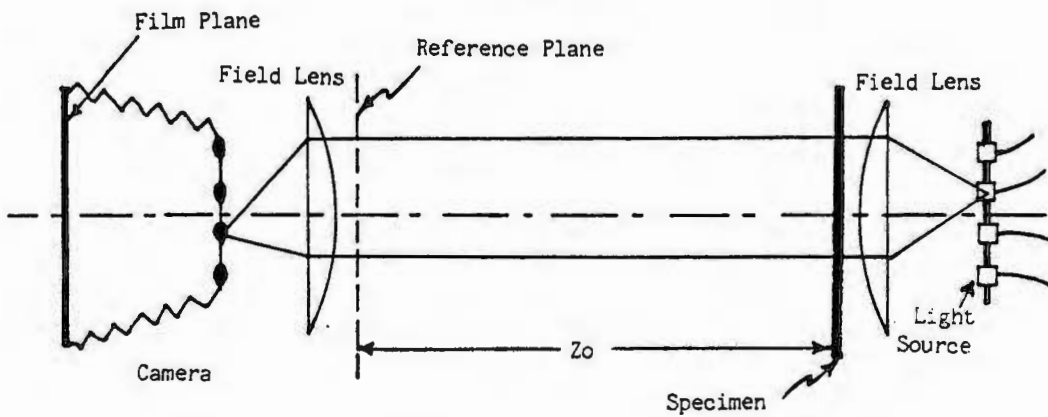
Fig.3. Optical arrangement of the camera for obtaining caustics.
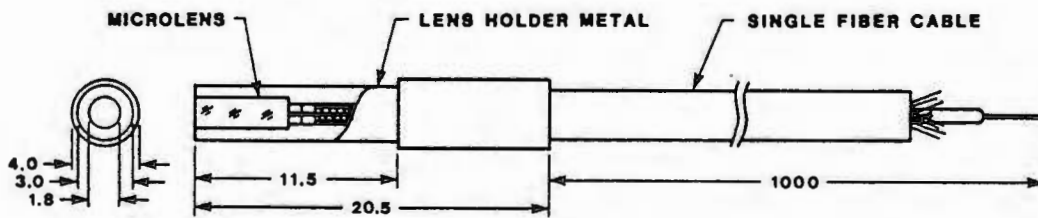
ALL DIMENSIONS IN mm

Fig.4. Physical characteristics of the optical fiber used for caustics.

PULSING CIRCUIT
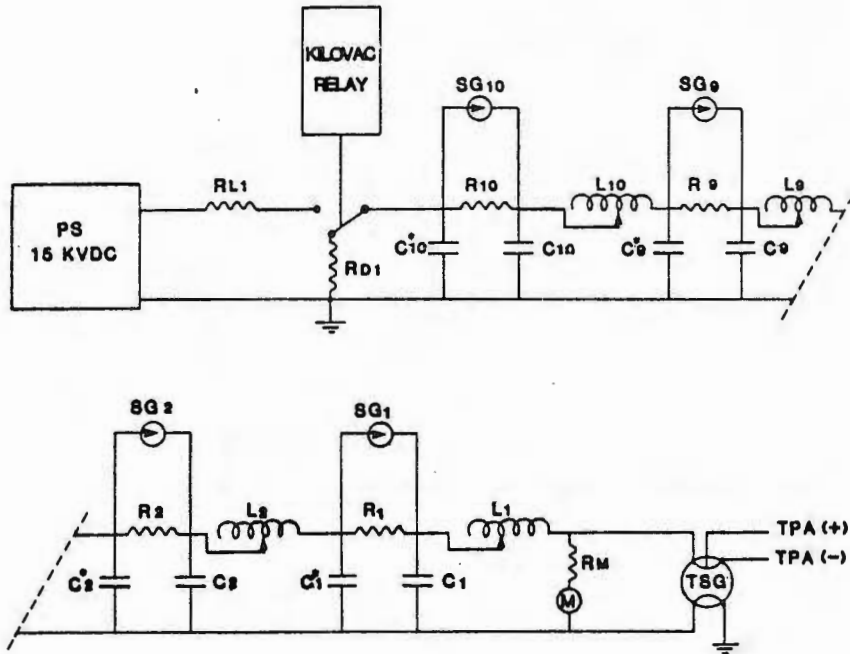
RL1	LOAD RESISTOR 3MΩ 24 Watts
RD1	DUMP RESISTOR 1MΩ, 16 Watts
C1 – C10	CAPACITORS 0.05μF, 20 KVDC
C*1 – C*10	
L1 – L10	INDUCTORS
SG1 – SG10	SPARK GAPS
RM	METER RESISTOR 400MΩ
M	METER 0–50μA
TSG	TRIGGER SPARK GAP
R – R10	BLEED RESISTORS 2MΩ

Fig.5. Pulsing circuit of the camera.

59
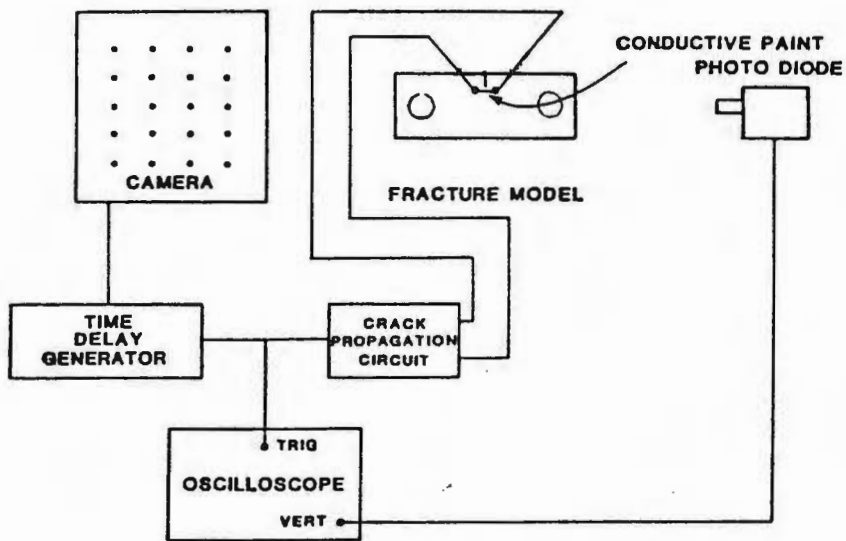
Fig.6. Schematic diagram for the synchronization
        circuit.
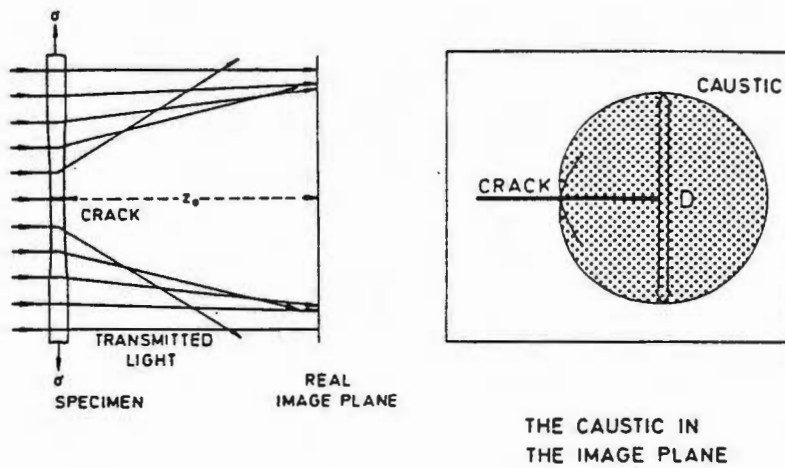
Fig.7. The principle of the method of shadow
        patterns.(from[1]).

60
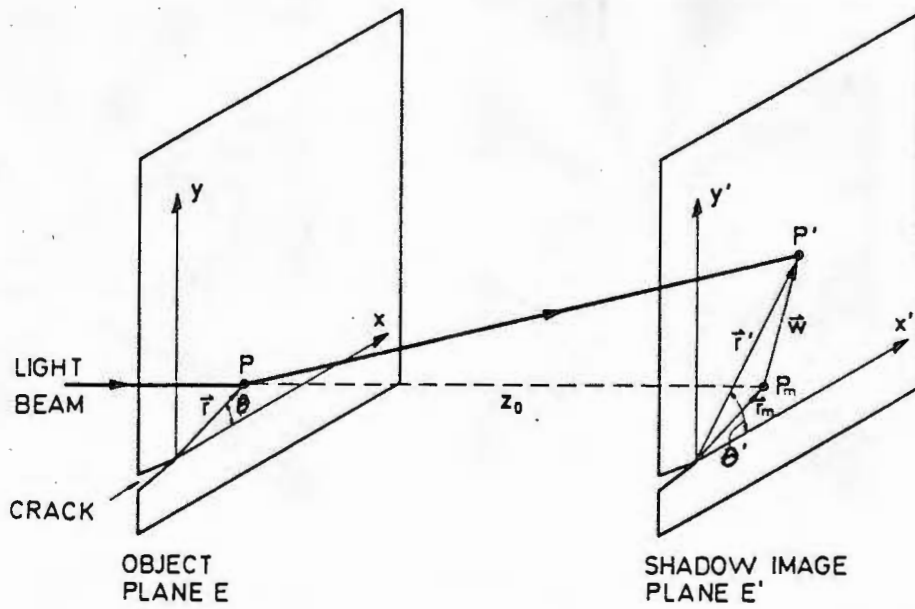
Fig.8. Geometrical conditions of the shadow optical analysis.(from[1]).
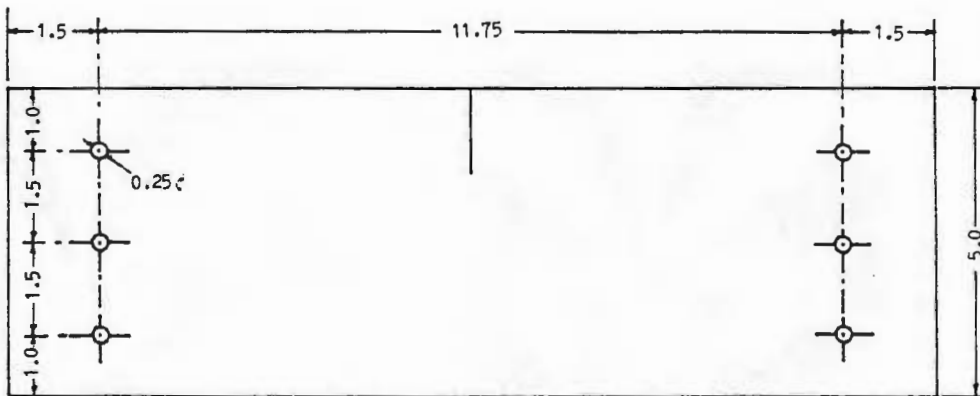
ALL DIMENSIONS IN INCHES

Fig.9. Geometry of the specimen used for photoelastic experiments.
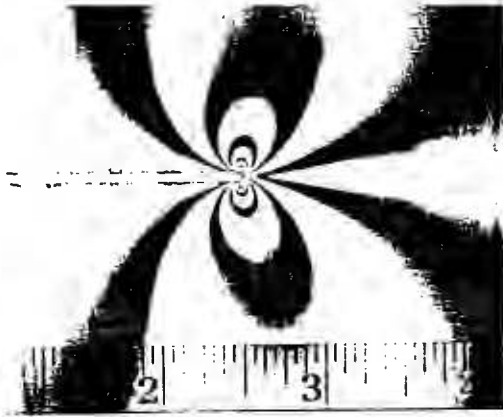
P=289N
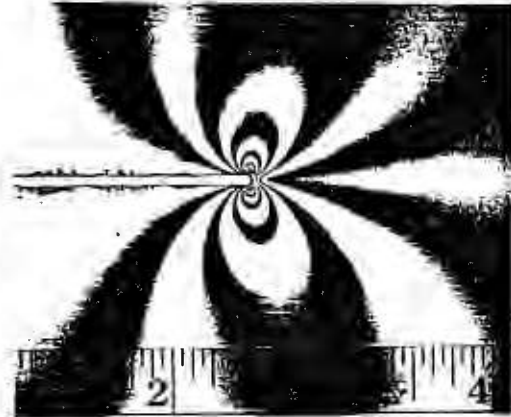
P=360N
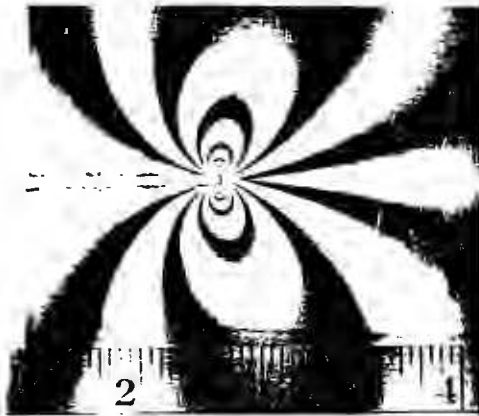
P=403N
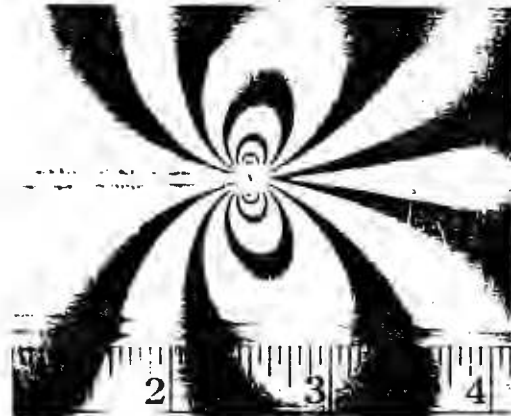
P=445N

Fig.10. A typical set of photographs from static photoelastic experiments.(l/w=0.5)
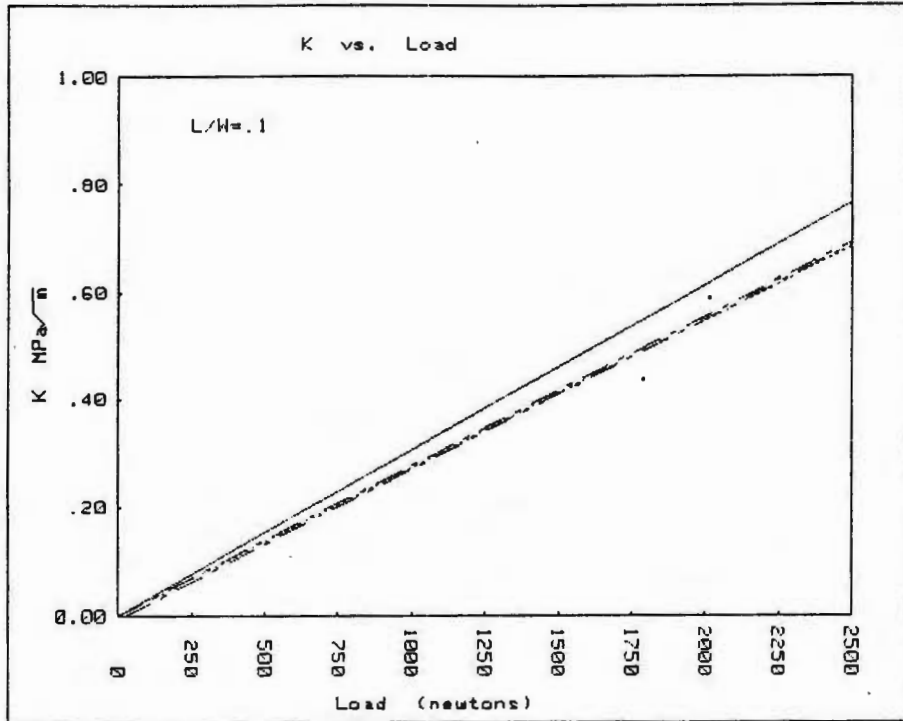
Fig.11.   KI3 vs P plot with l/w=0.1.(stat. iso. expt.)
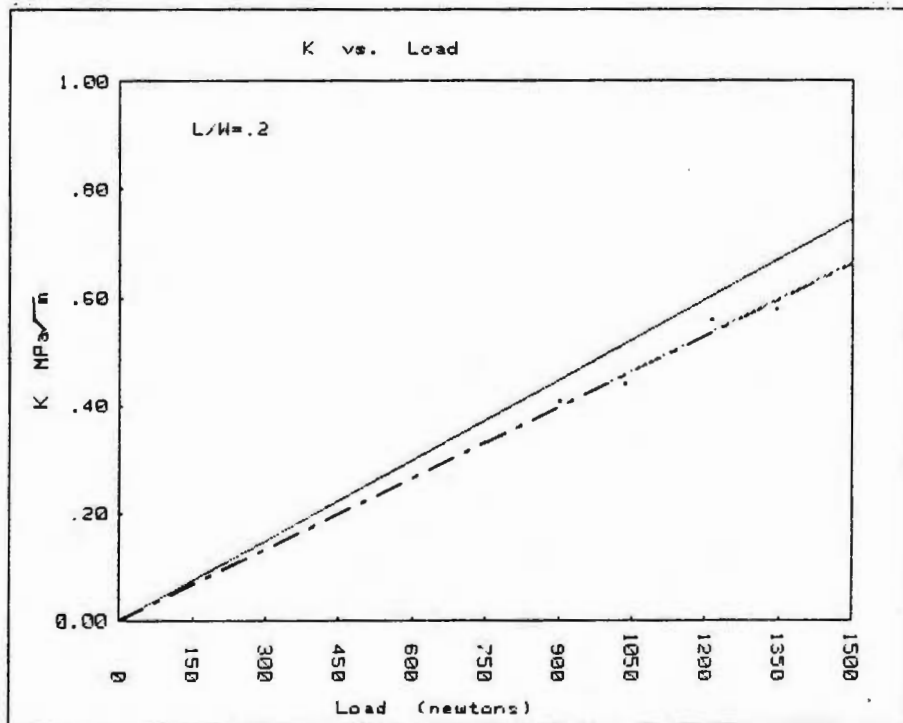
Fig.12.   KI3 vs P plot with l/w=0.2.(stat. iso. expt.)
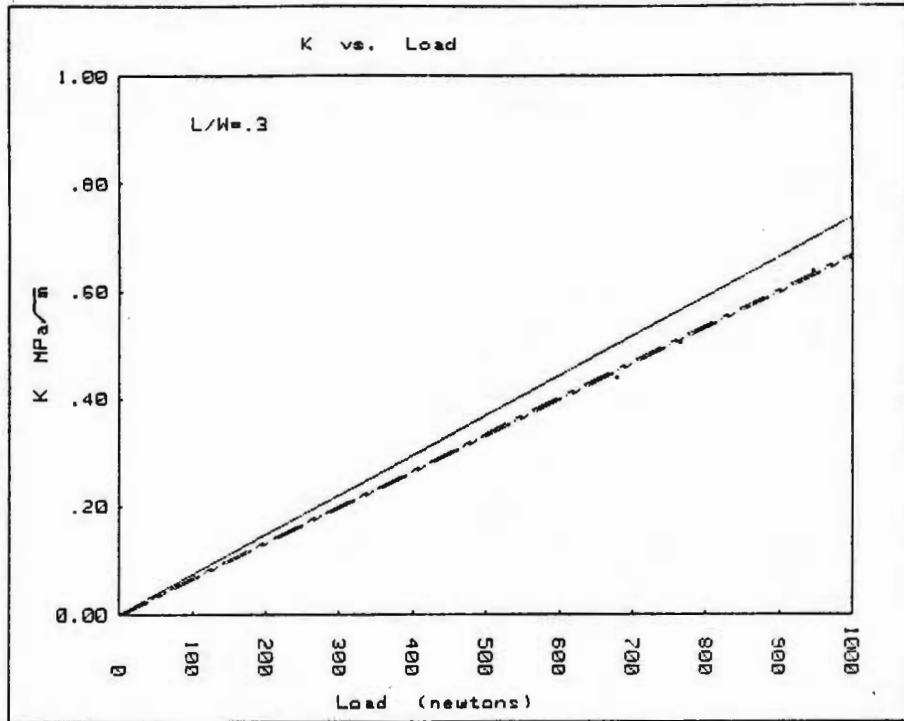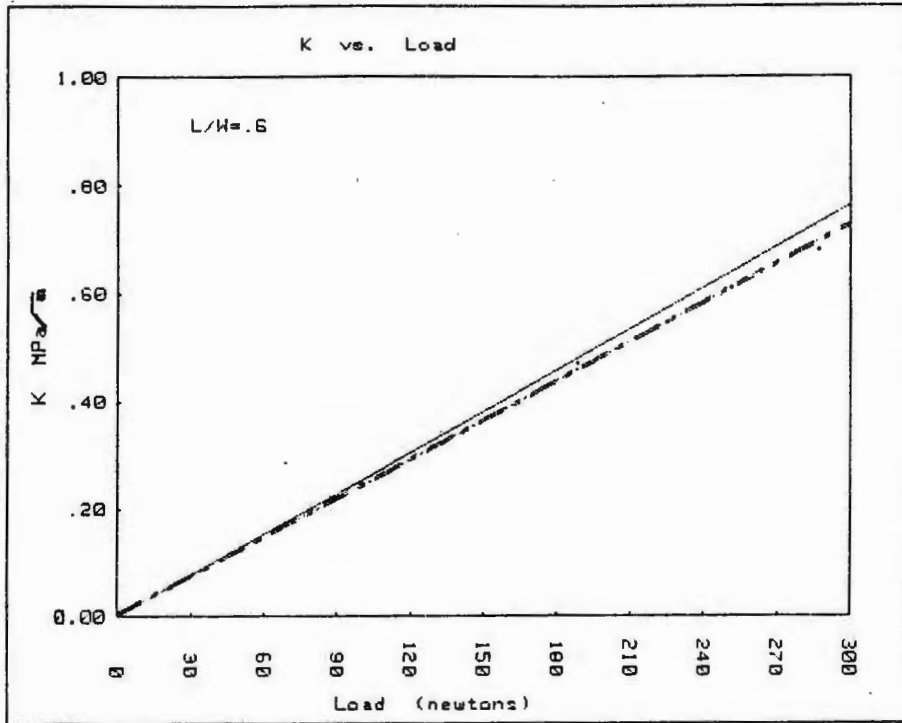
Fig.13. KI3 vs P plot with l/w=0.3.(stat. iso. expt.)
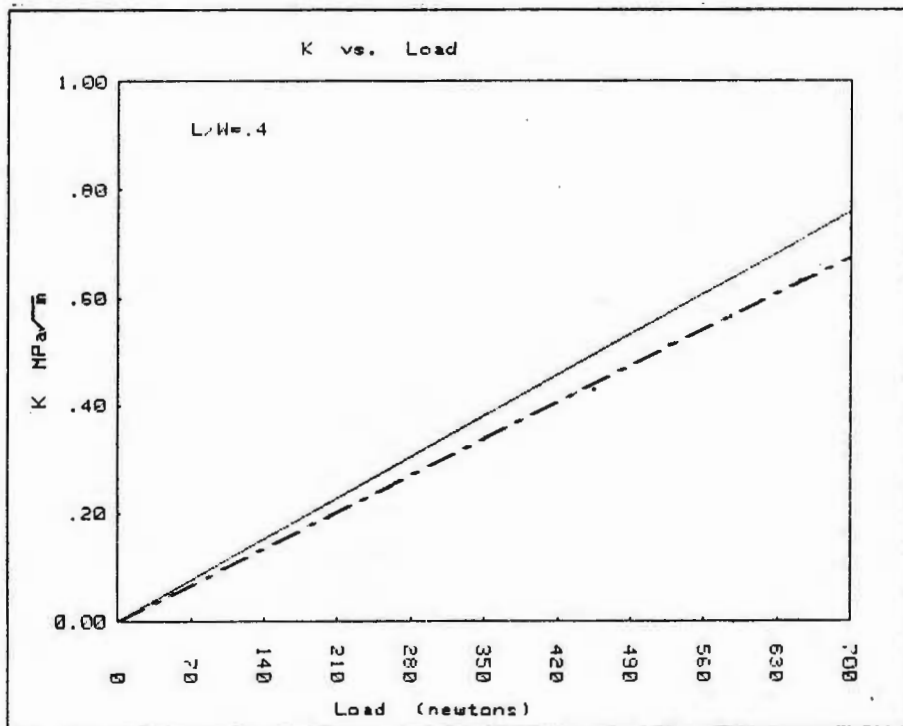
Fig.14. KI3 vs P plot with l/w=0.4.(stat. iso. expt.)

64
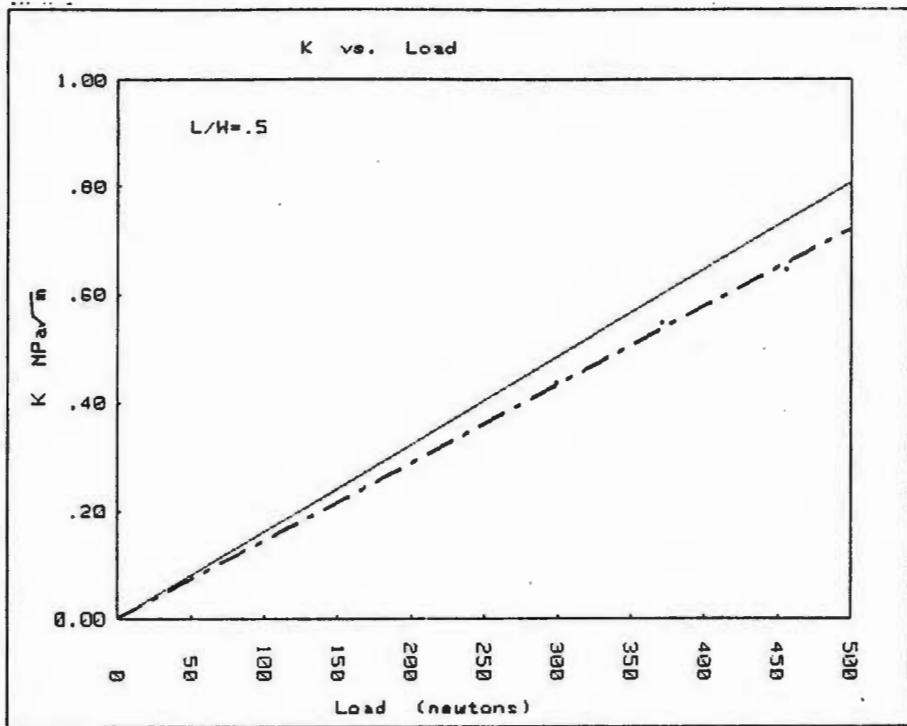
Fig.15. KI3 vs P plot with l/w=0.5.(stat. iso. expt.)
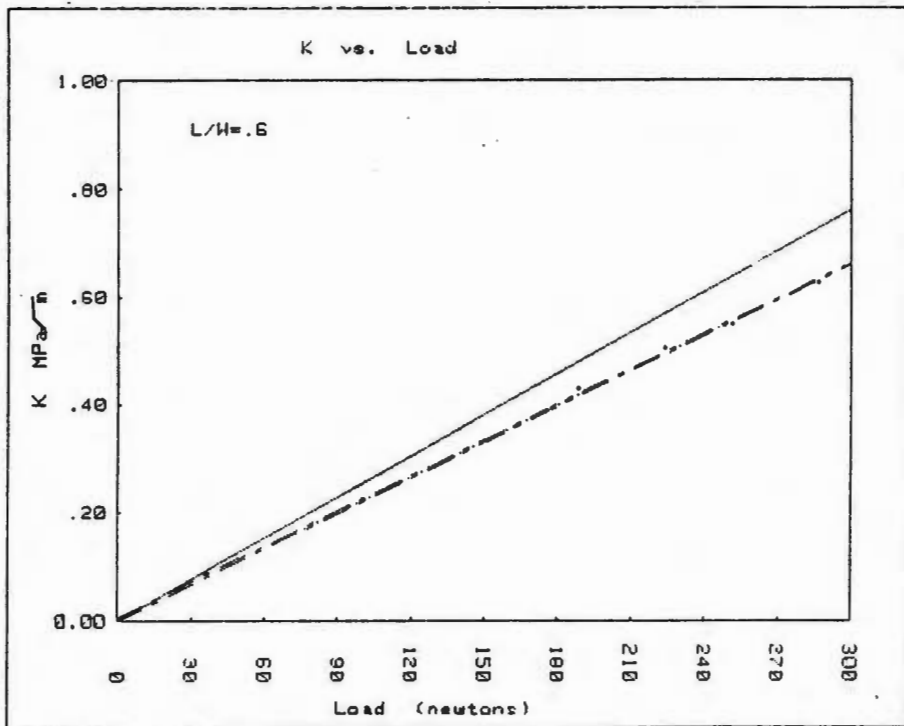
Fig.16. KI3 vs P plot with l/w=0.6.(stat. iso. expt.)

65
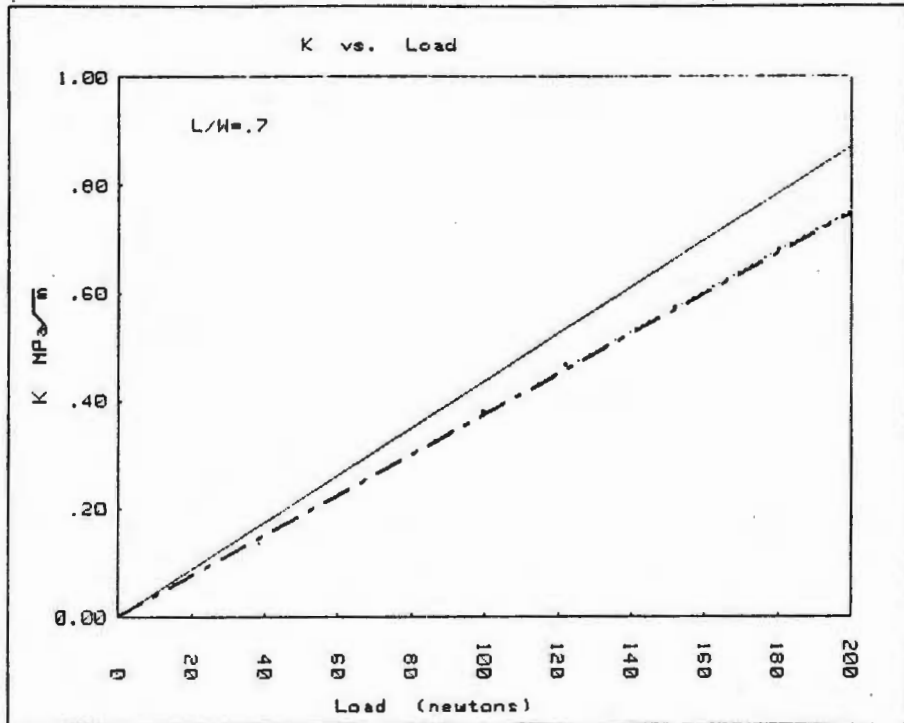
Fig.17. KI3 vs P plot with l/w=0.7.(stat. iso. expt.)
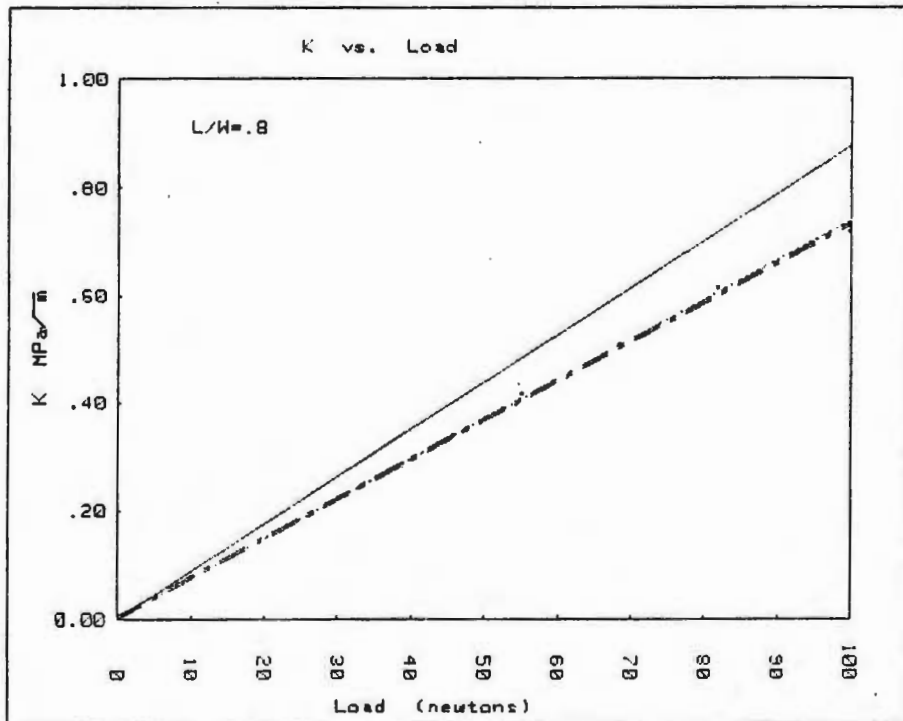
Fig.18. KI3 vs P plot with l/w=0.8.(stat. iso. expt.)
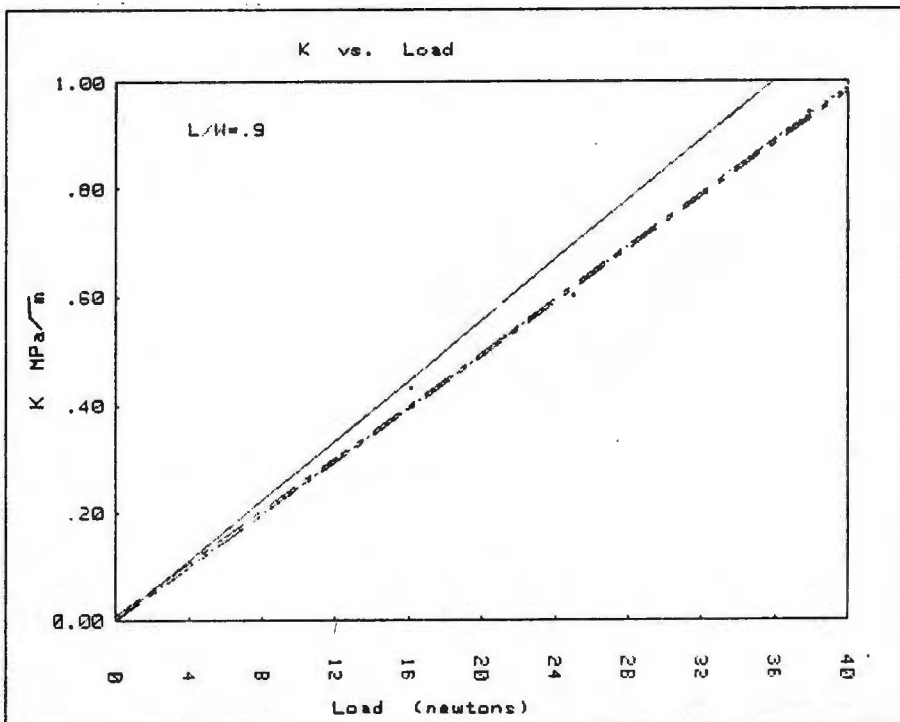
66
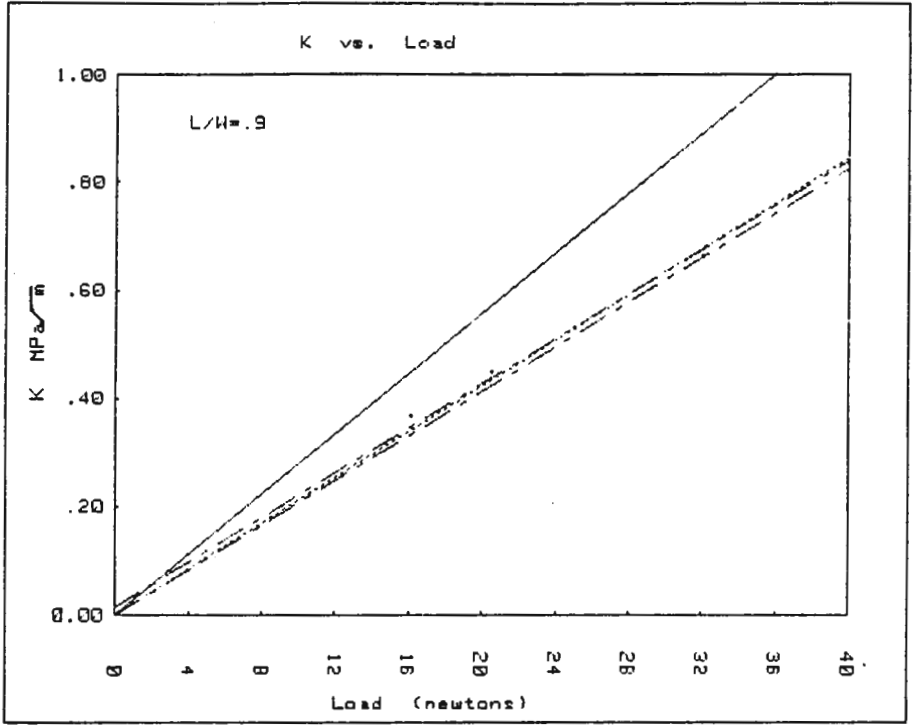
Fig.19. KI3 vs P plot with l/w=0.9.(stat. iso. expt.)
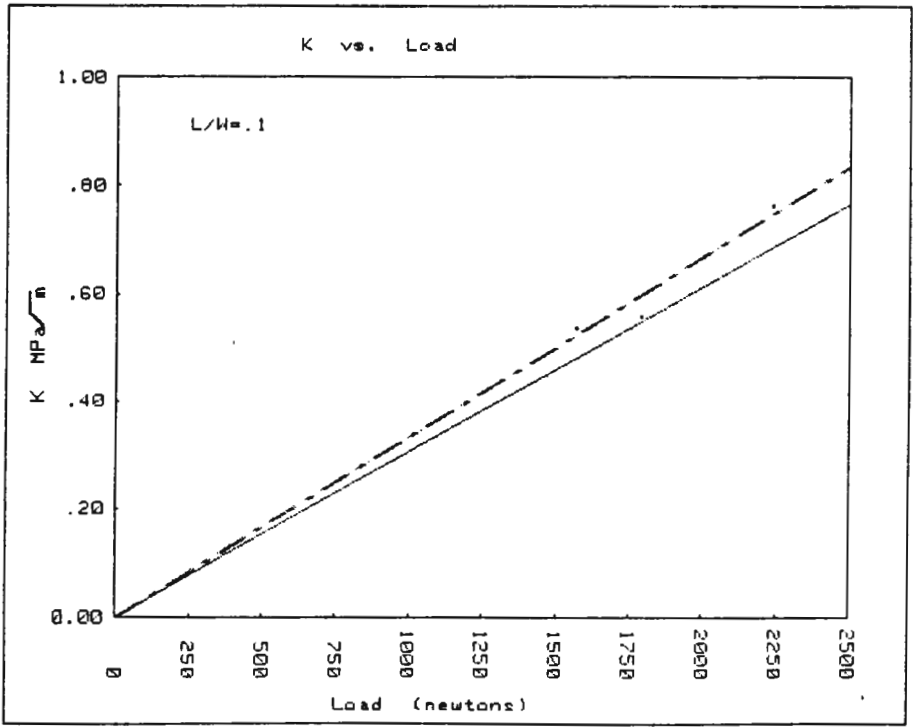
Fig.20. KI6 vs P plot with l/w=0.1.(stat. iso. expt.)
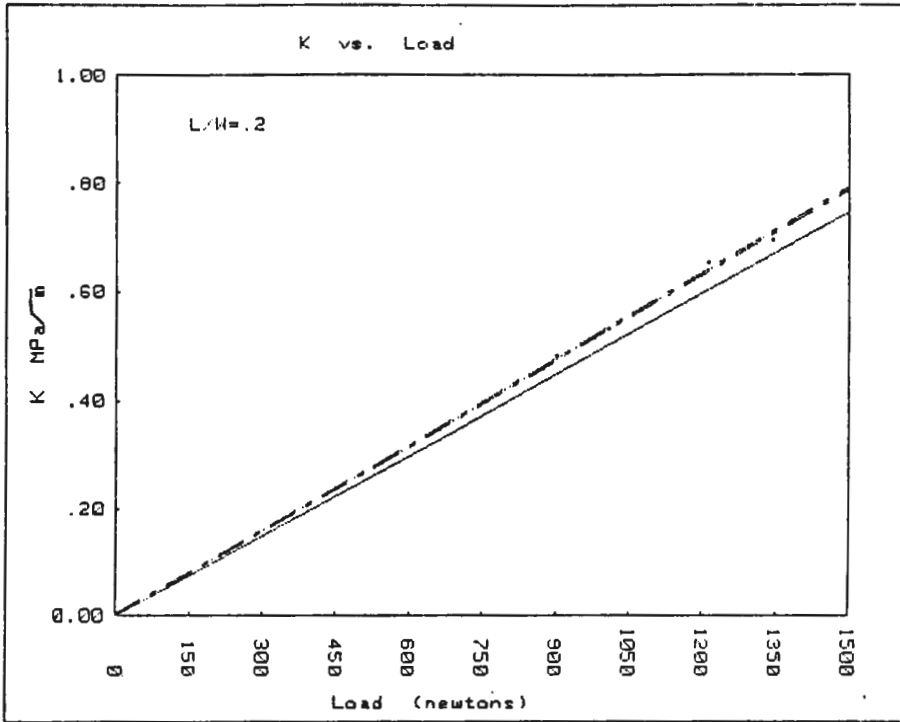
Fig.21. KI6 vs P plot with l/w=0.2.(stat. iso. expt.)
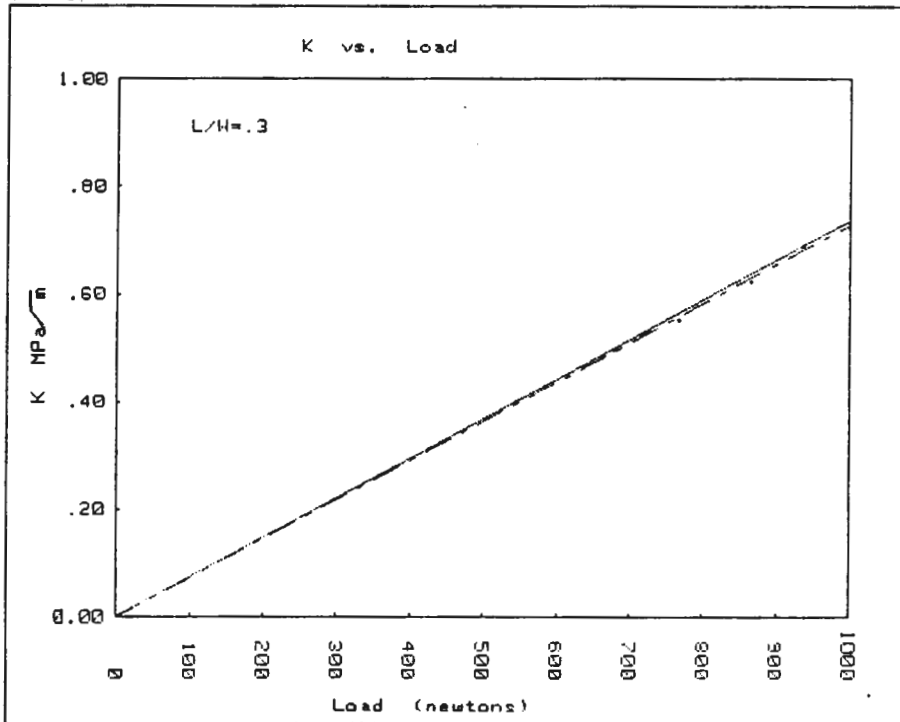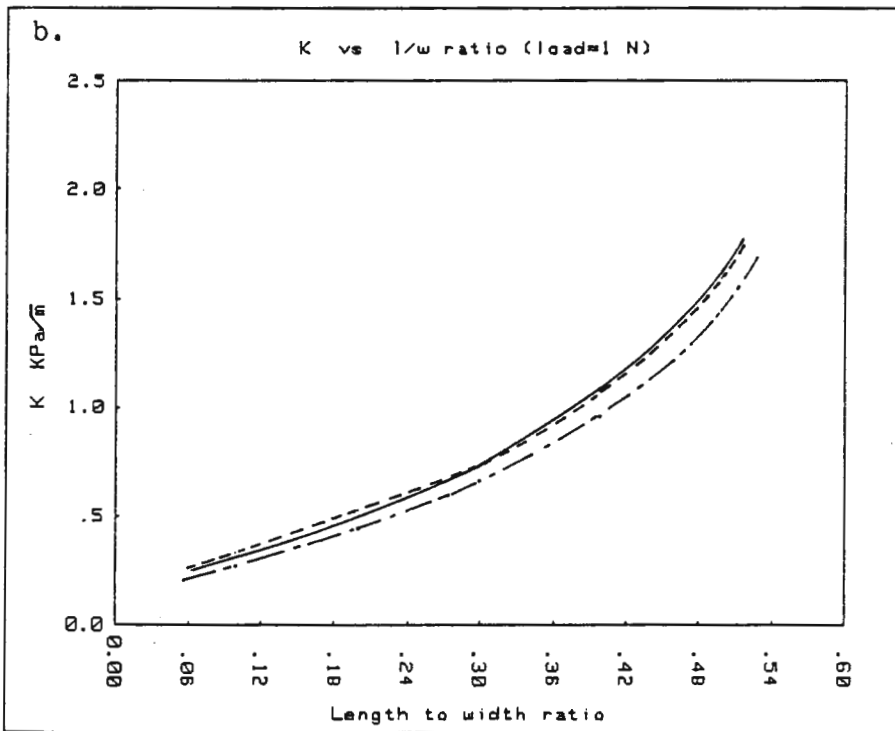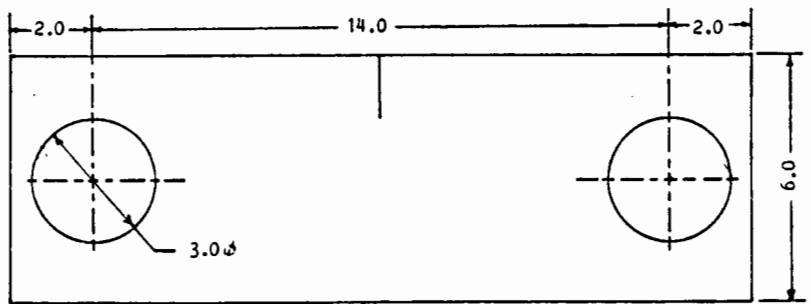

Fig.22. KI6 vs P plot with l/w=0.3.(stat. iso. expt.)

68
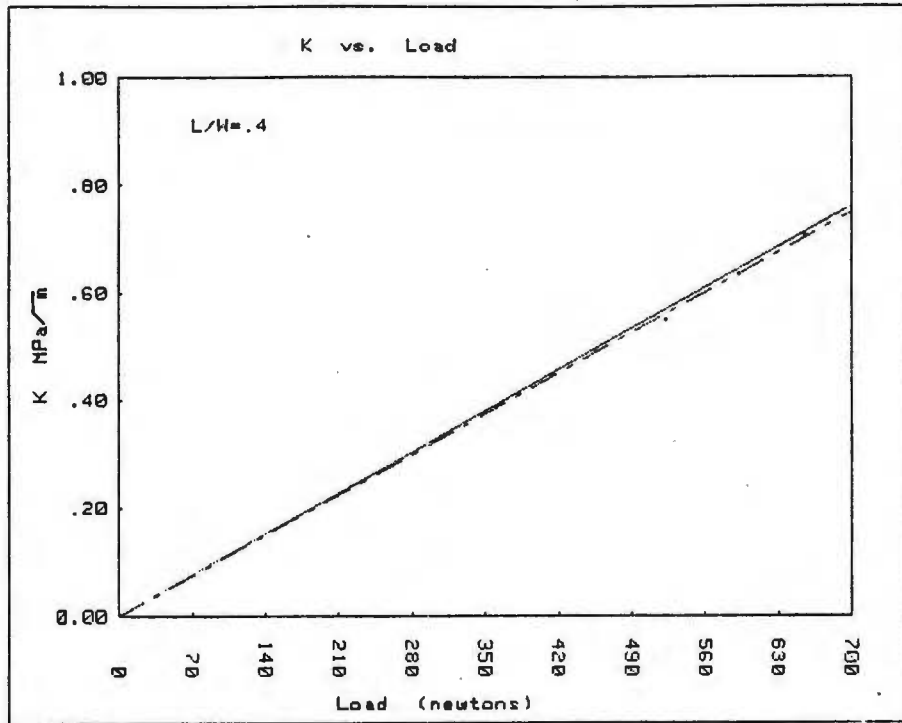
Fig.23. KI6 vs P plot with l/w=0.4.(stat. iso. expt.)
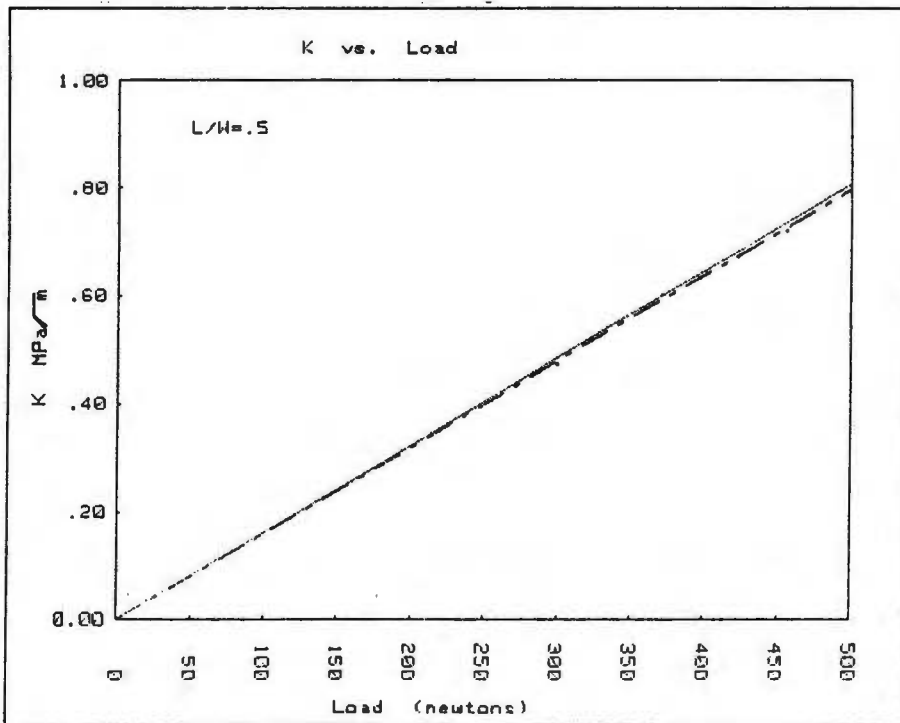
Fig.24. KI6 vs P plot with l/w=0.5.(stat. iso. expt.)

Fig.25. KI6 vs P plot with l/w=0.6.(stat. iso. expt.)
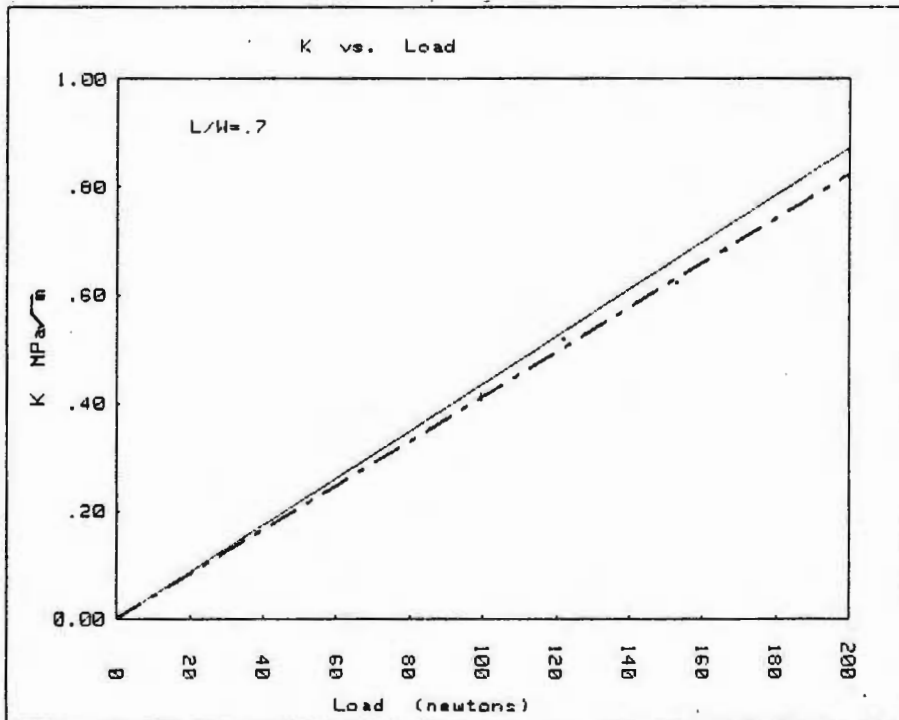
Fig.26. KI6 vs P plot with l/w=0.7.(stat. iso. expt.)
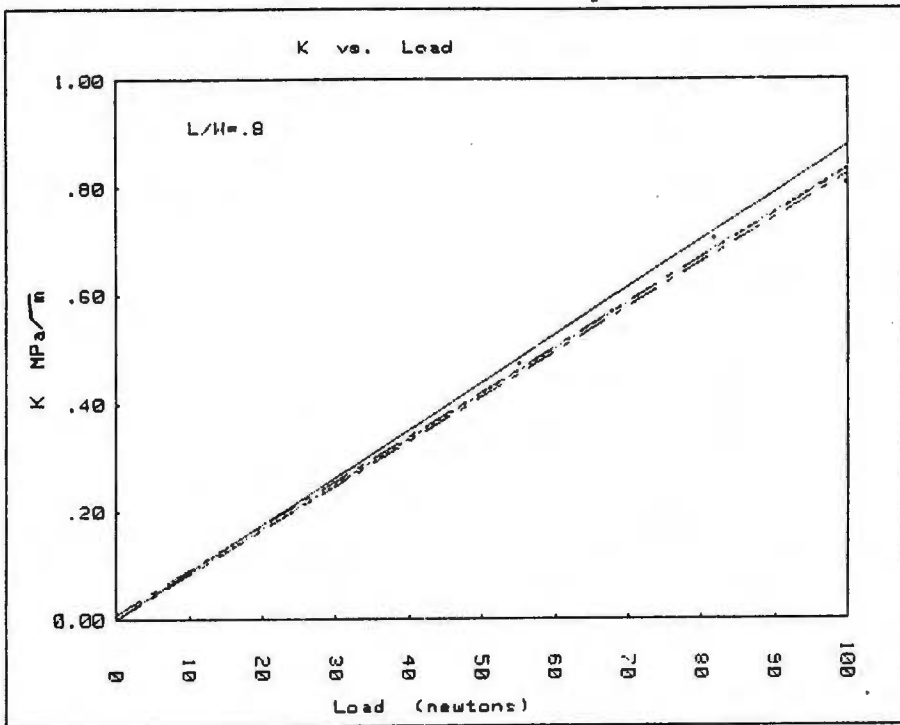
Fig.27. KI6 vs P plot with l/w=0.8.(stat. iso. expt.)

Fig.28. KI6 vs P plot with l/w=0.9.(stat. iso. expt.)

a.

K vs l/w ratio (load=1 N)

y-axis: K KPa√m̄ (0.0, 6.0, 12.0, 18.0, 24.0, 30.0)

Kth

KI6

KI3

x-axis: Length to width ratio (0.00, .10, .20, .30, .40, .50, .60, .70, .80, .90, 1.00)

b.

K vs l/w ratio (load=1 N)

y-axis: K KPa√m̄ (0.0, .5, 1.0, 1.5, 2.0, 2.5)

x-axis: Length to width ratio (0.00, .06, .12, .18, .24, .30, .36, .42, .48, .54, .60)
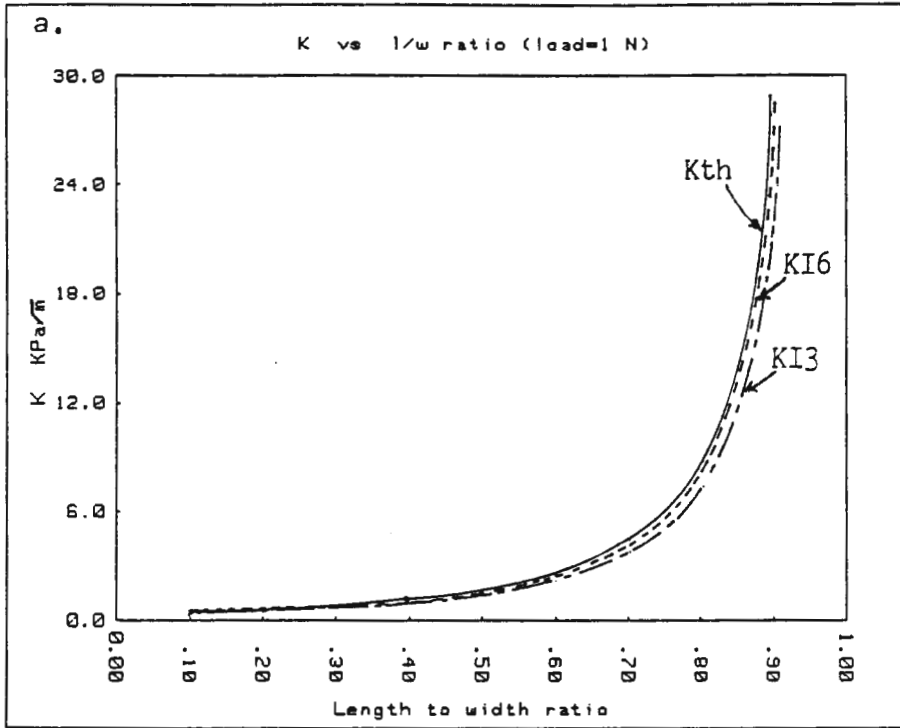
Fig.29. Photoelastic K as a function of l/w for a load of 1N. a: Entire range. b: 0< l/w <0.6.

72

ALL DIMENSIONS IN INCHES

Fig.30. Geometry of the SEN specimen used for static
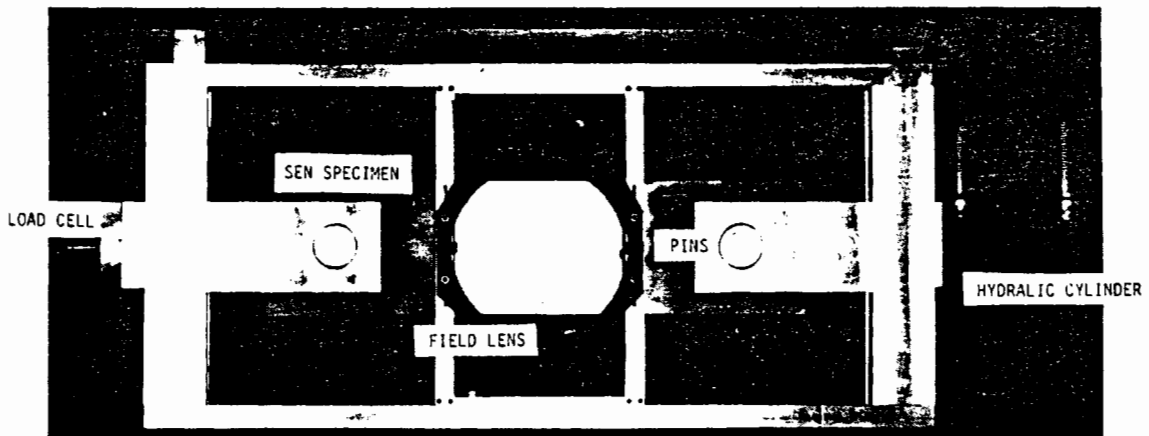caustic and dynamic experiments.

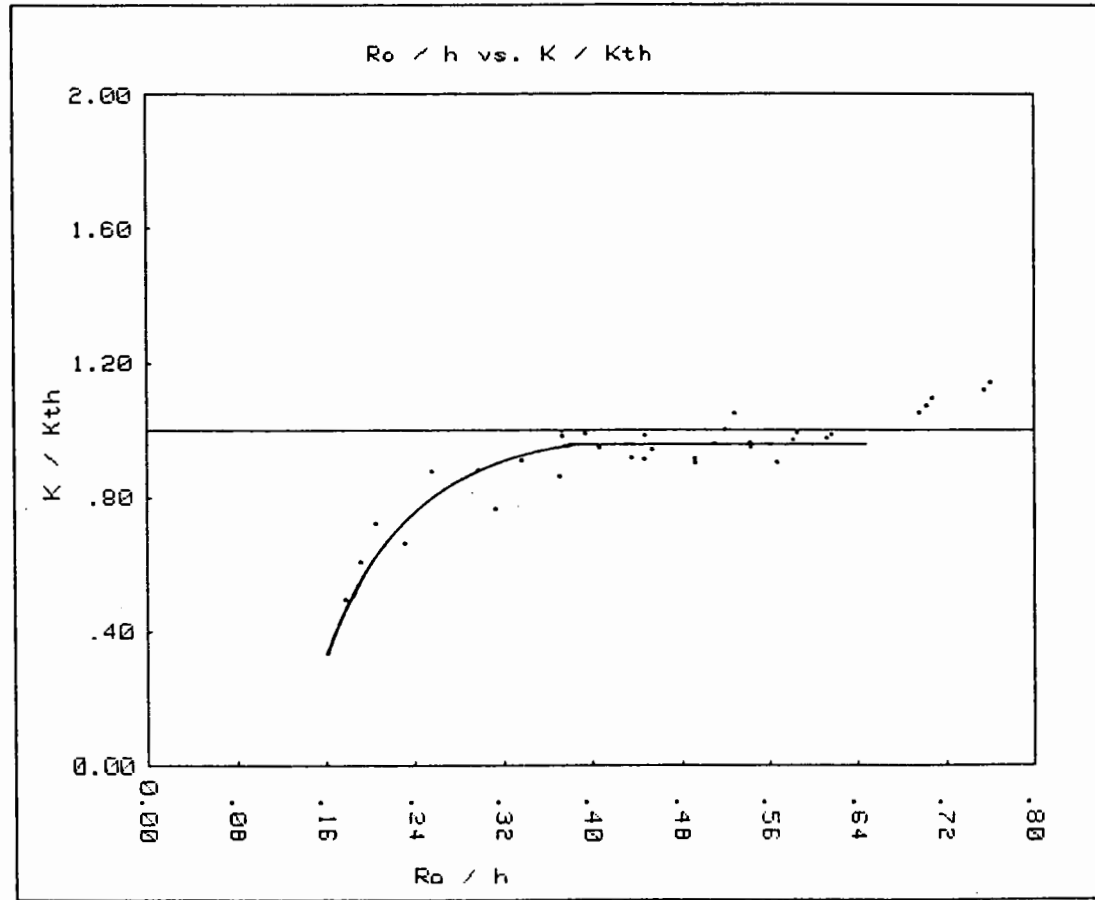
Fig.31. Loading fixture for the SEN specimens.(from[5])

Fig.32. K/Kth vs ro/h for plexiglas with 1/w=0.5.

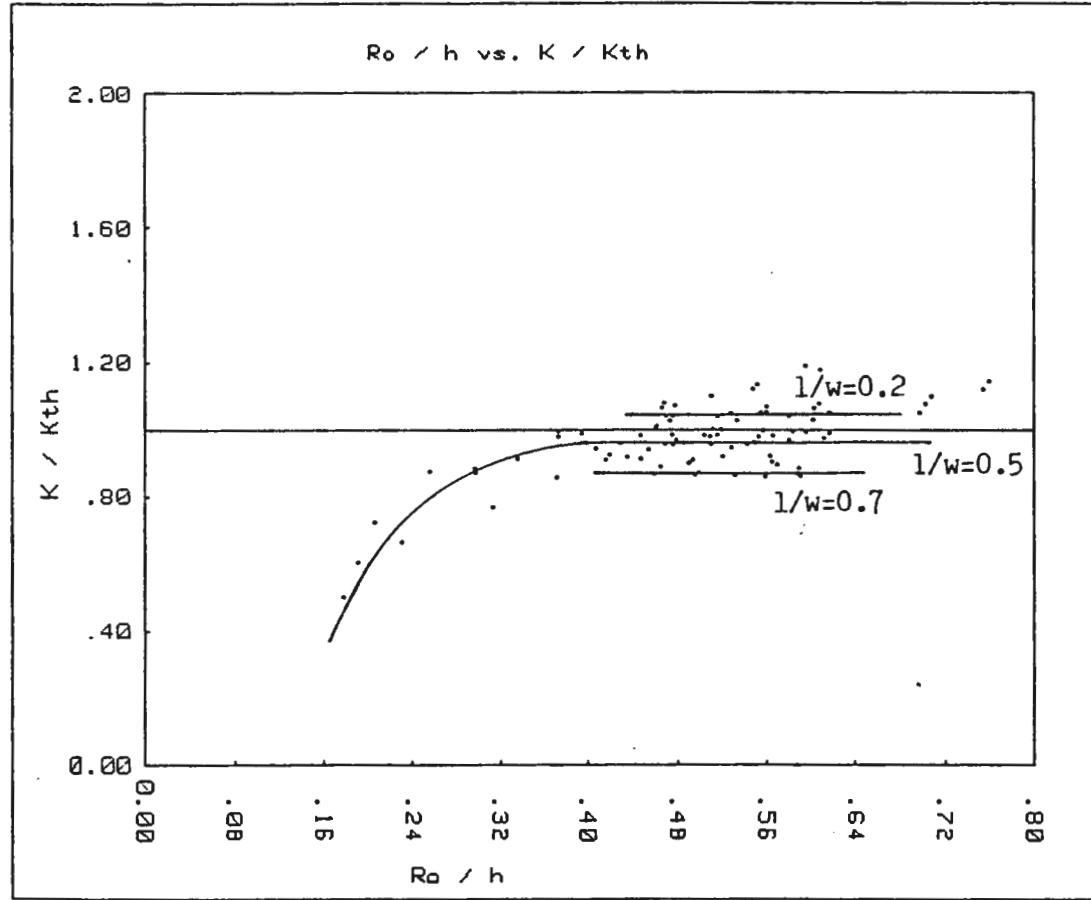Ro / h vs. K / Kth

Fig.33. K/Kth vs ro/h for plexiglas with varying crack lengths.
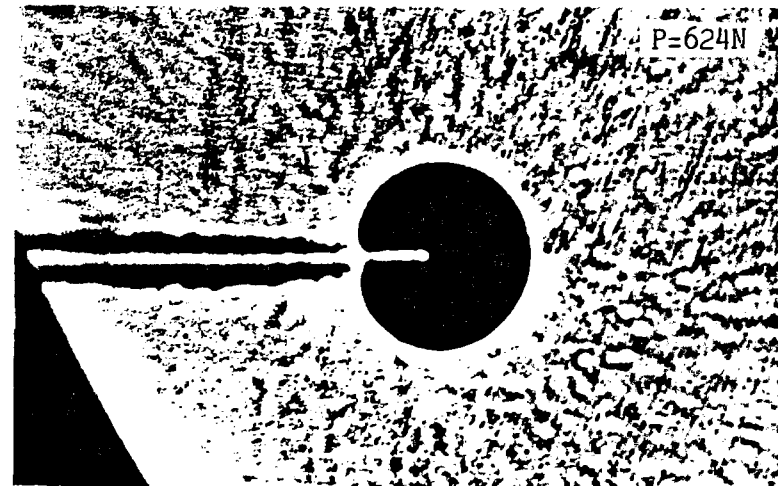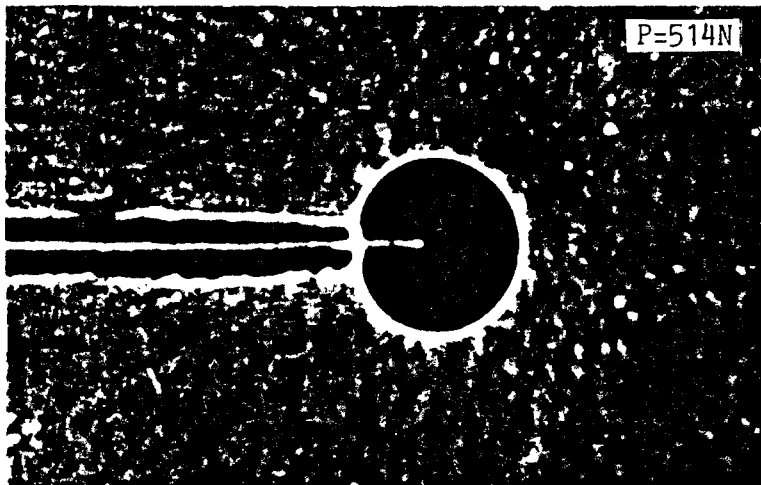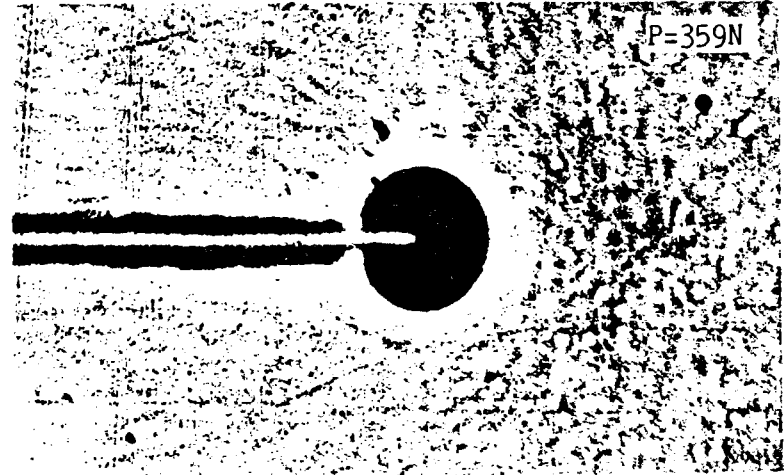
P=286N

P=359N

P=514N

P=624N
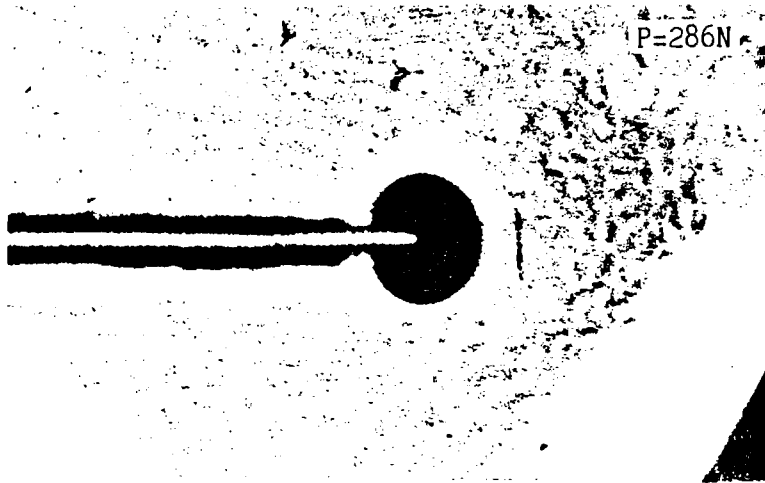
Fig.34. A typical set of photographs from static
caustic experiments.(l/w=0.6)
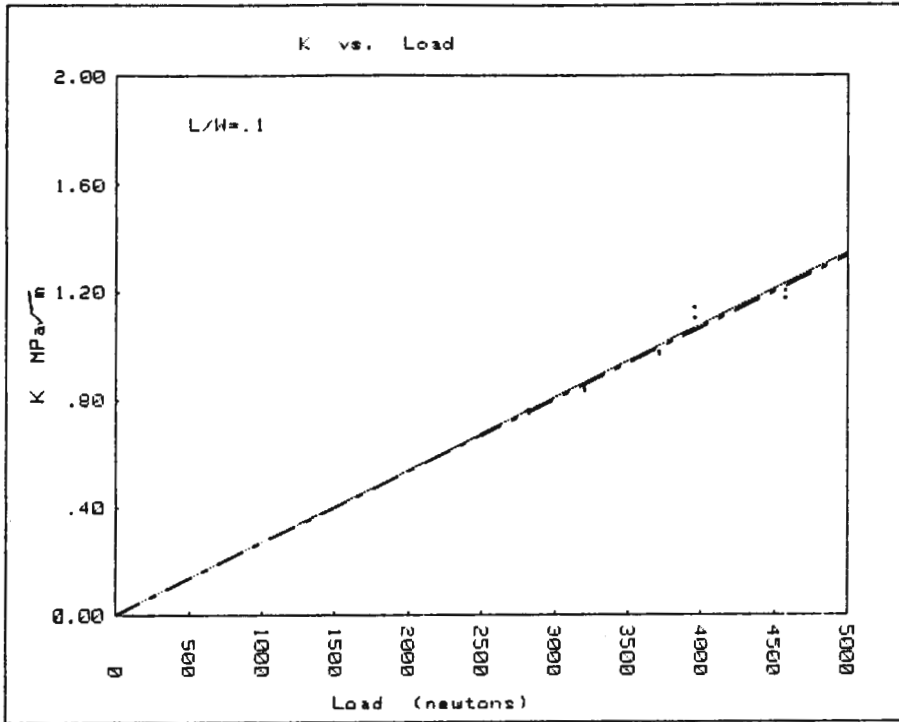
Fig.35. KI vs P plot with l/w=0.1.(stat. caus. expt.)

Fig.36. KI vs P plot with l/w=0.2.(stat. caus. expt.)
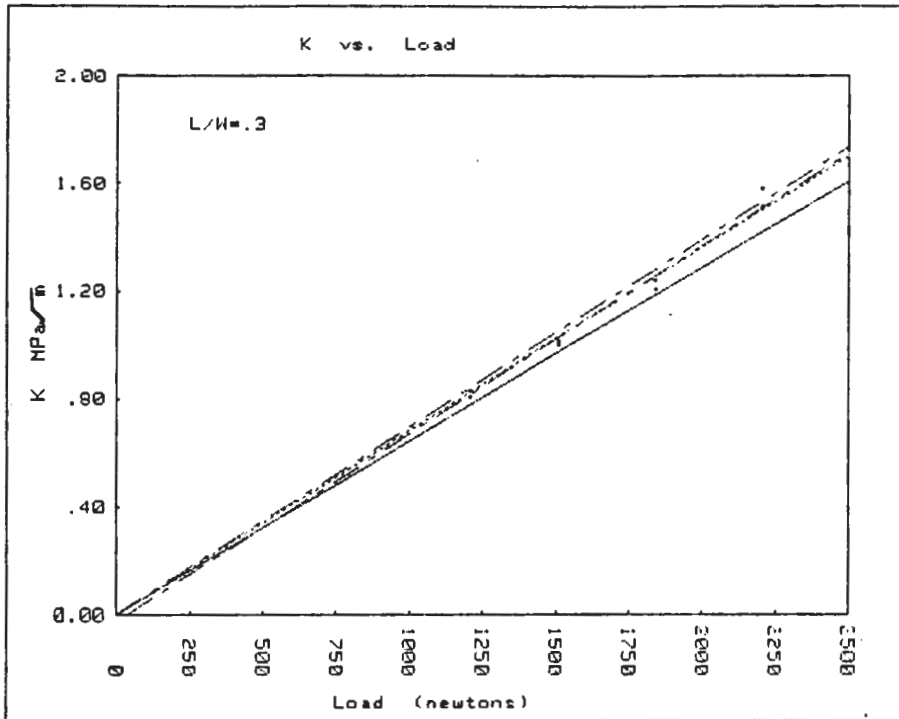
Fig.37. KI vs P plot with l/w=0.3.(stat. caus. expt.)
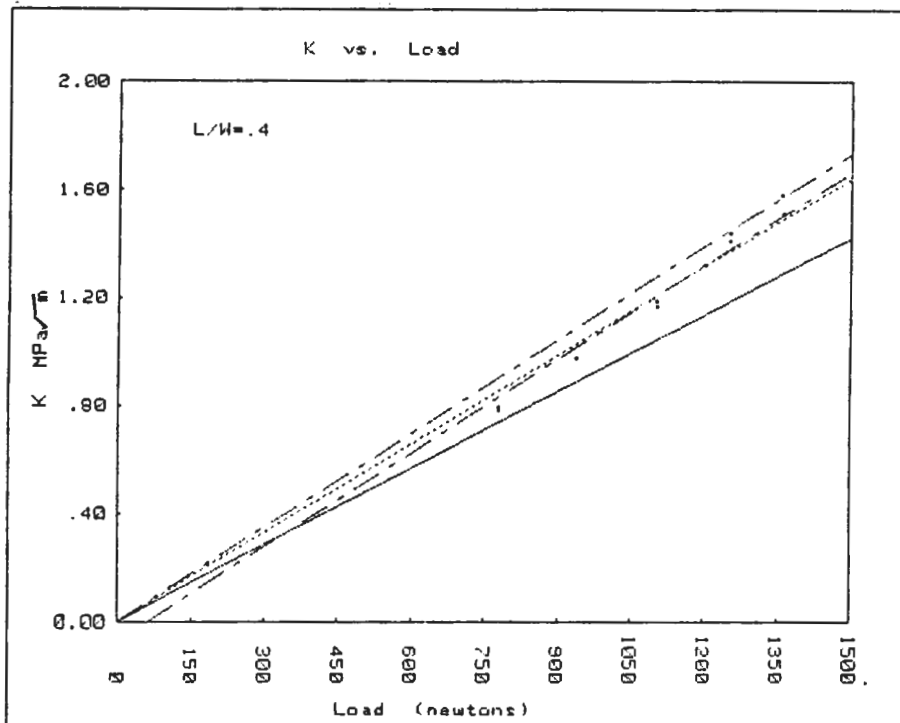
Fig.38. KI vs P plot with l/w=0.4.(stat. caus. expt.)

78
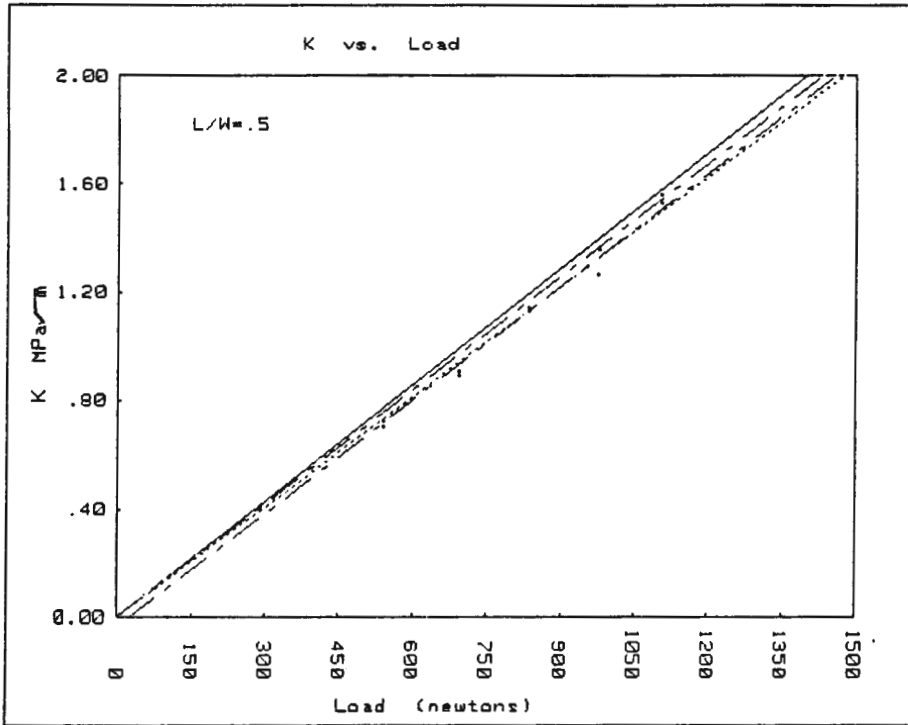
Fig.39. KI vs P plot with l/w=0.5.(stat. caus. expt.)
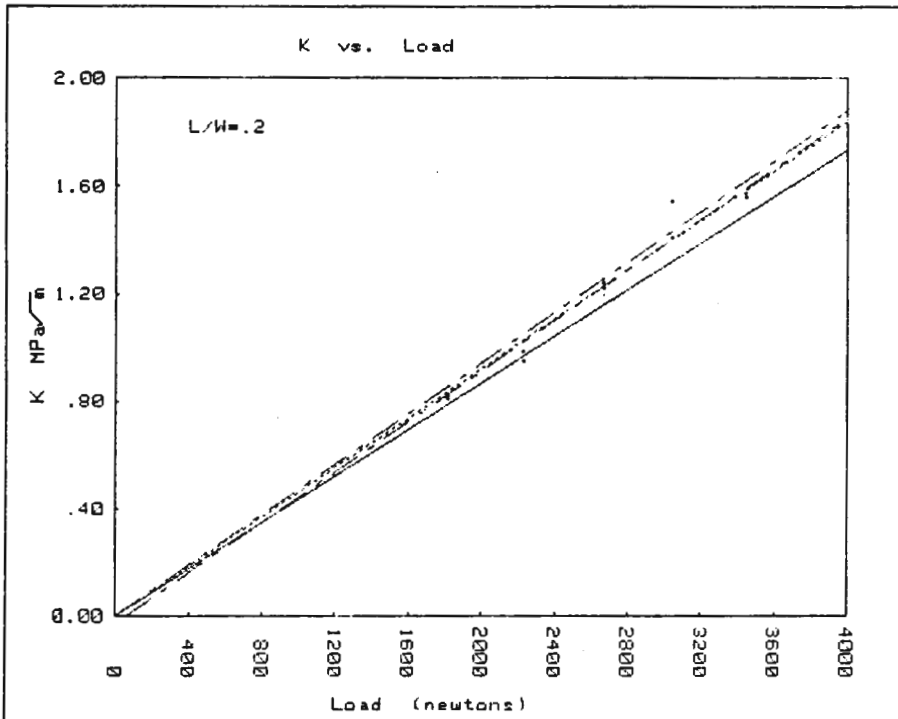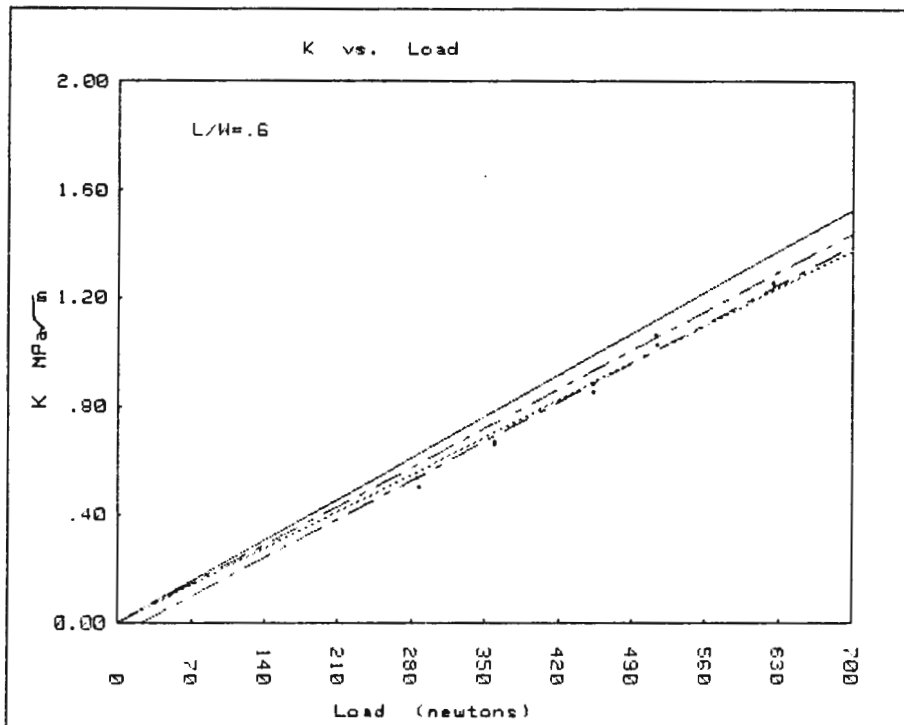

Fig.40. KI vs P plot with l/w=0.6.(stat. caus. expt.)
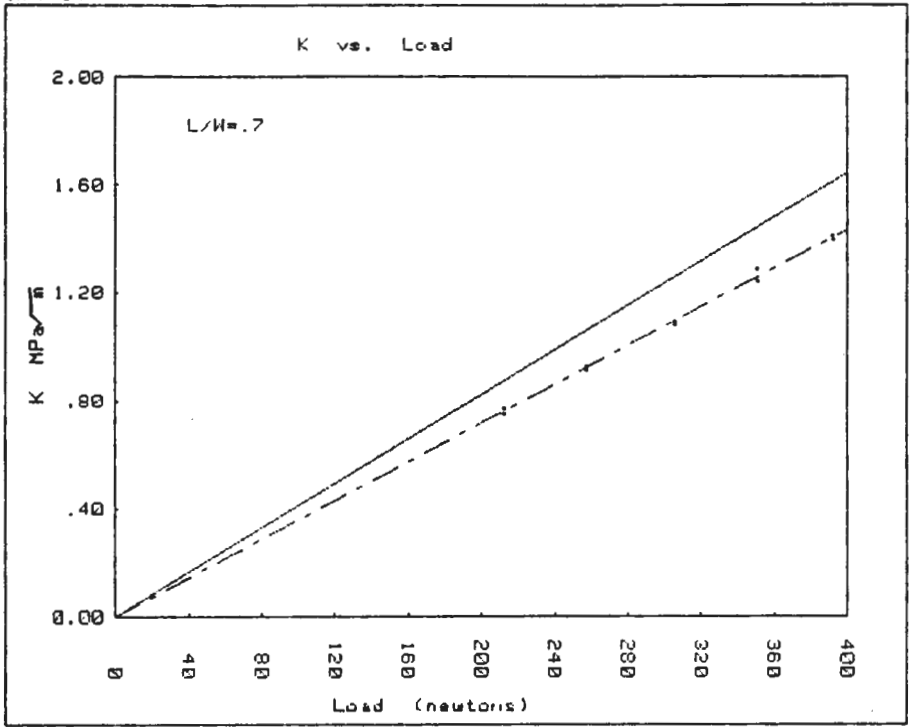
Fig.41. KI vs P plot with l/w=0.7.(stat. caus. expt.)
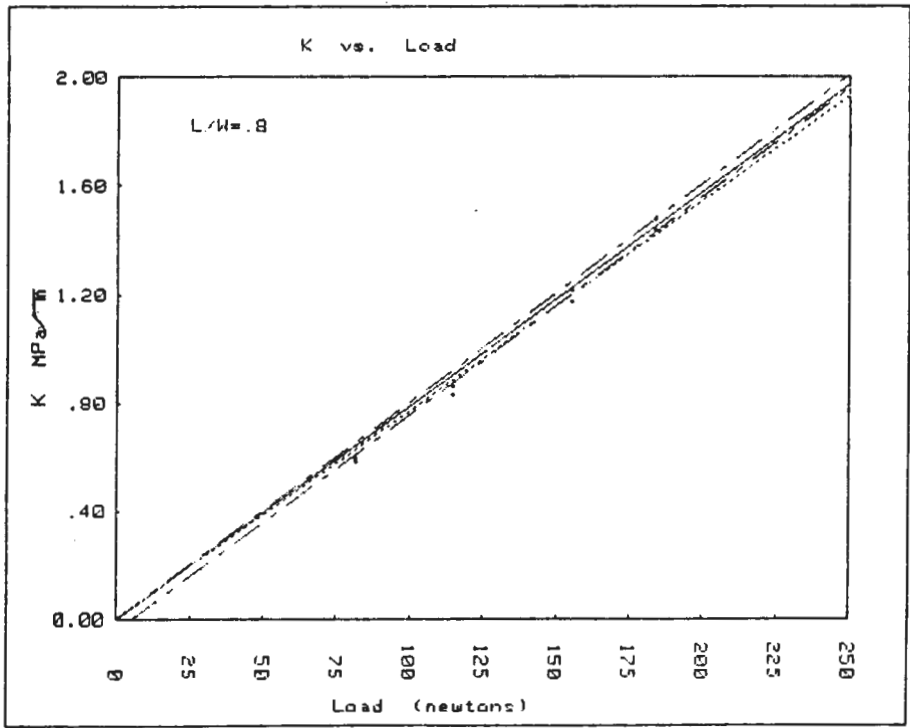
Fig.42. KI vs P plot with l/w=0.8.(stat. caus. expt.)
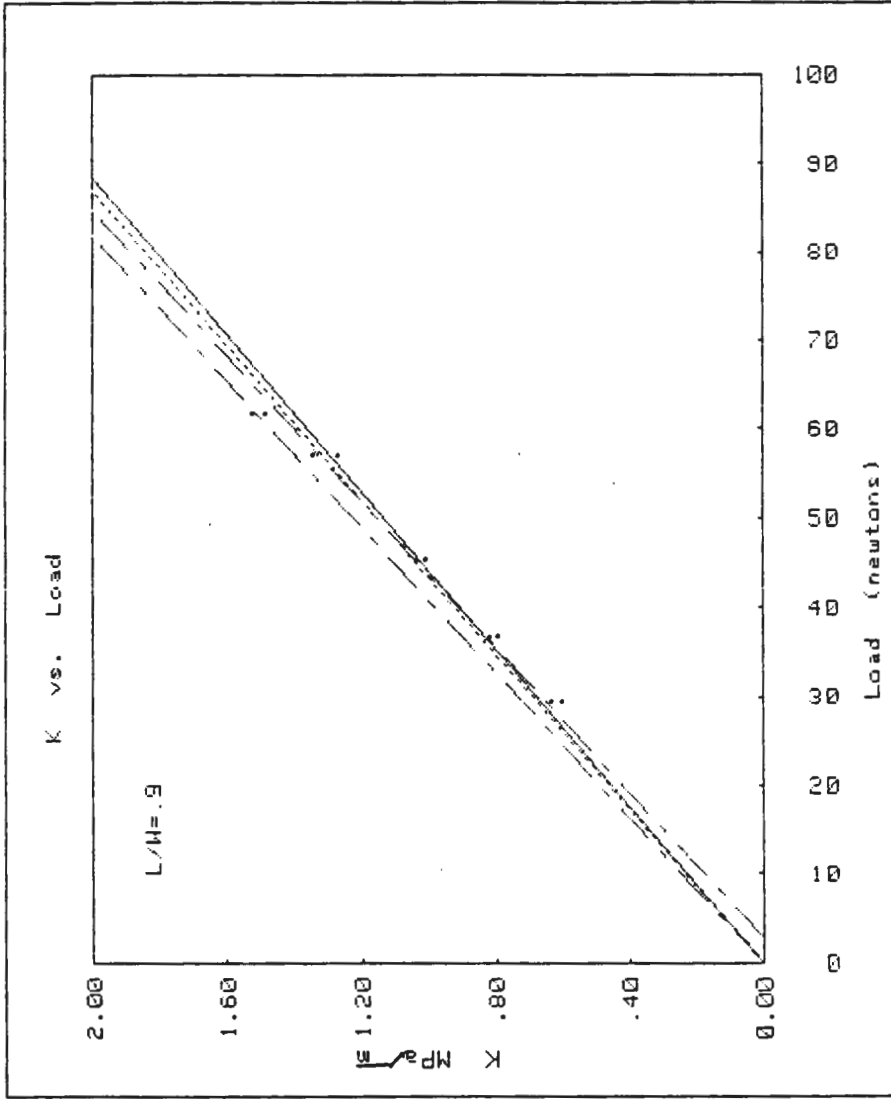
Fig.43. KI vs P plot with l/w=0.9.(stat. caus. expt.)

81
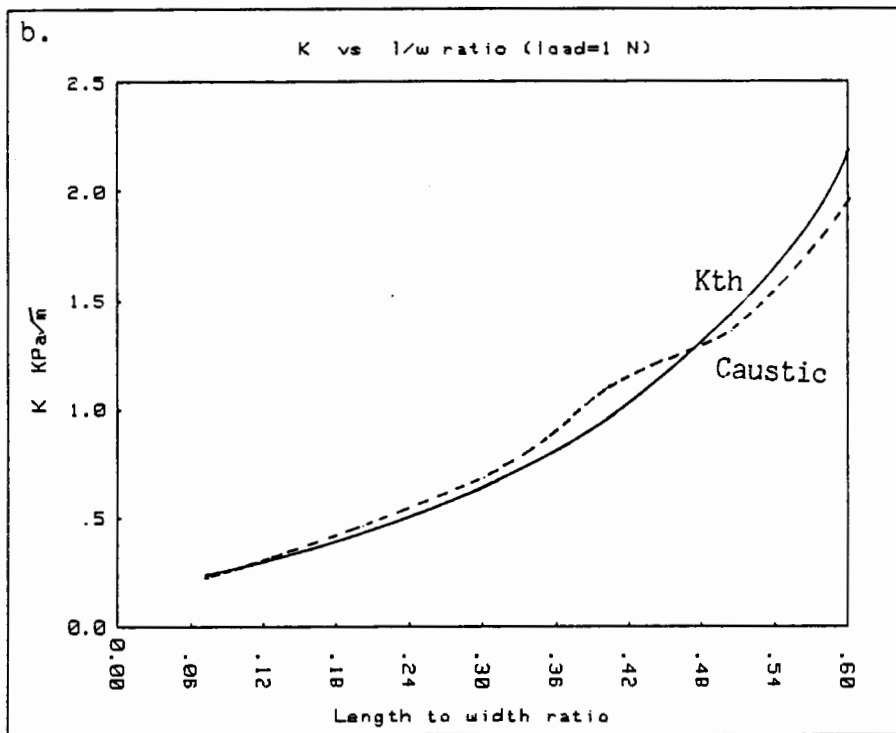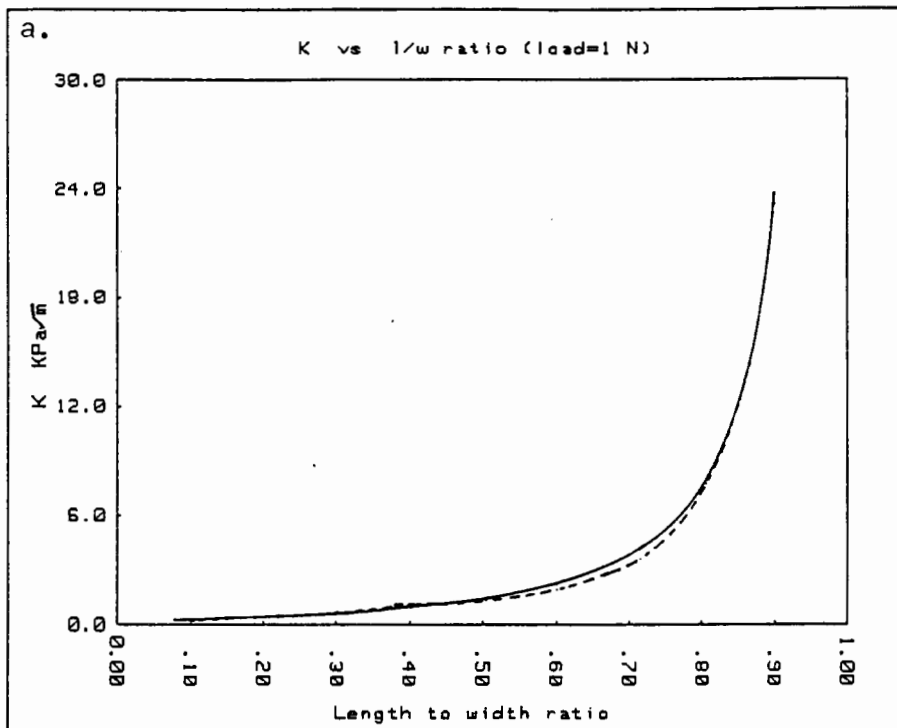
Fig.44. Photoelastic K as a function of l/w for a load of 1N. a: Entire range. b: 0< l/w <0.6.

82
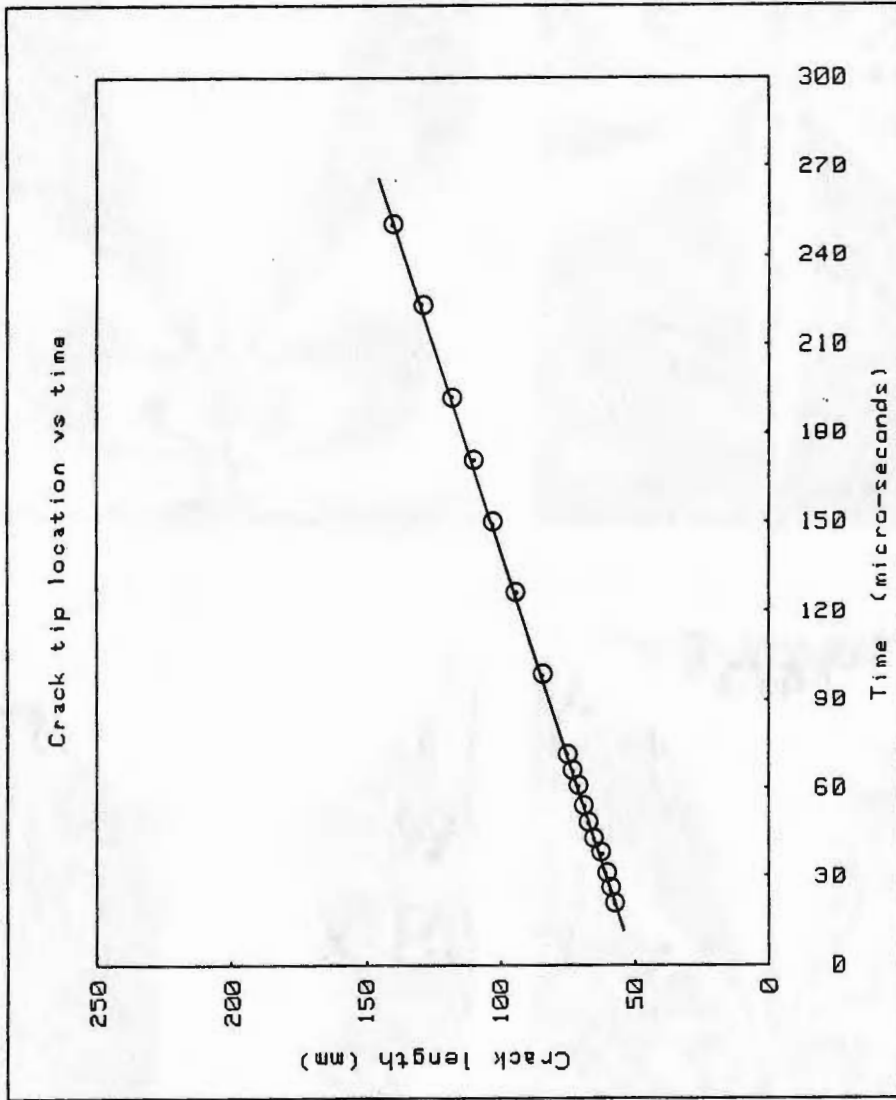
Fig.45. l vs t plot for dynamic SEN expt.1.

t=20.5μs

t=42.5μs

t=126μs

t=191.5μs
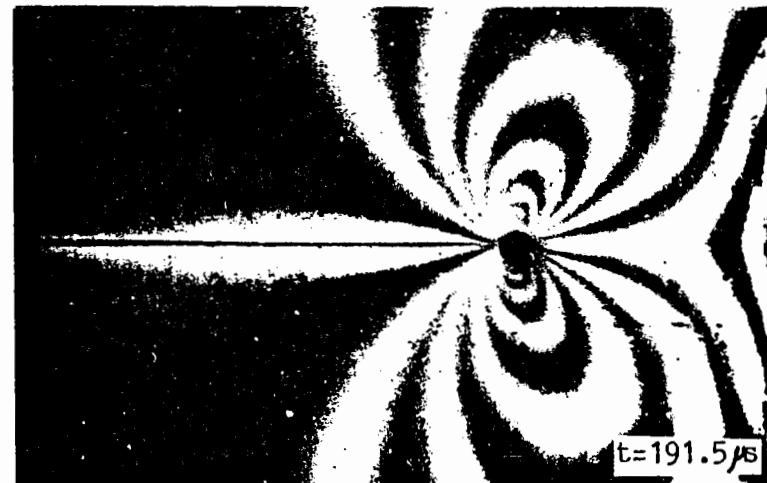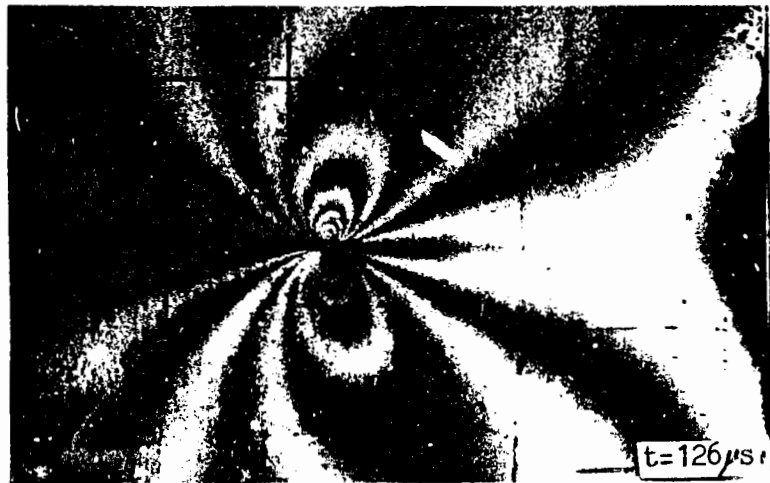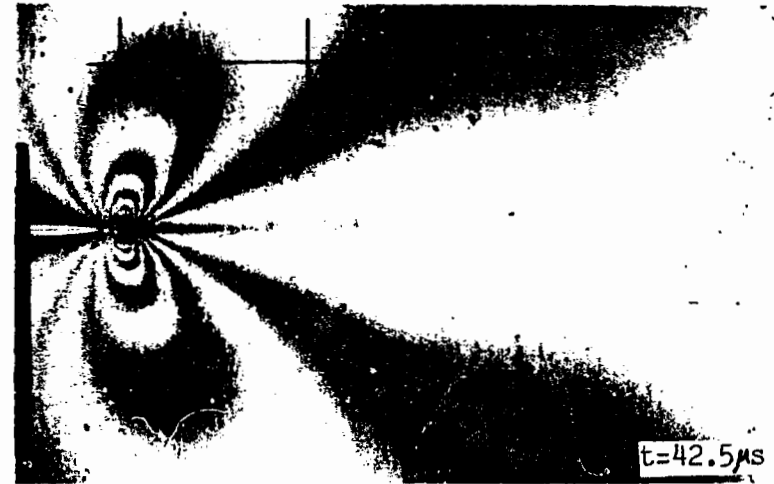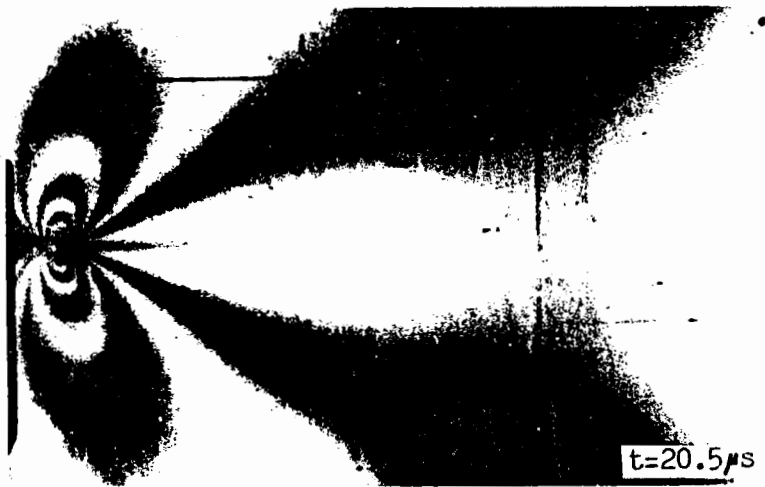
Fig.46. Fringe patterns from the dynamic SEN expt.1.
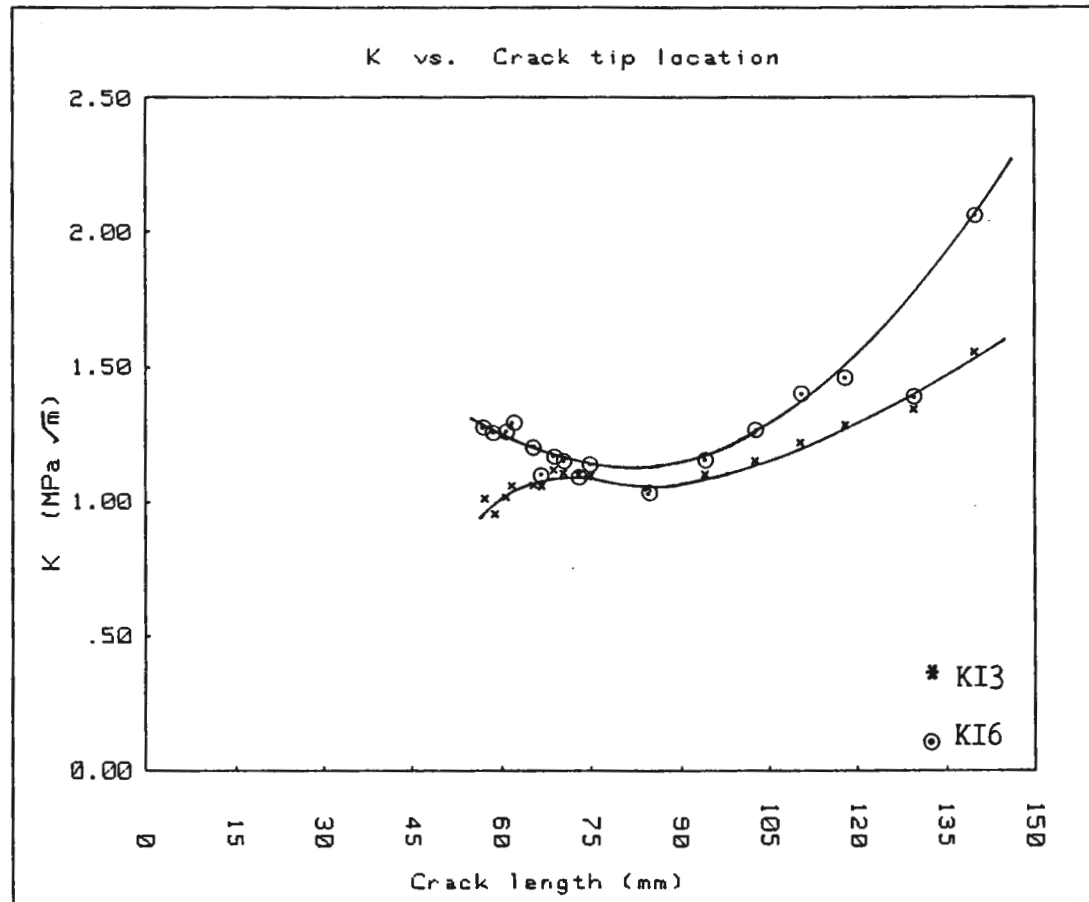
Fig.47. KI3 & KI6 vs l for SEN expt.1.
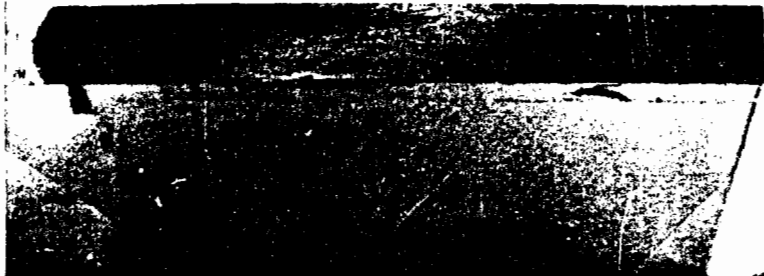
Fig.48. Fracture surface of the SEN specimen.
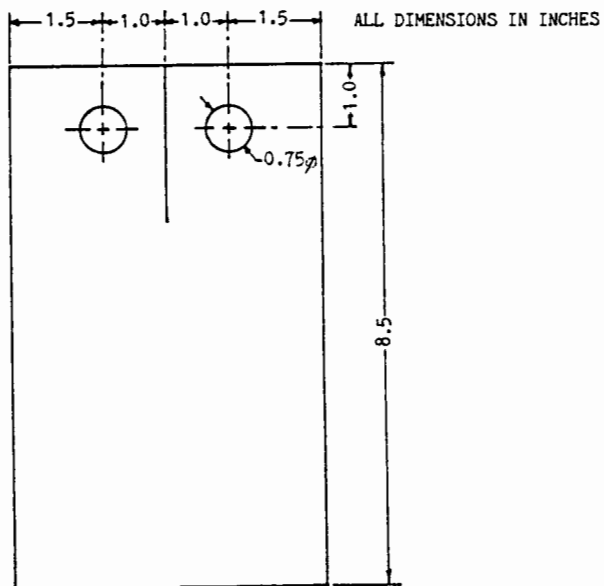
Fig.49. Geometry of the DCB specimen.
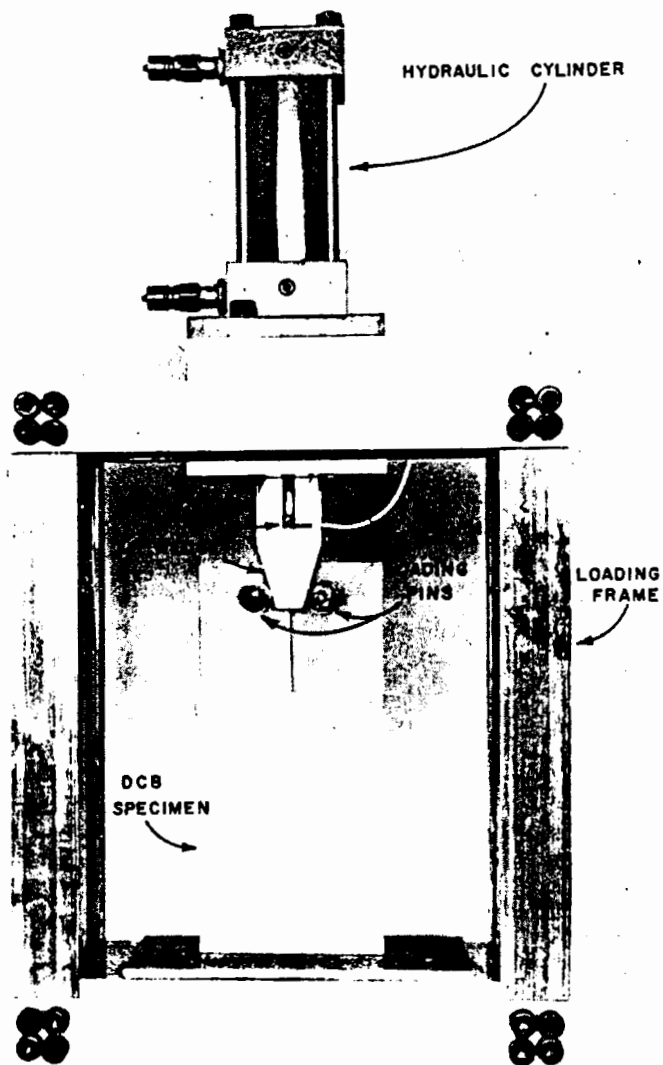
Fig.50. Loading arrangement for DCB & DCB/SEN specimens.(from [5])
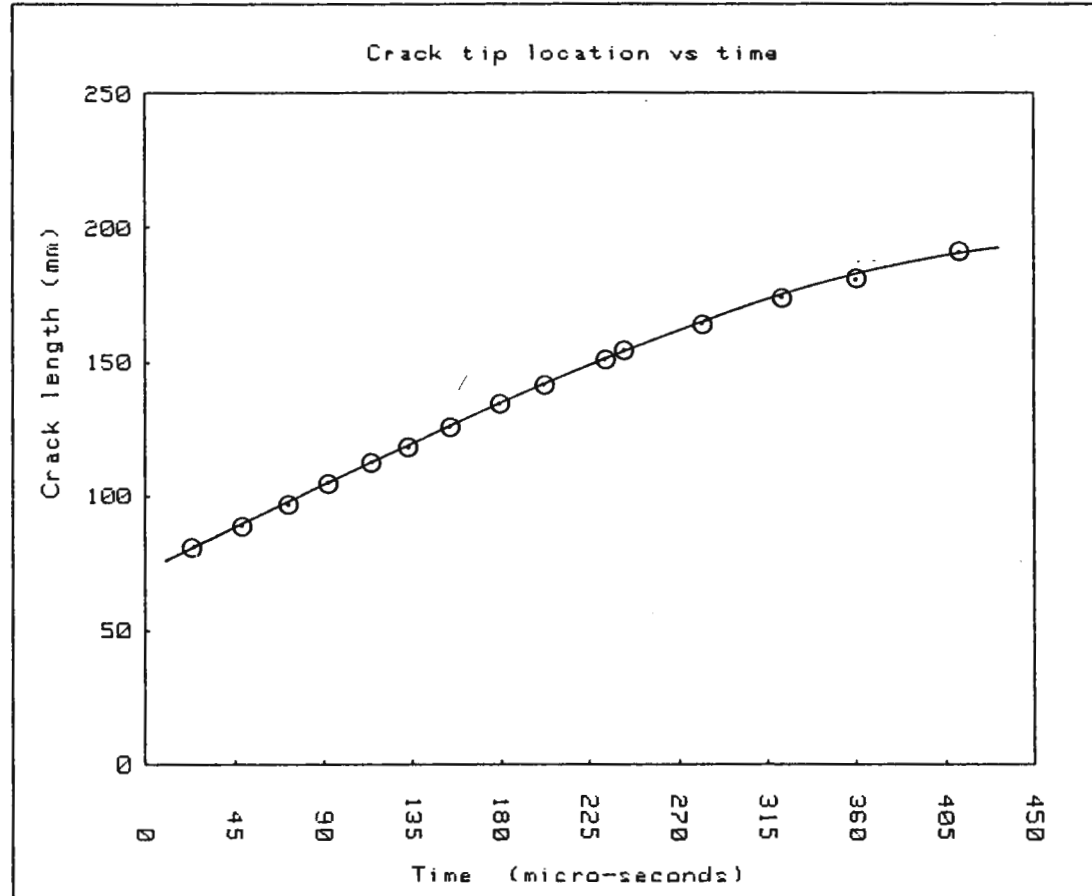
Fig.51. l vs t plot for the DCB experiment.

t=24.5μs

t=132.5μs

t=202.5μs

t=359.5μs
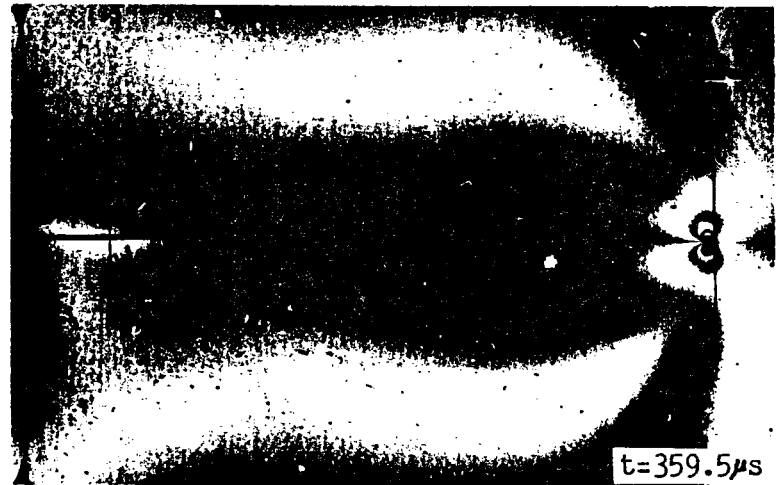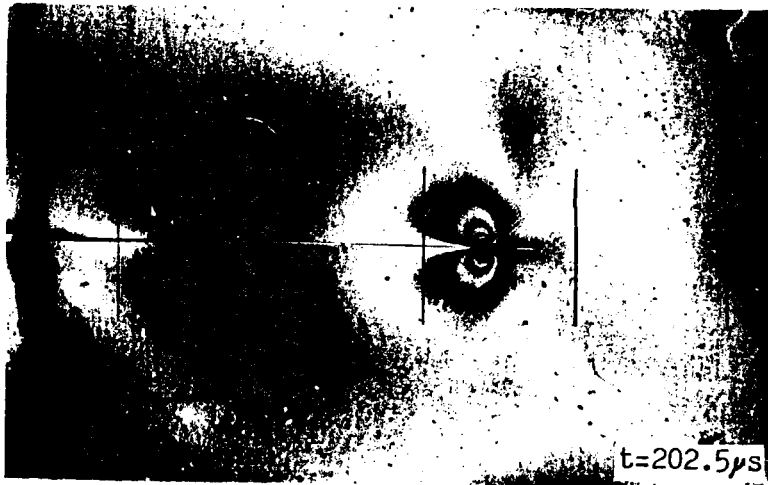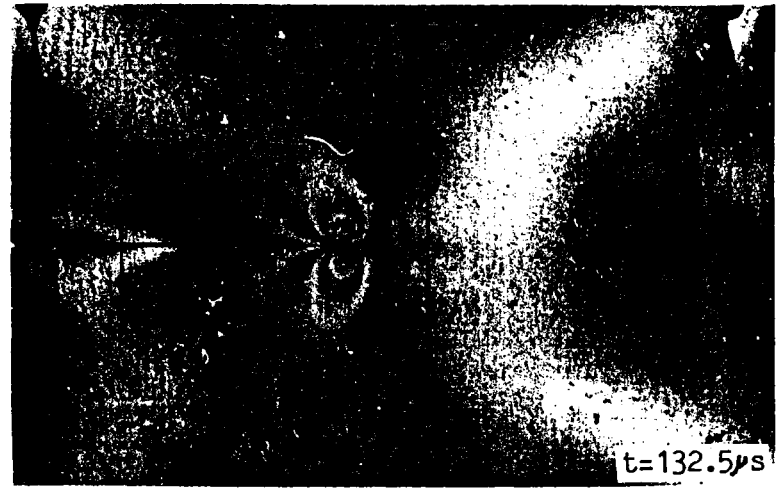
Fig.52. Varying fringe patterns in the DCB specimen.
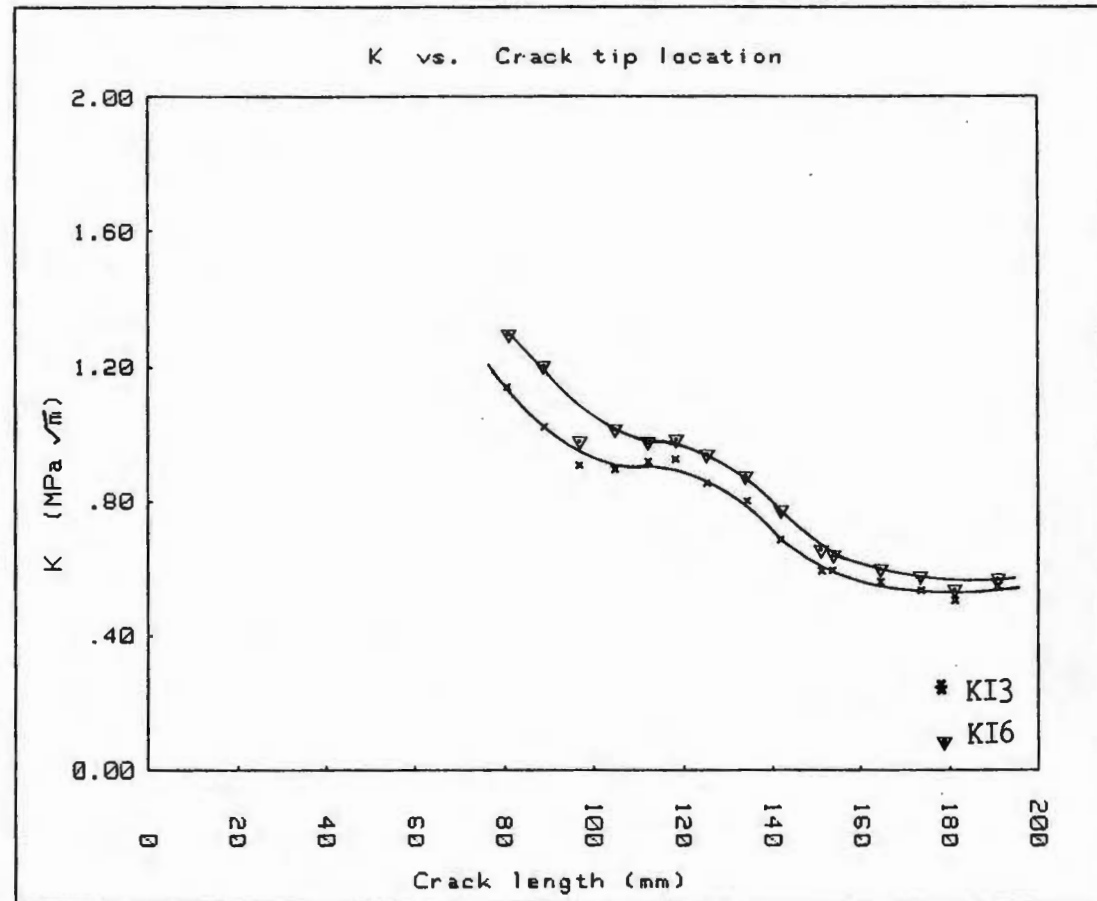
Fig.53. KI3 & KI6 vs l for the DCB experiment.

Fig.54. Fracture surface of the DCB specimen.

ALL DIMENSIONS IN INCHES
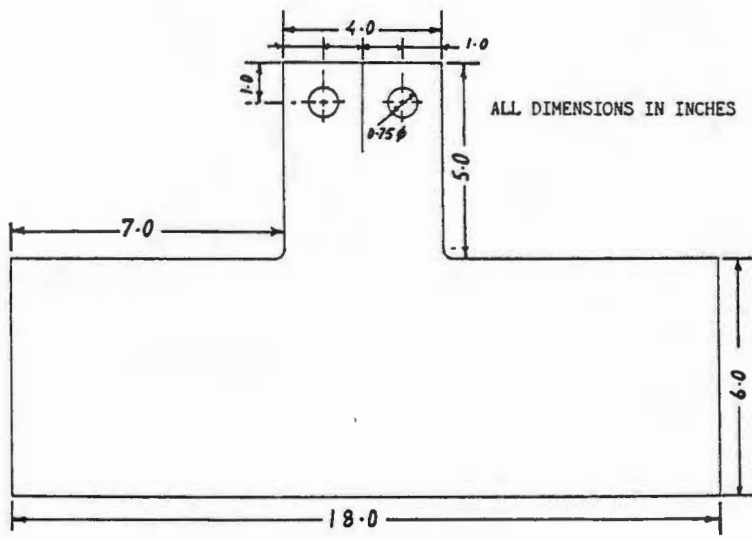
Fig.55. Geometry of the DCB/SEN specimen.

91
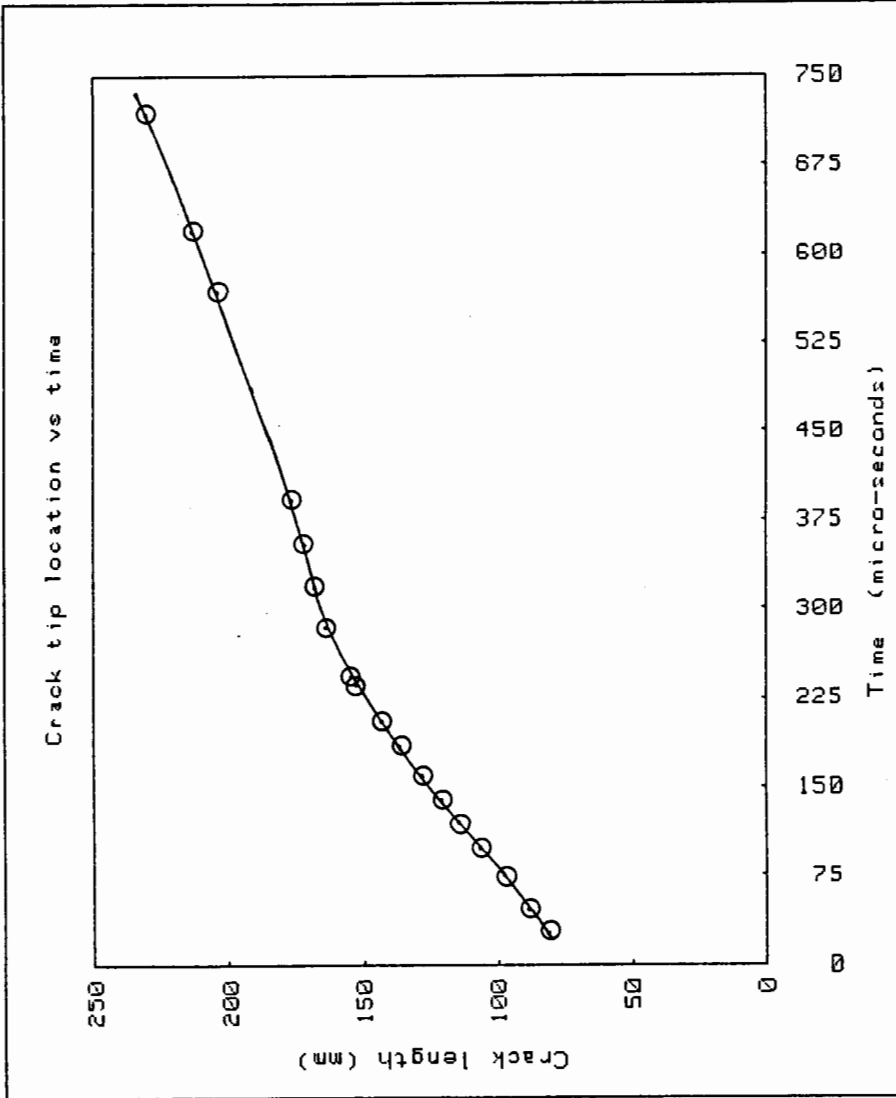
Fig.56. l vs t plot for DCB/SEN experiment.
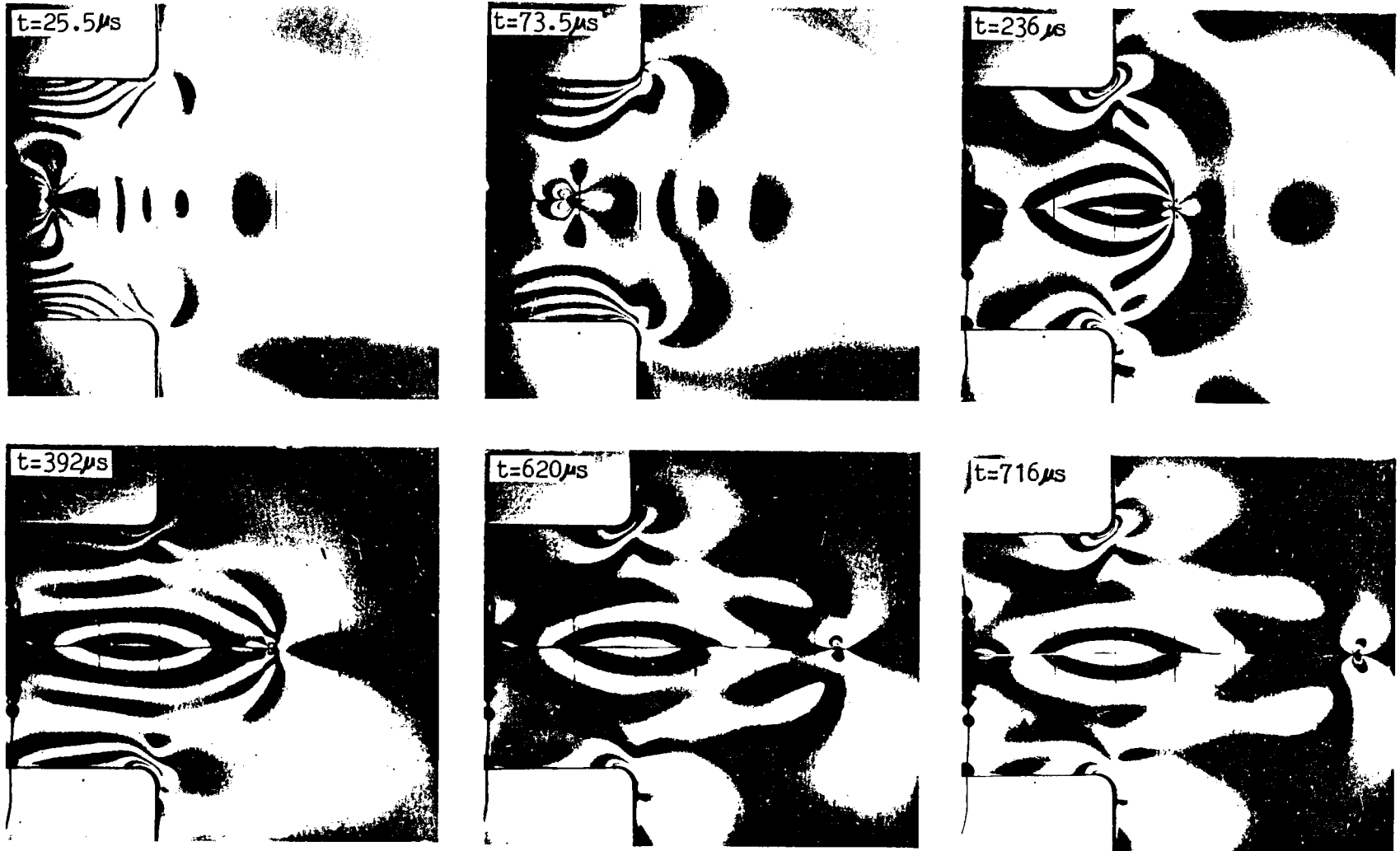
Fig.57. Photographs from the DCB/SEN experiment showing the changing size and the tilt of the fringe patterns.
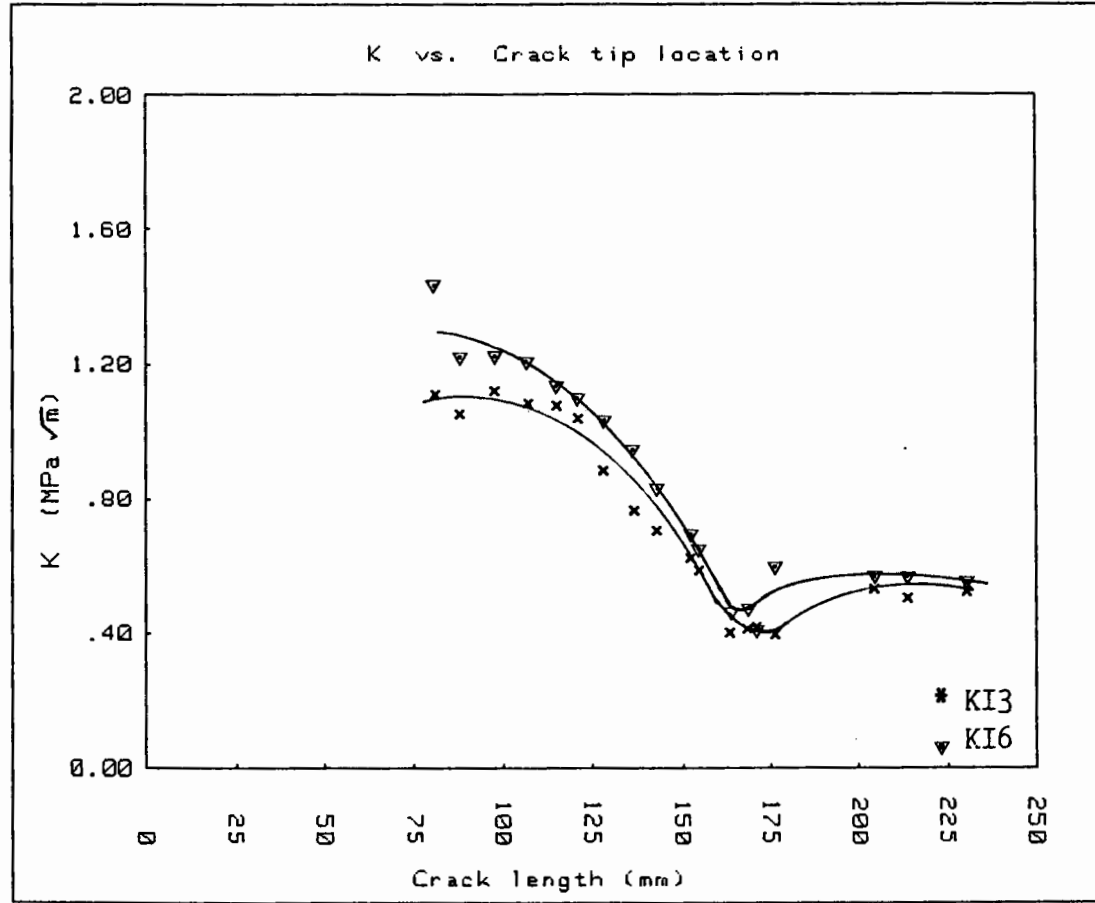
Fig.58. KI3 & KI6 vs l for DCB/SEN experiment.
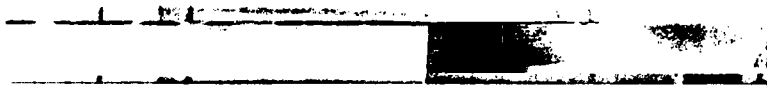
Fig.59. Fracture surface of the DCB/SEN specimen.
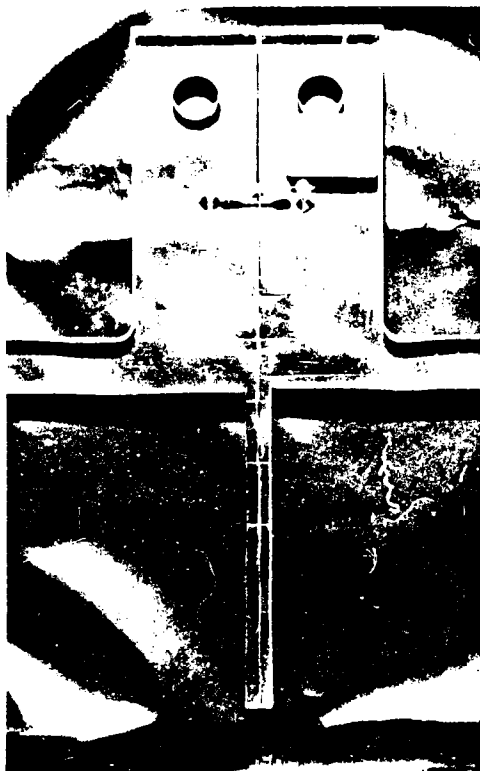
Fig.60. Post mortem picture of the DCB/SEN specimen.
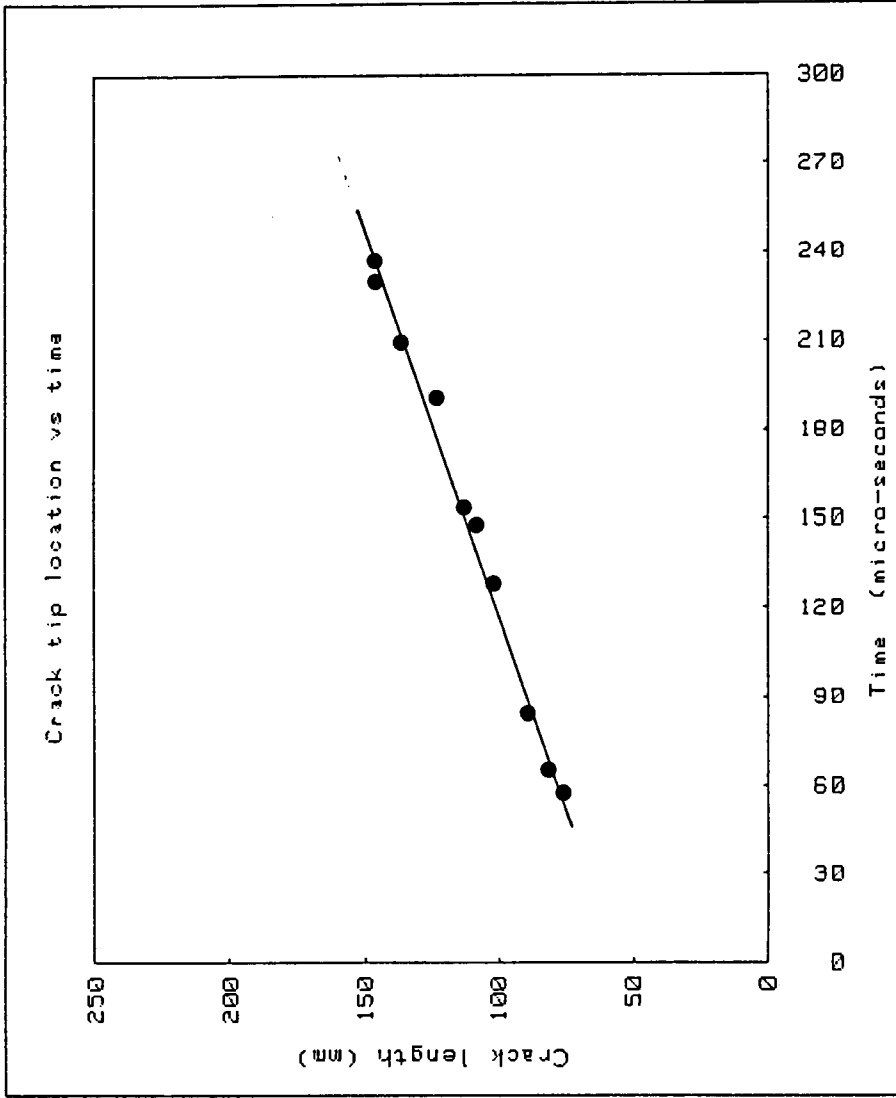
Fig.61. l vs t plot for dynamic caustic experiment.
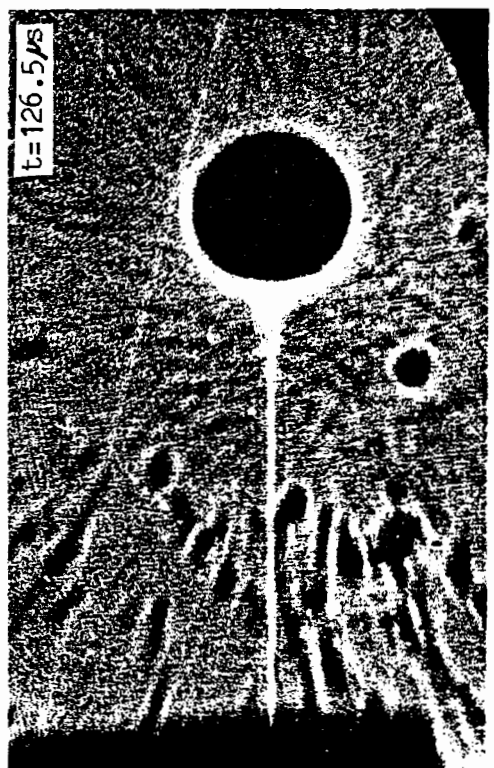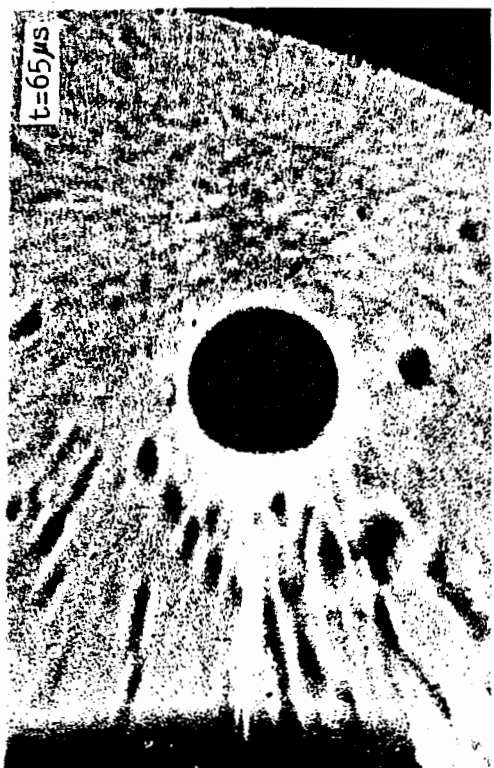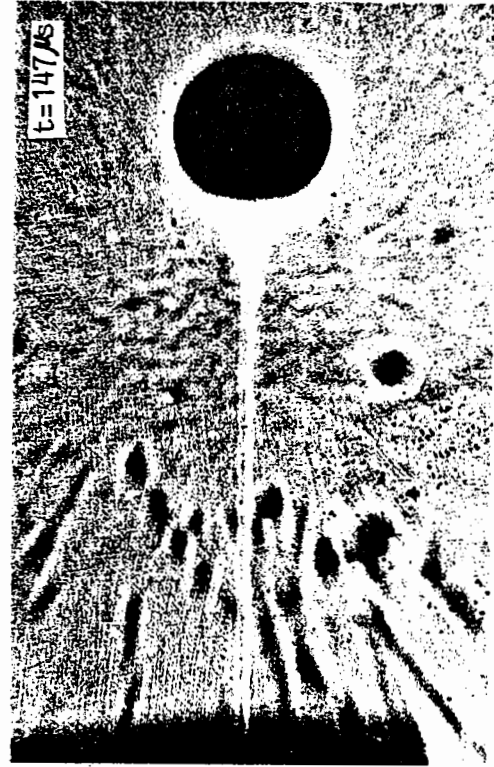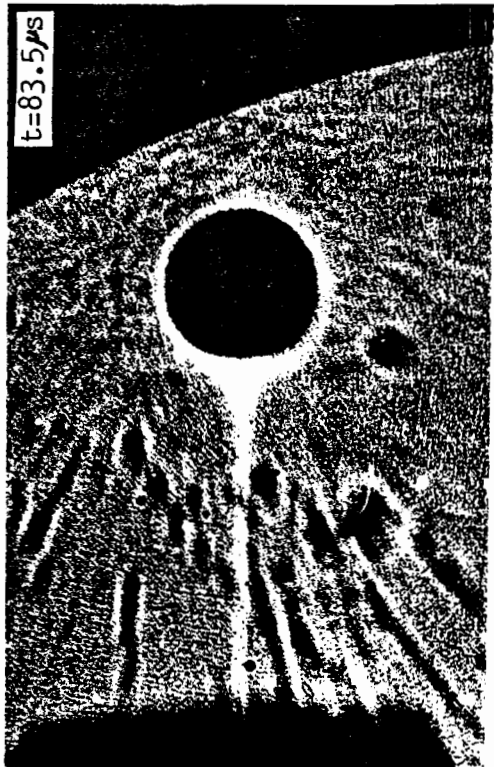
Fig.62. Photographs from the dynamic caustic experiment.

97
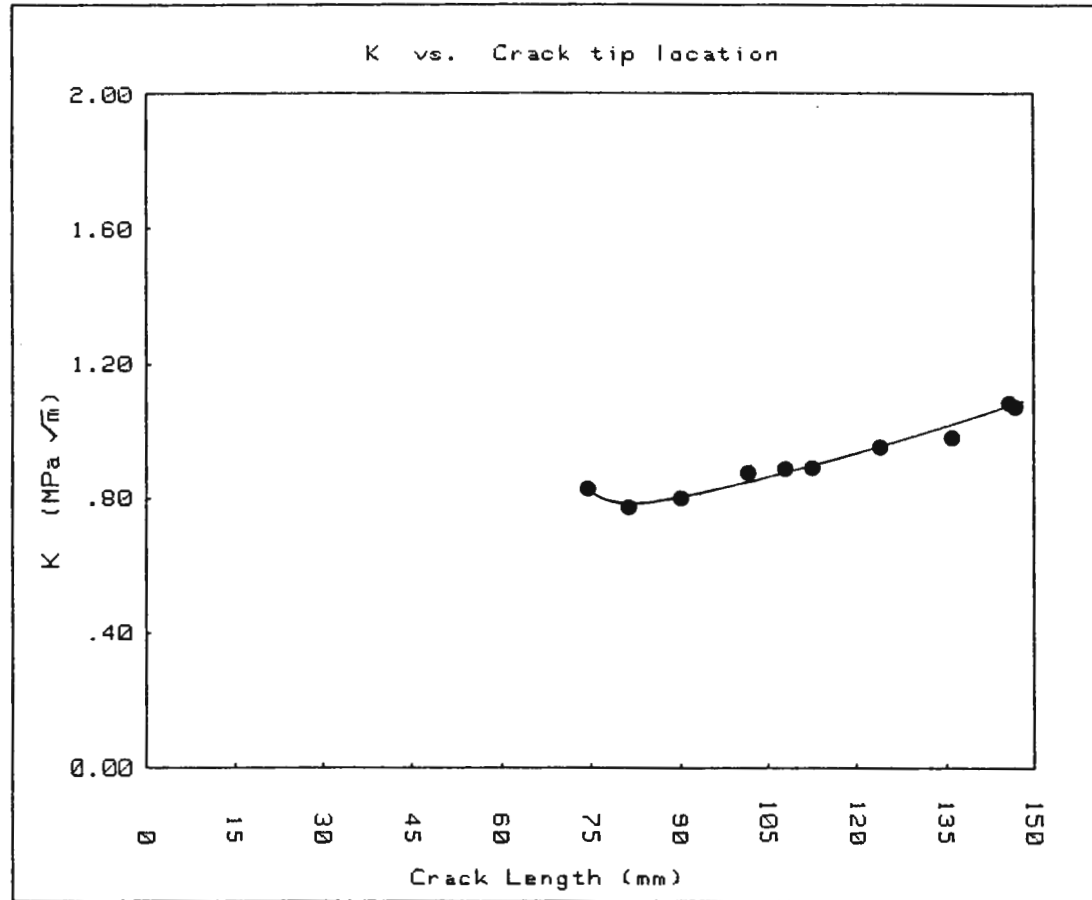
Fig.63. KI vs l plot for dynamic caustic experiment.
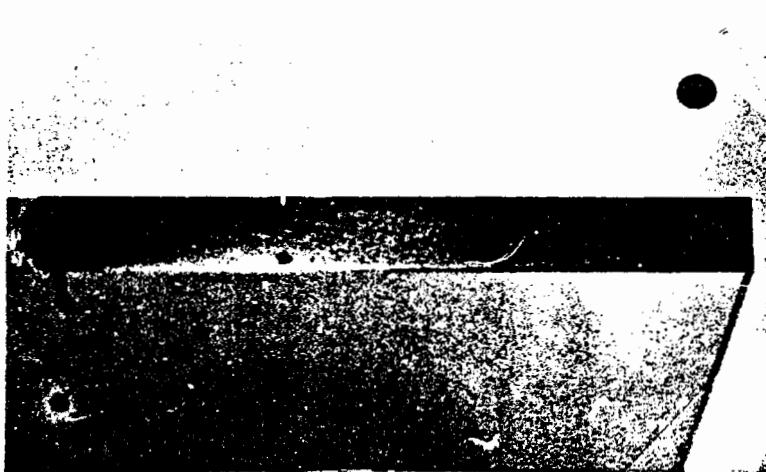
Fig.64. Fracture surface of the dynamic caustic specimen.
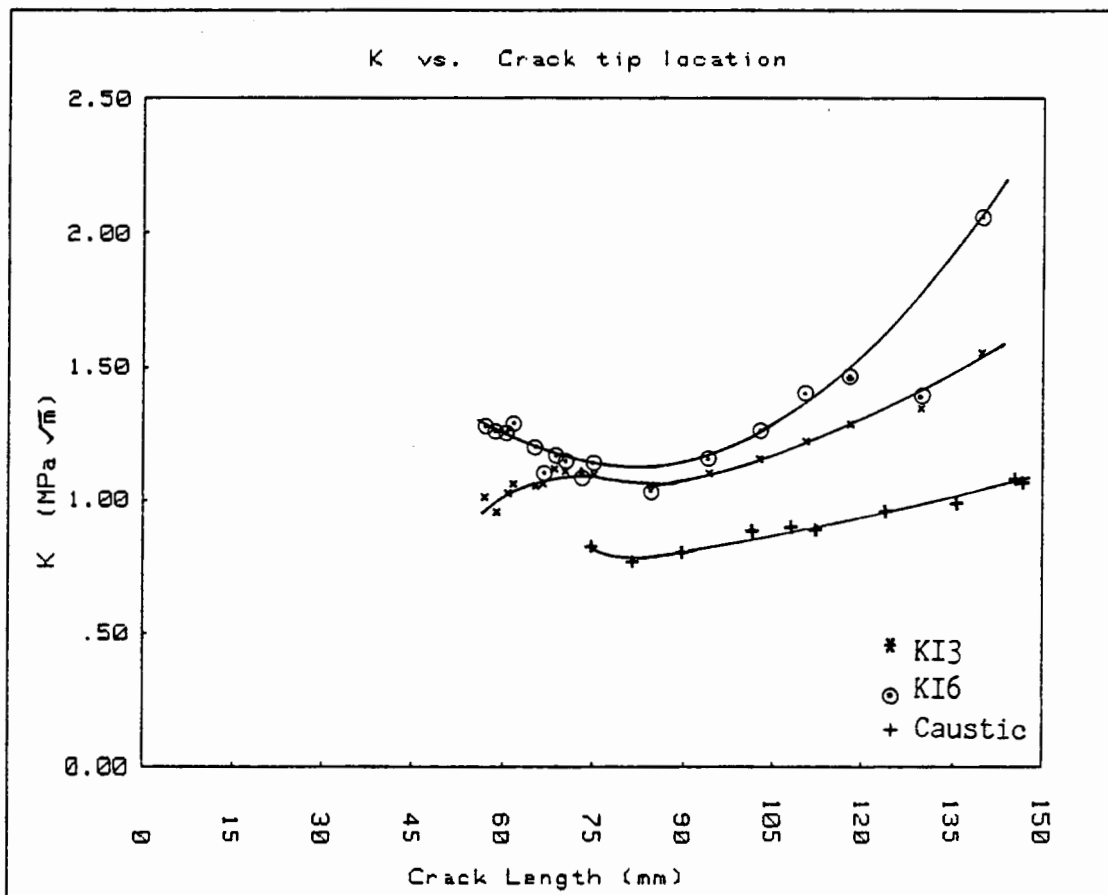
Fig.65. Comparison of the dynamic photoelastic and caustic data for SEN specimen.

99
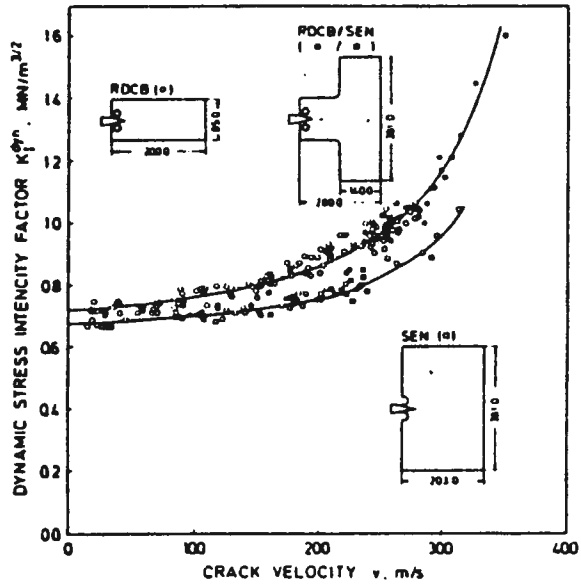
Fig.66. K-v data for DCB/SEN-combination specimens of
         Araldite B. (from[6])
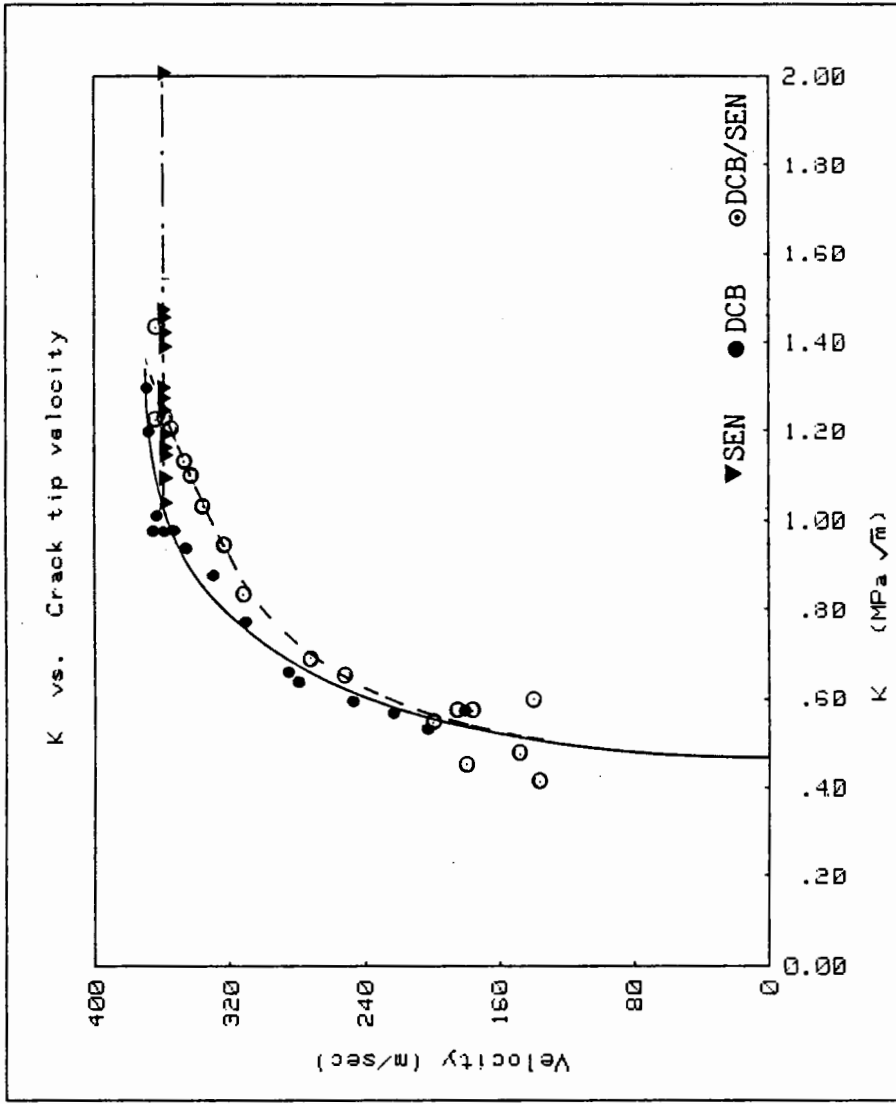
Fig.67.   KI6 vs v plot for Homalite-100.
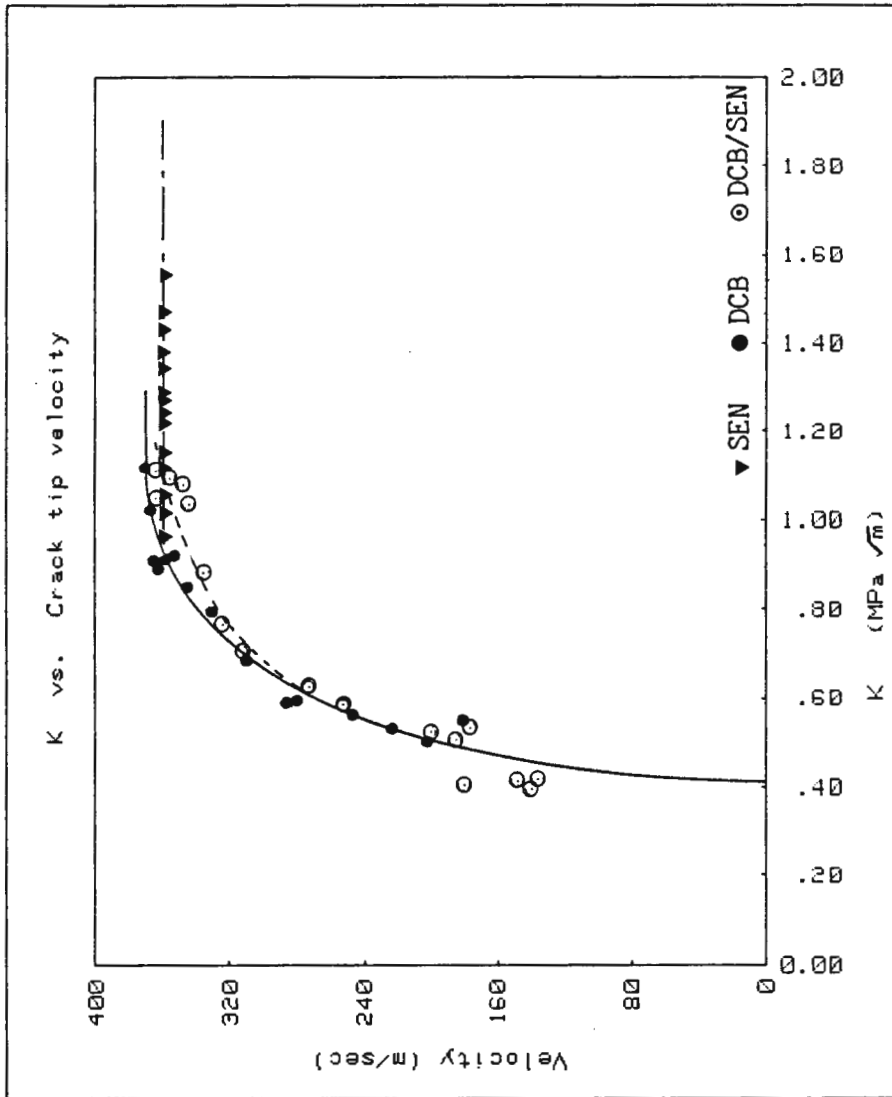
Fig.68. KI3 vs v plot for Homalite-100.

TABLE 1

DATA FROM THE STATIC PHOTOELASTIC TESTS

1/w	load N	Kth MPa√m̄	KI3 MPa√m̄	KI6 MPa√m̄
0.1	1567.4	0.481	0.426	0.537
0.1	1789.8	0.549	0.436	0.559
0.1	2012.2	0.618	0.589	0.671
0.1	2234.6	0.686	0.623	0.764
0.2	900.2	0.447	0.408	0.482
0.2	1033.6	0.514	0.441	0.548
0.2	1211.5	0.602	0.557	0.653
0.2	1345.0	0.668	0.578	0.693
0.3	677.8	0.499	0.437	0.497
0.3	766.7	0.565	0.502	0.553
0.3	864.6	0.637	0.578	0.623
0.3	944.7	0.696	0.637	0.696
0.4	455.4	0.495	0.428	0.489
0.4	522.1	0.567	0.506	0.548
0.4	588.8	0.640	0.570	0.631
0.4	655.5	0.712	0.636	0.705
0.5	299.7	0.485	0.438	0.474
0.5	370.9	0.600	0.547	0.602
0.5	413.1	0.668	0.597	0.659
0.5	455.4	0.736	0.647	0.720
0.6	188.5	0.478	0.428	0.469
0.6	224.1	0.571	0.505	0.568
0.6	250.8	0.638	0.549	0.607
0.6	286.4	0.729	0.627	0.681
0.7	99.5	0.433	0.378	0.407
0.7	121.8	0.531	0.466	0.518
0.7	152.9	0.666	0.571	0.623
0.7	179.6	0.782	0.669	0.738
0.8	55.05	0.483	0.417	0.474
0.8	68.39	0.600	0.510	0.573
0.8	81.74	0.717	0.614	0.704
0.8	99.53	0.873	0.719	0.808
0.9	16.10	0.448	0.366	0.430
0.9	20.54	0.572	0.450	0.507
0.9	24.99	0.696	0.529	0.603
0.9	31.64	0.881	0.651	0.775
0.9	37.86	1.055	0.795	0.942

TABLE 2

RESULTS OF STATIC ISOCHROMATIC TESTS WITH SIX PARAMETER ANALYSIS

No.	1/w	Cth *.0001	m *.0001	b *.0001	a *.001	%err.
1	.0989	3.07	3.333	3.347	-2.84	-8.55
2	.1999	4.97	5.283	5.252	3.56	-6.29
3	.2986	7.37	7.283	7.290	-.58	1.19
4	.3992	10.87	10.685	10.704	-1.02	1.70
5	.4977	16.17	15.947	15.932	.58	1.38
6	.6004	25.46	24.405	24.140	6.45	4.14
7	.7022	43.56	41.233	41.087	2.12	5.34
8	.8045	87.67	83.657	82.603	8.40	4.58
9	.8955	278.57	247.56	244.89	7.62	11.13

TABLE 3

RESULTS OF STATIC ISOCHROMATIC TESTS WITH THREE PARAMETER ANALYSIS

No.	1/w	Cth *.0001	m *.0001	b *.0001	a *.001	%err.
1	.0989	3.07	2.738	2.776	-7.40	10.82
2	.1999	4.97	4.413	4.395	2.06	12.20
3	.2986	7.37	6.634	6.684	-4.18	9.99
4	.3992	10.87	9.644	9.688	-2.51	11.28
5	.4977	16.17	14.459	14.377	3.26	10.58
6	.6004	25.46	22.157	21.985	4.17	12.97
7	.7022	43.56	37.555	37.309	3.56	13.79
8	.8045	87.67	73.918	73.102	6.50	15.69
9	.8955	278.57	211.36	206.52	13.82	24.13

TABLE 4

DATA FOR Ro/h vs K/Kth PLOT

l/w	Ro/h	K/Kth	l/w	Ro/h	K/Kth
0.1	0.460	1.002	0.1	0.461	1.009
0.1	0.479	0.967	0.1	0.477	0.958
0.1	0.510	0.980	0.1	0.534	1.030
0.1	0.509	0.974	0.1	0.554	0.979
0.1	0.550	0.955	0.2	0.474	1.028
0.2	0.476	1.038	0.2	0.504	0.982
0.2	0.513	1.022	0.2	0.557	1.051
0.2	0.561	1.066	0.2	0.591	0.863
0.2	0.616	1.044	0.2	0.617	1.048
0.3	0.471	1.037	0.3	0.477	1.068
0.3	0.517	1.040	0.3	0.561	1.049
0.3	0.608	1.072	0.4	0.469	1.073
0.4	0.467	1.060	0.4	0.510	1.099
0.4	0.548	1.119	0.4	0.551	1.135
0.4	0.596	1.187	0.4	0.608	1.175
0.5	0.454	0.940	0.5	0.447	0.910
0.5	0.493	0.902	0.5	0.494	0.911
0.5	0.543	0.955	0.5	0.542	0.949
0.5	0.565	0.904	0.5	0.581	0.968
0.5	0.616	0.989	0.5	0.611	0.972
0.5	0.374	0.992	0.5	0.373	0.980
0.5	0.204	0.721	0.5	0.190	0.603
0.5	0.177	0.501	0.5	0.336	0.911
0.5	0.314	0.765	0.5	0.256	0.872
0.5	0.230	0.665	0.5	0.298	0.879
0.5	0.297	0.874	0.5	0.394	0.988
0.5	0.371	0.855	0.5	0.415	0.996
0.5	0.406	0.945	0.5	0.448	0.983
0.5	0.435	0.914	0.5	0.529	1.050
0.5	0.519	1.002	0.5	0.510	0.955
0.5	0.584	0.994	0.5	0.585	0.996
0.5	0.754	1.124	0.5	0.760	1.144
0.5	0.709	1.099	0.5	0.697	1.052
0.5	0.709	1.097	0.5	0.703	1.076
0.6	0.491	0.896	0.6	0.521	0.916
0.6	0.528	0.944	0.6	0.564	0.916
0.6	0.564	0.918	0.7	0.465	0.885
0.7	0.460	0.861	0.7	0.498	0.871
0.7	0.496	0.860	0.7	0.532	0.862
0.7	0.532	0.865	0.7	0.561	0.859
0.7	0.570	0.894	0.7	0.591	0.878
0.7	0.589	0.868	0.8	0.416	0.912
0.8	0.419	0.923	0.8	0.487	0.959
0.8	0.557	0.993	0.8	0.550	0.962
0.8	0.595	0.992	0.8	0.603	1.025
0.9	0.429	0.954	0.9	0.517	0.983
0.9	0.469	0.954	0.9	0.566	0.981
0.9	0.580	1.040	0.9	0.475	0.983
0.9	0.517	0.983	0.9	0.603	1.065

TABLE 5

DATA FROM THE STATIC CAUSTIC TESTS

l/w	load N	Dia. mm	Kth MPa√m̄	KI MPa√m̄
0.1	2795.3	9.26	0.751	0.753
0.1	2795.3	9.28	0.751	0.758
0.1	3203.4	9.64	0.861	0.833
0.1	3203.4	9.60	0.861	0.825
0.1	3705.3	10.27	0.996	0.976
0.1	3705.3	10.25	0.996	0.970
0.1	3958.3	10.76	1.064	1.096
0.1	3958.3	10.91	1.064	1.136
0.1	4570.4	11.17	1.229	1.204
0.1	4570.4	11.05	1.229	1.173
0.2	1815.9	9.54	0.789	0.811
0.2	1815.9	9.58	0.789	0.819
0.2	2224.0	10.16	0.967	0.949
0.2	2224.0	10.32	0.967	0.988
0.2	2672.9	11.23	1.162	1.221
0.2	2672.9	11.30	1.162	1.238
0.2	3040.1	11.90	1.321	1.411
0.2	3040.1	12.35	1.321	1.547
0.2	3448.2	12.40	1.499	1.564
0.2	3448.2	12.43	1.499	1.572
0.3	1203.8	9.50	0.774	0.802
0.3	1203.8	9.61	0.774	0.826
0.3	1509.9	10.41	0.970	1.009
0.3	1509.9	10.35	0.970	0.995
0.3	1836.3	11.30	1.180	1.239
0.3	1836.3	11.17	1.180	1.204
0.3	2199.5	12.25	1.414	1.516
0.3	2199.5	12.46	1.414	1.581
0.4	779.4	9.44	0.737	0.791
0.4	779.4	9.40	0.737	0.781
0.4	938.6	10.27	0.888	0.976
0.4	938.6	10.27	0.888	0.976
0.4	1101.8	11.03	1.042	1.166
0.4	1101.8	11.10	1.042	1.183
0.4	1252.8	11.89	1.185	1.407
0.4	1252.8	11.99	1.185	1.437
0.4	1358.9	12.48	1.286	1.587
0.4	1358.9	12.23	1.286	1.511
0.5	542.7	9.14	0.775	0.730
0.5	542.7	9.02	0.775	0.705
0.5	693.7	9.92	0.991	0.894
0.5	693.7	9.96	0.991	0.903
0.5	836.5	10.93	1.195	1.141

TABLE 5(contd.)

DATA FROM THE STATIC CAUSTIC TESTS

l/w	load N	Dia. mm	Kth MPa√m	KI MPa√m
0.5	836.5	10.91	1.195	1.134
0.5	979.4	11.39	1.399	1.264
0.5	979.4	11.71	1.399	1.354
0.5	1101.8	12.38	1.574	1.557
0.5	1101.8	12.29	1.574	1.529
0.6	285.7	8.11	0.624	0.541
0.6	285.7	7.90	0.624	0.506
0.6	359.1	8.76	0.785	0.655
0.6	359.1	8.80	0.785	0.662
0.6	453.0	9.72	0.990	0.850
0.6	453.0	9.89	0.990	0.887
0.6	514.2	10.49	1.123	1.029
0.6	514.2	10.62	1.123	1.060
0.6	624.4	11.34	1.364	1.249
0.6	624.4	11.35	1.364	1.253
0.7	212.2	9.35	0.871	0.771
0.7	212.2	9.24	0.871	0.750
0.7	257.1	10.03	1.055	0.919
0.7	257.1	9.98	1.055	0.907
0.7	306.1	10.71	1.256	1.083
0.7	306.1	10.72	1.256	1.086
0.7	350.9	11.30	1.440	1.238
0.7	350.9	11.48	1.440	1.288
0.7	391.7	11.90	1.608	1.410
0.7	391.7	11.85	1.608	1.395
0.8	81.6	8.38	0.644	0.587
0.8	81.6	8.42	0.644	0.594
0.8	114.3	9.78	0.901	0.864
0.8	114.3	9.64	0.901	0.833
0.8	155.1	11.21	1.223	1.214
0.8	155.1	11.07	1.223	1.176
0.8	183.6	11.99	1.448	1.437
0.8	183.6	12.15	1.448	1.484
0.9	29.38	8.49	0.664	0.606
0.9	29.38	8.64	0.664	0.633
0.9	36.73	9.57	0.830	0.817
0.9	36.73	9.45	0.830	0.792
0.9	45.30	10.40	1.024	1.007
0.9	45.30	10.40	1.024	1.007
0.9	57.13	11.40	1.292	1.267
0.9	57.13	11.67	1.292	1.343
0.9	61.62	12.27	1.393	1.523
0.9	61.62	12.15	1.393	1.484

TABLE 6

RESULTS OF STATIC CAUSTIC TESTS

No.	l/w	Cth *.0001	m *.0001	b *.0001	a *.001	%err.
1	.1015	2.688	2.666	2.658	3.11	0.84
2	.2018	4.346	4.607	4.712	-29.13	-6.00
3	.3014	6.427	6.819	6.959	-24.71	-6.10
4	.4013	9.461	10.964	11.595	-71.09	-15.90
5	.5044	14.282	13.552	13.947	-34.75	5.11
6	.6006	21.850	19.609	20.853	-46.63	10.32
7	.7157	41.044	35.743	35.823	-2.54	12.90
8	.8049	78.850	77.258	80.296	-44.03	2.02
9	.8981	226.12	230.15	244.04	-68.32	-1.78

TABLE 7

DATA FOR THE DYNAMIC ISOCHROMATIC TEST
WITH THE SINGLE EDGE NOTCH SPECIMEN

No.	Time mic.sec	crk.lngth mm	KI3 MPa$\sqrt{m}$	KI6 MPa$\sqrt{m}$
1	20.5	57.15	1.010	1.274
2	24.5	58.78	0.954	1.252
3	31.0	60.17	1.017	1.253
4	37.5	61.90	1.059	1.290
5	42.5	65.28	1.058	1.205
6	48.5	66.75	1.057	1.098
7	54.0	68.53	1.118	1.165
8	60.5	70.31	1.107	1.146
9	65.5	72.92	1.101	1.105
10	71.5	75.11	1.092	1.139
11	98.5	84.58	1.051	1.038
12	126.0	94.08	1.104	1.155
13	149.5	102.82	1.154	1.264
14	170.5	110.36	1.216	1.403
15	191.5	118.08	1.284	1.463
16	223.0	129.34	1.344	1.390
17	250.5	139.88	1.555	2.064

Velocity = 360m/s

108

TABLE 8

DATA FOR THE DYNAMIC ISOCHROMATIC TEST WITH THE DOUBLE CANTILEVERED BEAM SPECIMEN

No.	Time mic.sec	crk.lngth mm	Velocity m/s	KI3 MPa$\sqrt{m}$	KI6 MPa$\sqrt{m}$
1	24.5	80.59	370	1.137	1.299
2	48.0	88.77	368	1.023	1.202
3	72.5	97.05	365	0.905	0.977
4	92.5	104.65	363	0.895	1.012
5	114.0	112.22	358	0.917	0.977
6	132.5	118.31	353	0.922	0.978
7	153.5	125.55	345	0.849	0.940
8	179.0	134.21	330	0.797	0.877
9	202.5	141.71	310	0.685	0.771
10	233.0	151.23	285	0.590	0.660
11	242.5	153.90	280	0.594	0.640
12	281.5	164.11	247	0.564	0.596
13	322.0	173.66	223	0.531	0.568
14	359.5	180.80	202	0.503	0.531
15	412.0	190.68	180	0.550	0.571

TABLE 9

DATA FOR THE DYNAMIC ISOCHROMATIC TEST WITH THE DCB/SEN SPECIMEN

No.	Time mic.sec	crk.lngth mm	Velocity m/s	KI3 MPa√m̄	KI6 MPa√m̄
1	25.5	81.1	364	1.111	1.432
2	45.5	88.1	364	1.048	1.224
3	73.5	97.9	360	1.124	1.224
4	97.0	106.5	356	1.090	1.207
5	120.0	114.8	348	1.080	1.133
6	139.0	121.1	344	1.037	1.099
7	159.5	128.4	336	0.882	1.032
8	184.0	136.5	324	0.768	0.943
9	205.5	143.3	312	0.706	0.834
10	236.0	152.6	272	0.623	0.691
11	242.5	154.7	252	0.585	0.653
12	284.0	163.6	180	0.404	0.454
13	317.0	168.3	148	0.413	0.477
14	354.0	171.0	136	0.419	0.414
15	392.0	176.3	140	0.397	0.598
16	567.0	204.0	176	0.533	0.572
17	620.0	213.6	184	0.506	0.571
18	716.0	230.3	200	0.523	0.547

TABLE 10

DATA FOR THE DYNAMIC CAUSTIC TEST WITH THE SINGLE EDGE NOTCH SPECIMEN

No.	Time mic.sec	crk.lngth mm	Dia. mm	KI3 MPa√m̄
1	57.5	74.6	15.04	0.825
2	65.0	81.5	14.63	0.770
3	83.5	89.8	14.83	0.797
4	126.5	101.5	15.42	0.878
5	147.0	108.1	15.53	0.894
6	153.0	112.0	15.49	0.889
7	191.0	123.5	15.97	0.959
8	209.0	135.8	16.13	0.983
9	229.0	145.5	16.75	1.080
10	236.5	146.6	16.70	1.072

Velocity = 384m/s

TABLE 11

MATERIAL PROPRETIES

Materials used for photoelastic tests:

Material	f' N/m/fringe
Polycarbonate	66.67
Homalite-100	218.8

Materials used for caustic tests:
(Inner caustic under plane stress)

Material	c m /N	f	k
Plexiglas	1.080E-10	3.17	0.526
Homalite-100	0.929E-10	3.11	0.518

:Expression for c given by equation(4.44).

BIBLIOGRAPHY

1. Atluri,S.N. and Nishioka,T., Engr. Fract. Vol. 18, No.1, pp1-22, (1983).

2. Beinert,J. and Kalthoff,J.F., "Experimental determination of dynamic stress intensity factors by shadow patterns", Mechanics of Fracture, vol VII, G.C.Sih,ed., Noordhoff Int. Publishing, London, The Netherlands, 1981.

3. Beinert,J., Kalthoff,J.F. and Maier,M., "Neuere Ergebnesse zur Anwendung des Schatten-fleckverfahrens auf stehende und Schnellaufende Bruche", VIth Intl. Conf. Expt. Stress Analysis, VDI Nr.313, 791-798 (1978).

4. Bradley,W.B. and Kobayashi,A.S., "An Investigaion of Propagating Crack by Dynamic Photoelasicity", Exptl. Mech., 10(3), 106-113 (1970).

5. Broek,D., "Elementary Engineering Fracture Mechanics", Marinus Nijhoff Publishers, 1982.

6. Chona,R., Fourney,W.L., Sanford,R.J. and Shukla,A., "Determining Stress Intensity Factor for Running Cracks", Proceedings of CFC10, "Modeling Problems in Crack Tip Mechanics", held at the Univ. of Waterloo, Aug.24-26,1983.

7. Collins,J.A., "Failure of Materials in Mechanical Designs", Wiley Intersciences Publications.

8. Cranz,C. and Schardin,H., Zeits.f.Phys., 56, 147-83, (1929).

9. Dally,J.W., "Dynamic Photoelastic Studies of Fracture", Expt. Mech., vol.19, No.10, pp.349-361, Oct(1979).

10. Dally,J.W., Kobayashi,T. and Fourney,W.L., "Influences of Specimen Geometry on Crack Propagation and Arrest Behaviour", VIth Intl. Conf. Exptl. Stress Analysis, Society for Exptl. Stress Analysis, Munich, West Germany, Sept. 18-22, 1978.

11. Dally,J.W. and Riley,W.F., "Experimental Stress Analysis", McGraw-Hill, (1978).

12. Etheridge,J.M. and Dally,J.W., "A Critical Review of Methods for Determining Stress Intensity Factors from Isochromatic Fringes", Exptl. Mech., 17(7), 248-254

(1977).

13. Etheridge,J.M. and Dally,J.W., "A Three Parameter
Method for Determining Stress Intensity Factor from
Isochromatic Fringe Loops", J. Strain Analysis, 13(2),
91-94 (1978).

14. Irwin,G.R., "Discussion of Wells and Post Paper (in
Proc. of SESA, 16(1)), Proc. of SESA, 16(1),
93-96(1958).

15. Irwin,G.R., "Series Representation of the Stress Field
Around Constant Speed Cracks", Univ. of Maryland
Lecture Notes, 1980.

16. Irwin,G.R., Dally,J.W. and Fourney,W.L., "On the
Uniqueness of the Stress Intensity Factor-Crack Velocity
Relationship", To be published.

17. Irwin,G.R., Dally,J.W, Kobayashi,T., Fourney,W.L.,
Etheridge,M.J. and Rossmanith,H.P., "On he
Determination of the a-K Relaionship for Birefringent
Polymers", Experimental Mechanics, vol. 19, No. 4,
121-128, April 1979.

18. Kalthoff,J.F., "On some Current problems in Experimental
Fracture Dynamics"

19. Kalthoff,J.F., Beinert,J. and Winkler,S., "Influence of
Dynamic Effects on Crack Arrest", EPRI 1022-1, First
Semi-annual Progress Report, Report V9/78, Institut fur
Festkopermechanik, Freiburg, Germany, Aug (1978).

20. Kobayashi,A.S. et al., "Crack Branching in Homalite-100
Sheets", Engr. Frac. Mech., vol.6, pp.81-92, (1974).

21. Kobayashi,A.S. and Mall,S., "Dynamic Fracture Toughness
of Homalite-100", Experimental Mechanics, 18(1978)
11-18.

22. Kobayashi,A.S. and Ramulu,M., "Dynamic Stress Intensity
Factors for Unsymmetric Dynamic Isochromatics", Exptl.
Mech., vol.21, No.1, Jan 1981, 1141-1148.

23. Manogg,P., "Anwendung der Schattenoptik zur Untersuchung
des Zerreissvorgangs von Platten", Dissertation,
Freiburg, Germany (1964).

24. Manogg,P., "Investigation of the rupture of a Plexiglas
Plate by means of an Optical Method Involving High-speed
Filming of the Shadows Originating Around Holes Drilling
in the Plate", Intl. J. Frac. Mech., 2,pp 604-613
(1966).

25. Phillips,J.W. and Sanford,R.J., "Effect of Higher-order Stress Terms on Mode-1 Caustics in Birefringent Materials", Special Technical Publication 743, ASTM.

26. Post,D., "Photoelasitc Stress Analysis for an Edge Crack in a Tensile Field", Proc. of SESA, 12(1), 99-116(1954).

27. Ravi-Chander,K. and Knauss,W.G., "Process Controlling the Dynamic Fracture of Brittle Solids", Workshop on Dynamic Fracture, Calif. Inst. of Tech., pp.119-128, Feb.(1983).

28. Rice,J.R., "Mathematical Analysis in the Mechanics of Fracture", Fracture, ed. Liebowitz,H., Academic press, NY-London, pp235-238(1968).

29. Rosakis,A.J., "Analysis of the Optical Method of Caustics for Dynamic Crack Propagation", Report ONR-79-1 Division of Engineering Brown Univ., Mar.1979, Engineerring Fracture Mech., vol.13, pp.331-347, (1980).

30. Rosakis,A.J., Duffy,J. and Freund,L.B., "Experimental Study of the Dynamic Crack Propagation Resistance of a Structured Steel by the Optical Method of Caustics"

31. Rosakis,A.J. and Freund,L.B., "The Effect of Crack Tip Plasticity on the Determination of Dynamic Stress Intensity Factors by the Optical Method of Caustics", Trans. of the ASME, J. Appl. Mech., vol.48, pp.302-308, June 1981.

32. Rosakis,A.J. and Ravi Chander,K., "On Crack Tip Stress State: An Experimental Evaluation of Three Dimensional Effects", Caltech Report, SM84-2, March 1984.

33. Rossmanith,H.P., "Determination of Stress Intensity Factors by the Dynamic Method of Caustics for Optically Isotropic Materials", Ingenieur Archiv, 362-381, 48(1979)

34. Rossmanith,H.P., "General Mode-1 Caustic Evaluation for Optically Anisotropic Materials", Ingenieur-Archiv, 73-83, 50(1981).

35. Rossmanith,H.P. and Irwin,G.R., "Analysis of Dynamic Isochromatic Crack Tip Stress Patterns", Univ. of Maryland Report.

36. Sanford,R.J., Chona,R., Fourney,W.L. and Irwin,G.R., "A Photoelastic Study of the Influence of Non-singular Stresses in Fracture Test Specimens", Univ. of Maryland Report, p.1, Aug.1981.

37. Sanford,R.J. and Dally,J.W., "A General Method for Determining Mixed-mode Stress Intensity Factor from Isochromatic Fringe Patterns, J. of Engr. Fract. Mech., 11,621-633 (1979).

38. Schroedl,M.A. and Smith,C.W., "Local Stresses near Deep Surface Flaws Under Cylindrical Bending Fields", Progress in Flaw Growth and Fracture Toughness Testing, ASTM STP 536, pp.45-63 (1973).

39. Shockey,D.A., Kalthoff,J.F., Klemm,W. and Winkler,S., "Simultaneous Measurements of Stress Intensity and Toughness for Fast Running Cracks in Steel", Expt. Mech. Vol.23, No.2, June 1983.

40. Shukla,A., "Crack Propagation in Ring Type Fracture Specimens", M.S.Thesis, Univ. of Maryland, p.50, (1978).

41. Tada,Irwin,G.R. and Paris, "The Stress Analysis of Cracks Handbook", Del Research Corporation, 1973.

42. Theocaris,P.S., "Caustics for the Determination of Singularities in Cracked Plates", Proc. IUT Symposium on Optical Methods in Mechanics of Solids, Univ. of Poitires, (1979).

43. Theocaris,P.S., "Local Yielding Around a Crack Tip in Plexiglas", J. Appl. Mech., 37 ,509-514, (1970).

44. Theocaris,P.S. and Gdoutos,E.E., "The Modified Dugdale-Barenblatt Model Adapted to Various Fracture Configurations in Metals", Intl. J. Frac., vol 10, pp 549-564, (1974).

45. Theocaris,P.S. and Gdoutos,E.E., "Verification of the Validity of the Dugdale-Barenblatt Model by the Method of Caustics", Engr. Frac. Mech., vol.6, pp 523-535,(1974).

46. Wells,A. and Post,D, "The Dynamic Stress Distribution Surrounding a Running Crack- A Photoelasic Analysis", Proc. of SESA, 16(1), 69-92(1958).

47. Williams,M.L., "On the Stress Distribution at the Base of a Stationary Crack", J.Appl. Mech., 24, pp.109-114(1957).

48. Yoffe,E.H., "The Moving Griffith Crack", Philosophical Magazine, Series 7, 42,739(1951).